Stony Brook University

Some Results on One-Dimensional Models with Broken and Deformed Symmetries

A Dissertation Presented

by

Francis Norman Claridades Paraan

to

The Graduate School

in Partial Fulfillment of the Requirements

for the Degree of

Doctor of Philosophy

in

Physics

Stony Brook University

December 2012

Stony Brook University

The Graduate School

Francis Norman Claridades Paraan

We, the dissertation committee for the above candidate for the Doctor of Philosophy degree, hereby recommend acceptance of this dissertation.

Vladimir E. Korepin – Dissertation Advisor
Professor, C. N. Yang Institute for Theoretical Physics and Department of Physics and Astronomy

Dominik A. Schneble – Chairperson of Defense
Associate Professor, Department of Physics and Astronomy

Tzu-Chieh Wei – Committee Member
Assistant Professor, C. N. Yang Institute for Theoretical Physics and Department of Physics and Astronomy

Alexander Kirillov, Jr. – Committee Member
Associate Professor, Department of Mathematics
Stony Brook University

This dissertation is accepted by the Graduate School.

Charles Taber
Interim Dean of the Graduate School

Abstract of the Dissertation

Some Results on One-Dimensional Models with Broken and Deformed Symmetries

by

Francis Norman Claridades Paraan

Doctor of Philosophy

in

Physics

Stony Brook University

2012

We present analytic results for the ground state properties and entanglement in the Lieb–Liniger model and q-deformed Affleck–Kennedy–Lieb–Tasaki (AKLT) models. The translational invariance of the Lieb–Liniger model is broken by an external harmonic potential in one case and by coarse-grained measurements of particle number in another. Meanwhile, anisotropy is introduced into the AKLT model by generalizing its SU(2) invariant hamiltonian into one that is $\mathrm{SU}_q(2)$ invariant.

The Lieb–Liniger model describes a one-dimensional gas of bosons that mutually interact by a zero-range interaction term. Under longitudinal harmonic confinement, the exact spectrum of the hamiltonian is known only for free and impenetrable bosons. We use a pseudopotential approach and perturbation theory to calculate the ground state energy of this gas near the limit of infinite repulsion.

We further study entanglement in the periodic homogeneous Lieb–Liniger model. When the particle number in a spatial partition of the ground state is measured, entanglement in the resulting state arises only from interparticle interactions. We demonstrate that entanglement in these projected states increases monotonically with the strength of interactions.

Finally, we discuss how anisotropy reduces entanglement in the valence-bond-solid ground state of the q-deformed AKLT model. We propose effective thermal models that describe block entanglement in terms of boundary degrees of freedom. The anisotropy parameter q enters these models as an effective temperature.

Contents

List of Figures

Acknowledgments

Academic.

I thank my advisor Prof. Vladimir Korepin. Advancing in physics requires a continuous sharpening of intuition. After each consultation with him his ability to simplify physical and mathematical concepts allowed me to see further. Additionally, he took every opportunity to introduce me to his colleagues and their work. This led to successful collaborations with Prof. Andreas Klümper, Prof. Sougato Bose, and Prof. Javier Molina-Vilaplana. Working with them was a pleasure and very educational. I am also grateful to Prof. Dominik Schneble, Prof. Alexander Abanov, and Fabio Franchini for sharing their time and expertise. The work presented here benefitted greatly from my interactions with them. I further thank Prof. Tzu-Chieh Wei and Prof. Alexander Kirillov, Jr. for their critical reading of this manuscript as committee members of my defense.

I am indebted to my colleague and co-author Raul Santos. I consider him my second advisor.

I am grateful to Prof. Akio Hosoya for his gracious hospitality during my stay at the Tokyo Institute of Technology. Some of the material in this manuscript was presented there. Also, I thank Yutaka Shikano and Hosho Katsura for the scientific exchanges we shared in Tokyo.

I have always maintained ties with my previous group at the University of the Philippines. Along with Prof. Perry Esguerra, my former labmates Mike Solis, Soli Garcia, Lexter Dy, Hauser Villegas, Mikhail Solon, and Michiko Alcanzare have clarified many issues while I was working on this thesis.

Financial.

I acknowledge support by the U.S. National Science Foundation through Grants No. DMS-0905744 and No. DMS-1205422. My stay in Tokyo was funded by the Foreign Graduate Student Invitation Program of the Tokyo Institute of Technology. My attendance at the 5^{th} Asia Pacific Workshop on Quantum Information Science at Nanyang Technological University in Singapore was supported by an International travel grant from the C. N. Yang Institute for Theoretical Physics.

Social.

I wish to thank those who made my stay in Stony Brook pleasant through personal communication.

Related Publications

This thesis is mainly based on the following manuscripts:

I Francis N. C. Paraan, Vladimir E. Korepin, "Perturbative correction to the ground-state properties of one-dimensional strongly interacting bosons in a harmonic trap," Phys. Rev. A **82**, 065603 (2010), preprint arXiv:1011.1706.

II Francis N. C. Paraan, Javier Molina-Vilaplana, Vladimir E. Korepin, Sougato Bose, "Entanglement in bipartite pure states of an interacting boson gas obtained by local projective measurements," Phys. Rev. A **84**, 032330 (2011), preprint arXiv:1105.1211.

III Raul A. Santos, Francis N. C. Paraan, Vladimir E. Korepin, Andreas Klümper, "Entanglement spectra of the q-deformed Affleck-Kennedy-Lieb-Tasaki model and matrix product states," Europhys. Lett. **98**, 37005 (2012), preprint arXiv:1112.0517.

IV Raul A. Santos, Francis N. C. Paraan, Vladimir E. Korepin, Andreas Klümper, "Entanglement spectra of q-deformed higher spin VBS states," J. Phys. A: Math. Theor. **45**, 175303 (2012), preprint arXiv:1201.5927.

V Raul A. Santos, Francis N. C. Paraan, Vladimir E. Korepin, "Quantum phase transition in a multicomponent anyonic Lieb-Liniger model," Phys. Rev. B **86**, 045123 (2012), preprint arXiv:1204.4149.

Chapter 1

Introduction

One-dimensional quantum models are important and interesting. Their reduced dimensionality can make them analytically tractable and in some cases exactly solvable. This feature has led to many advances in mathematical physics such as the development of integrable models, quantum groups, and others as specialized fields. Additionally, one of the original motivating factors for the study of these models was the extraction of physical insight that would be useful for the analysis of their higher-dimensional counterparts. This perspective has expanded in recent decades because of scientific and technological advances. The focus is now on the understanding of actual and quasi one-dimensional physical systems. This drive is pushed by current experimental methods that allow one to manufacture and manipulate low-dimensional structures under controlled conditions. For example, the physical systems of particular relevance to this thesis are: ultracold gases in optical lattices (recent reviews are [1–3]), photonic valence-bond-solid states [4–6], and molecular antiferromagnetic chains [7].

One-dimensional systems are inherently strongly interacting and have nontrivial physical features. For example, in Chapters 2 and 3 we consider the Lieb–Liniger model, which describes a boson gas with contact interactions. In the strong repulsion limit of this system a dynamically-induced exclusion principle leads to thermodynamic properties that are similar to that of a free-fermion gas. Additionally, the ground state of the quantum spin chain pre-

sented in Chapter 4 can be pictured as a crystal made up of valence bonds. The quantum state of a block of spins in this ground state may be represented by a product of vector-valued matrices. A notable feature of this construction is that the dimension of the Hilbert space of such a block does not depend on the number of spins in the block (more than two spins). As we discuss in more detail in the following chapters, the tractability of these models is related to certain symmetries they possess. When some of these symmetries are broken or deformed, the conventional approach to the problem may need to be abandoned or generalized.

In Chapter 2 the translational invariance of the Lieb–Liniger model of interacting bosons is broken by an external harmonic trapping potential. The homogeneous model (no trapping potential) is integrable and solvable by the Bethe ansatz. However, in the presence of the trap the many-body problem has no known exact solution for general values of the interaction parameter. The hamiltonian, however, is analytically diagonalizable in the limit of infinite repulsion. In this limit of impenetrable bosons, the quantum mechanical eigenvalue problem can be mapped onto an equivalent non-interacting fermionic problem. We can therefore analyze the ground state properties of the trapped gas near the extreme limit of infinitely repulsive particles by a perturbative pseudopotential approach.

Chapters 3 and 4 are devoted to the study of quantum correlations in the pure ground states of two different one-dimensional models. These correlations are quantified by a physical quantity called entanglement. From the perspective of quantum information, entanglement is a resource that may be used to perform quantum computations. In this thesis the amount of entanglement in these pure states is measured by the entanglement entropy and entanglement spectrum.

In Chapter 3 the translational symmetry of the Lieb–Liniger ground state is broken by a projective measurement. This measurement results in a projected pure state with a fixed number of particles in a spatial region of the gas. As a consequence of this procedure, entanglement in this projected state arises only from interparticle interactions. Our strategy here is to use the many-particle wavefunction (which is derived from the coordinate Bethe ansatz) for exact

numerical calculations of the entanglement entropy. Our results therefore show how particle interactions affect entanglement in a direct manner.

In Chapter 4 we study entanglement in the ground state of an anisotropic integer-spin model on a linear chain. This model is a q-deformed generalization of the SU(2) invariant Affleck–Kennedy–Lieb–Tasaki model of antiferromagnets. That is, the anisotropy introduced in this generalized model does not completely break SU(2) symmetry, but continuously deforms it to that of the $\mathrm{SU}_q(2)$ quantum group. Through a unified approach involving the appropriately generalized rules of angular momentum addition, we are able to quantify entanglement in this model from the undeformed isotropic limit to the fully deformed limit with no entanglement.

Each chapter in this thesis follows the same format. An introductory section is followed by a discussion of results. This chapter introduction will provide a more detailed survey of historical material, definitions, and preliminary calculations that are needed to properly frame the main result. A concluding section summarizes these results and poses possible future problems. Some details of additional calculations are provided in a section of derivations at the end of each chapter.

Chapter 2

Strongly repulsive boson gas in a harmonic trap

The contents of this chapter are based on the manuscript [**I**].

2.1 Lieb–Liniger model

The Lieb–Liniger (LL) gas [8, 9] is a model of interacting spinless bosons in one-dimension. Pairwise interactions in this model have zero range and are represented by Dirac-delta functions. The quantum mechanical hamiltonian of this model is

$$H = -\sum_{i=1}^{N} \frac{\partial^2}{\partial x_i^2} + 2c \sum_{i<j} \delta(x_j - x_i), \tag{2.1}$$

where c is the strength of the interaction. We have used $\hbar^2/2mL^2$ as the unit of energy and L as the unit of length (m is the particle mass). Here we consider repulsive interactions ($c > 0$) because we are interested in the properties of the gas near the impenetrable Tonks–Girardeau (TG) limit $c \to \infty$. In terms of quantum fields, the Lieb–Liniger model is equivalently expressed as

$$\mathcal{H} = \int_0^1 \partial_x \Psi^\dagger(x) \partial_x \Psi(x) + c \Psi^\dagger(x) \Psi^\dagger(x) \Psi(x) \Psi(x) \, \mathrm{d}x. \tag{2.2}$$

The field operator $\Psi(x)$ obeys the canonical commutation relations

$$\begin{aligned}[\Psi(x), \Psi^\dagger(y)] &= \delta(x-y), \\ [\Psi(x), \Psi(y)] &= [\Psi^\dagger(x), \Psi^\dagger(y)] = 0.\end{aligned} \tag{2.3}$$

The corresponding equation of motion for the quantum hamiltonian (2.2) is the nonlinear Schrödinger equation (NLSE):

$$i\partial_t \Psi = \left[-\partial_x^2 + 2c\Psi^\dagger\Psi\right]\Psi. \tag{2.4}$$

The homogeneous Lieb–Liniger model has several features that make it a good starting point for the study of one-dimensional systems. One of the most important of its characteristics is its integrability. The quantum inverse scattering method (QISM) [10] may be used to construct a hierarchy of operators that commute with the quantum hamiltonian [11]. This method also allows one to obtain the energy spectrum of the model from the solution of set of algebraic equations known as the Bethe equations. Furthermore, a complete set of energy eigenfunctions for the model is explicitly given by the coordinate Bethe ansatz [8, 10, 12–15]. These wavefunctions and the corresponding Bethe equations are discussed in Section 3.2.

Though being a decades-old model, there is still much interest in it. Recent experimental developments in the physics of ultracold atoms has much to do with this activity [3]. With current technology and techniques it is possible to form and manipulate quasi one-dimensional boson gases with tunable interaction parameters [16–23]. These developments have led to many experimental breakthroughs. For example, the superfluid to Mott insulator quantum phase transition has been realized [24, 25], the ground and low-lying excited states of the Lieb–Liniger gas have been prepared and characterized at different interaction strengths [17–19, 26], and collision experiments between one-dimensional ultracold gases have been performed to probe their structural and transport properties [27–29]. Surveys of experimental results on one-dimensional boson systems are presented in the reviews [1–3].

The suitability of the LL model in describing the properties of these quasi

one-dimensional systems at low temperatures has been established. Given a gas of spinless bosonic atoms with short-ranged pairwise interactions that is confined transversally by tight harmonic potentials, the longitudinal s-wave scattering amplitudes are reproduced by one-dimensional pseudopotentials proportional to a Dirac delta function [30, 31]. With this result, the strength of the effective delta interaction may be obtained from measureable quantities such as the three-dimensional atomic scattering length $a_{3\mathrm{D}}$ and the linear dimension of the transverse confining potential $a_\perp$. For example, for a three-dimensional gas with a spherically symmetric interaction potential $V = \delta(\mathbf{r})\partial_r(r\,\cdot)$ (Huang potential [32]), the longitudinal scattering length $a_{1\mathrm{D}}$ in an effectively one-dimensional system under tight harmonic confinement is [30]

$$a_{1\mathrm{D}} = -\frac{a_\perp^2}{a_{3\mathrm{D}}}\left(1 - C\frac{a_{3\mathrm{D}}}{a_\perp}\right). \tag{2.5}$$

The constant C here is numerically equal to $1.4603\cdots$, $a_\perp$ is the transverse oscillator length $a_\perp = \sqrt{\hbar/\mu\omega_\perp}$, $\mu = m/2$ is the two-particle reduced mass, and $\omega_\perp$ is the transverse oscillator frequency. The effective one-dimensional interparticle potential is then

$$c\delta(x) = -\frac{\hbar^2}{\mu a_{1\mathrm{D}}}\,\delta(x). \tag{2.6}$$

Therefore, the interaction constant c may be tuned by changing the three-dimensional scattering length (e.g. via a Feshbach resonance [33, 34]) or by modifying the width of the transverse confining potential. The resonant behavior of c as $a_\perp \sim a_{3\mathrm{D}}$ is a phenomenon known as confinement-induced resonance. It is a general feature of ultracold gases with short-range interactions under transverse harmonic confinement [31].

2.1.1 Trapped Lieb–Liniger gas

The homogeneous Lieb–Liniger model (2.1) is still quite an idealization because it describes a gas that is not confined longitudinally. Thus, much effort has been devoted to studying the effects of longitudinal confinement of inter-

acting bosons [35–38]. For example, including an external harmonic potential to the free Lieb–Liniger model of spinless bosons leads to the many-particle Schrödinger eigenvalue equation

$$\bar{E}\Psi^{\mathrm{b}} = \left[\sum_{i=1}^{N} -\frac{\hbar^2}{2m}\frac{\partial^2}{\partial x_i^2} + \frac{m\omega^2 x_i^2}{2}\right]\Psi^{\mathrm{b}} - \frac{\hbar^2}{ma}\sum_{i<j}\delta(x_j - x_i)\Psi^{\mathrm{b}}. \tag{2.7}$$

Here ω is the angular frequency of the longitudinal trap and a is the effective one-dimensional s-wave scattering length. The superscript 'b' refers to the bosonic nature of the wavefunction, i.e. it is symmetric under interchanges of particle coordinates $x_i \leftrightarrow x_j$. Measuring energy in units of $\hbar\omega$ and length in units of the longitudinal oscillator length $\ell = \sqrt{\hbar/m\omega}$ gives the dimensionless eigenvalue equation

$$E\Psi^{\mathrm{b}} = \left[\sum_{i=1}^{N} -\frac{1}{2}\frac{\partial^2}{\partial x_i^2} + \frac{1}{2}x_i^2 + c\sum_{i<j}\delta(x_j - x_i)\right]\Psi^{\mathrm{b}}, \tag{2.8}$$

where we have introduced the dimensionless interaction strength $c = -\ell/a$.

Currently, there is no exact analytical solution for the spectrum of this model (2.8) for general values of the particle number N and interaction strength c. The addition of a harmonic confining potential to the Lieb–Liniger model breaks the translational invariance of the system and the total momentum of the gas is no longer a conserved quantity. Furthermore, the two-particle scattering phase becomes position-dependent due to the external potential, which destroys the general integrability of the model. However, there are certain limits where the harmonically confined boson gas remains solvable. For example, the energy eigenfunctions and spectrum are known for the separable two-particle case [39] and the Tonks–Girardeau (TG) limit of infinite repulsion $c \to +\infty$ [40, 41]. Additionally, the ground state and low-lying excitations of this confined model have been studied analytically in the Thomas–Fermi limit ($N \to \infty$ with $\sqrt{N}/c \to$ constant) [35–37, 42–44]. The Thomas–Fermi approach is sketched in Section 2.6.2.

The properties of the Lieb–Liniger gas under the influence of different trapping potentials has been investigated previously. The simplest case is that of

a flat-bottomed box where the many-body wavefunction is required to vanish at the boundaries of the box [45–47]. In this case the solvability of the model is preserved. Another example is that of a linear (wedge-shaped) confining potential [48]. In the limit of impenetrable bosons, the stationary states of this system involves a Slater determinant of single-particle Airy states.

2.1.2 Chapter outline

In this chapter, we develop a perturbative expansion for the ground state energy of the trapped boson gas about the known TG solution. An essential ingredient of the following analysis is the fermion-boson mapping for one-dimensional systems [49]. With this technique the wavefunctions and spectrum of the impenetrable boson gas are obtained from the wavefunction and spectrum of free-fermionic models. We use a generalization of this mapping in Section 2.2 that connects a strongly interacting boson gas and a weakly interacting spin-polarized fermion gas [50, 51]. The main result of this chapter is an analytic expression for the first-order $(1/c)$ correction to the ground state energy of the trapped gas for any number of bosons N (Section 2.3). We consider the case of two bosons and further discuss the large N behavior of our formula in Section 2.4. We find that the Thomas–Fermi limit is approached rapidly with increasing N. Finally, the details of some derivations of these results are provided in Section 2.6.

2.2 Fermion-boson mapping

In one dimension a bosonic model with pairwise contact interactions of strength c can be mapped into a fermionic model with interactions of strength $\sim 1/c$ and having the same energy spectrum [50]. Specifically, let us consider a fermionic many-particle wavefunction Φ^{f} that is antisymmetric under interchanges of particle coordinates $x_i \leftrightarrow x_j$ and satisfies the eigenvalue equation

$$E\Phi^{\mathrm{f}} = \left[\sum_{i=1}^{N} -\frac{1}{2}\frac{\partial^2}{\partial x_i^2} + \frac{1}{2}x_i^2 + \hat{V}^{\mathrm{f}}\right]\Phi^{\mathrm{f}}, \tag{2.9}$$

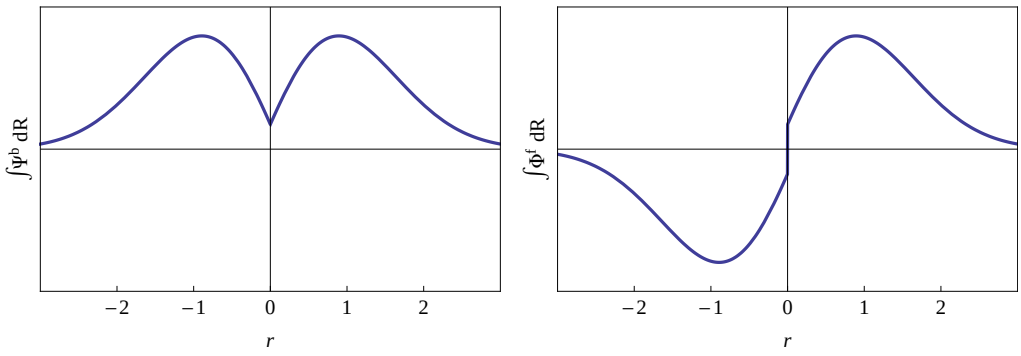

(a) Bosonic (b) Fermionic

Figure 2.1: (a) Relative coordinate part of the ground state wavefunction of two delta-interacting bosons $\int \Psi^{\mathrm{b}}\,\mathrm{d}R$ in a harmonic trap and (b) its fermionic counterpart $\int \Phi^{\mathrm{f}}\,\mathrm{d}R$. The interaction constant is $c = 10$ and $\sqrt{2}r = x_1 - x_2$.

An appropriate pseudopotential operator $\hat{V}^{\mathrm{f}}$ allows us to make the following correspondence between a bosonic wavefunction Ψ^{b} and its fermionic counterpart Φ^{f}

$$\Psi^{\mathrm{b}} = \mathcal{A}\Phi^{\mathrm{f}}(x_1, \ldots, x_N), \quad \mathcal{A} \equiv \prod_{i<j} \mathrm{sgn}(x_j - x_i), \tag{2.10}$$

such that Ψ^{b} satisfies the eigenvalue equation (2.8) with the same eigenvalue E. Such an operator has matrix elements in the coordinate representation given by [38]

$$\langle \varphi^{\mathrm{f}} | \hat{V}^{\mathrm{f}} | \phi^{\mathrm{f}} \rangle = -\frac{4}{c} \sum_{i<j} \int \lim_{r_{ij}\to 0} \left[\frac{\partial \varphi^{\mathrm{f}*}}{\partial r_{ij}} \times \frac{\partial \phi^{\mathrm{f}}}{\partial r_{ij}} \right] \mathrm{d}R_{ij}, \tag{2.11}$$

where $r_{ij} = x_j - x_i$ and $R_{ij} = \frac{1}{2}(x_j + x_i)$ are relative and central coordinates, and $\varphi^{\mathrm{f}}(x_1, \ldots, x_N)$ and $\phi^{\mathrm{f}}(x_1, \ldots, x_N)$ are the coordinate space wavefunctions corresponding to the fermionic state kets $|\varphi^{\mathrm{f}}\rangle$ and $|\phi^{\mathrm{f}}\rangle$. These matrix elements are also reproduced by an approximate pseudopotential $\hat{V}^{\mathrm{f}}_{\mathrm{a}} = -(2/c)\sum_{i<j} \delta''(x_i - x_j)$ [52, 53] provided the coordinate basis wavefunctions are continuous and vanish at the collisional nodes [38]. In this chapter we will use the exact pseudopotential (2.11).

As an illustration of the fermion-boson mapping idea, we plot the relative coordinate part (2.19) of the ground state wavefunction for the case of two

bosons in Figure 2.1a. The delta interaction results in a cusp in the bosonic wavefunction Ψ^{b} at the collisional node $r \equiv (x_1 - x_2)/\sqrt{2} = 0$. Meanwhile, multiplying the bosonic wavefunction by the unit antisymmetric function $\mathcal{A}$ results in a fermionic wavefunction Φ^{f} that changes sign under particle interchange. At $r = 0$ this fermionic wavefunction is discontinuous, but its first derivatives at $r = 0^+$ and $r = 0^-$ are equal (Figure 2.1b). It is precisely this discontinuity in the fermionic wavefunction that is reproduced by the pseudopotential $\hat{V}^{\mathrm{f}}$ (2.11). As the strength of the delta interaction increases $c \to \infty$, the discontinuity in Φ^{f} vanishes. The fermion-boson mapping (2.10) therefore relates impenetrable boson wavefunctions to free-fermionic ones. It is, however, also valid for arbitrary repulsion strengths c.

For an arbitrary number of bosons N, the bosonic eigenvalue equation (2.8) is solved in the TG limit by the symmetrized Slater determinant [40, 41]

$$\Psi^{\mathrm{b}}_{\mathrm{TG}} = \frac{\mathcal{A}}{\sqrt{N!}} \det \psi_n(x_m) \equiv \mathcal{A}\Phi^{\mathrm{f}}_{\mathrm{TG}}, \tag{2.12}$$

where $\Phi^{\mathrm{f}}_{\mathrm{TG}}$ is the fermionic wavefunction, $\{x_m\}$ are the particle coordinates and $\{\psi_n\}$ is a set of N single-particle harmonic oscillator eigenfunctions $\psi_n(x) = \pi^{-1/4}(2^n n!)^{-1/2} H_n(x) e^{-x^2/2}$. The $H_n(x)$ appearing here are the usual Hermite polynomials. For the ground state, the set $\{\psi_n\}$ consists of N orbitals with the lowest distinct quantum numbers n. The corresponding energy of this TG ground state (in units of $\hbar\omega$) is

$$E_{\mathrm{TG}} = \tfrac{1}{2}N^2. \tag{2.13}$$

For finite and large repulsion strengths we may use the quantity $1/c \ll 1$ as a perturbation parameter for the fermionic problem (2.9) about the Tonks–Girardeau solution. Thus, ordinary first-order perturbation theory gives the desired correction to the ground state energy

$$E_0 = \tfrac{1}{2}N^2 + \langle \Phi^{\mathrm{f}}_{\mathrm{TG}} | \hat{V}^{\mathrm{f}} | \Phi^{\mathrm{f}}_{\mathrm{TG}} \rangle + \mathcal{O}(1/c^2). \tag{2.14}$$

Our task in the following section is to perform an exact calculation for the

matrix element $\langle \Phi^{\mathrm{f}}_{\mathrm{TG}} | \hat{V}^{\mathrm{f}} | \Phi^{\mathrm{f}}_{\mathrm{TG}} \rangle$.

2.3 Perturbation result

In this section we give the leading $1/c$ correction $\delta E \equiv \langle \Phi^{\mathrm{f}}_{\mathrm{TG}} | \hat{V}^{\mathrm{f}} | \Phi^{\mathrm{f}}_{\mathrm{TG}} \rangle$ to the ground state energy E_0. The effective fermionic interaction operator $\hat{V}^{\mathrm{f}}$ is a sum of two-body operators $\hat{v}$ that has the matrix elements

$$v_{klmn} = -\frac{4}{c} \int \lim_{r \to 0} \left\{ \frac{\partial \big[\psi_k(x_1) \psi_l(x_2) \big]^*}{\partial r} \frac{\partial \big[\psi_m(x_1) \psi_n(x_2) \big]}{\partial r} \right\} \mathrm{d}R. \tag{2.15}$$

Since $\Phi^{\mathrm{f}}_{\mathrm{TG}}$ is a Slater determinant, we may calculate the perturbation δE using the Slater-Condon rule $\delta E = \sum_{m<n} (v_{mnmn} - v_{mnnm})$ [54, 55]. Prior to calculating the derivatives appearing inside the integral (2.15), we must be careful to write the coordinates $x_1 = R + \frac{1}{2} r$ and $x_2 = R - \frac{1}{2} r$ in terms of the relative and central coordinates r and R. Since the single-particle wavefunctions $\psi_m(x)$ are real, the symmetry of the integrand allows us to write and define $v_{mnmn} = -v_{mnnm} \equiv \tilde{v}_{mn}$ where

$$\tilde{v}_{mn} = -\frac{4}{c} \int \lim_{r \to 0} \left\{ \frac{\partial \big[\psi_m(x_1) \psi_n(x_2) \big]}{\partial r} \right\}^2 \mathrm{d}R. \tag{2.16}$$

Thus, the leading correction becomes $\delta E = 2 \sum_{m<n} \tilde{v}_{mn}$. It is always negative for $1/c > 0$: reducing the magnitude of interparticle repulsion decreases the energy of the ground state. After some manipulation (details are given in Section 2.6.1), we obtain a finite series expression for the energy correction:

$$\delta E = \frac{1}{c} \sqrt{\frac{2}{\pi^3}} \sum_{n=1}^{N-1} \frac{\Gamma\big(n - \frac{1}{2}\big)}{\Gamma(n+1)} \times \sum_{m=0}^{n-1} (m-n)^2 \frac{\Gamma\big(m - \frac{1}{2}\big)}{\Gamma(m+1)} \, {}_3F_2 \left[\begin{matrix} \frac{3}{2}, -m, -n \\ \frac{3}{2} - m, \frac{3}{2} - n \end{matrix} ; 1 \right]. \tag{2.17}$$

Here, ${}_3F_2 \left[\begin{smallmatrix} a_1, a_2, a_3 \\ b_1, b_2 \end{smallmatrix} ; z \right]$ is a hypergeometric function of argument z [56]. This the main result of this chapter and is exact for all values of N.

2.4 Ground state energy correction

2.4.1 Two particles

The special case of $N = 2$ particles is separable in relative ($\sqrt{2}r = x_1 - x_2$) and central ($\sqrt{2}R = x_1 + x_2$) coordinates. Therefore, the resulting eigenvalue problem for the energy spectrum is exactly solvable [39, 57] and provides an important test case for our approach. In these coordinates, the two-particle eigenvalue equation (2.8) becomes

$$E\Psi^{\mathrm{b}} = \left[-\frac{1}{2}\frac{\partial^2}{\partial R^2} + \frac{1}{2}R^2 - \frac{1}{2}\frac{\partial^2}{\partial r^2} + \frac{1}{2}r^2 + \frac{c}{\sqrt{2}}\delta(r)\right]\Psi^{\mathrm{b}}, \tag{2.18}$$

The eigenfunctions of this equation are $\Psi^{\mathrm{b}} = f_{E'}(r)\psi_n(R)$ and the corresponding eigenvalue is $E = \left(E' + n + \frac{1}{2}\right)$. Here ψ_n is a single-particle harmonic oscillator eigenfunction and the relative coordinate part of the wavefunction is [58]

$$f_{E'}(r) = \frac{1}{\mathcal{N}}\left\{M\left[\tfrac{1}{4} - \tfrac{1}{2}E', \tfrac{1}{2}; r^2\right] - \frac{c}{\sqrt{2}}\,|r|\,M\left[\tfrac{3}{4} - \tfrac{1}{2}E', \tfrac{3}{2}; r^2\right]\right\}e^{-r^2/2}. \tag{2.19}$$

The normalization factor is $\mathcal{N}$ and $M[a, b; z]$ is the confluent hypergeometric function [56].

Upon imposing vanishing boundary conditions on the two-body eigenfunction at infinity, we find that the ground state energy $E_0 = E_0' + \frac{1}{2}$ of the trapped two boson system satisfies the transcendental equation

$$\frac{2\,\Gamma\left[\frac{1}{2}(1 + E_0)\right]\tan\left[\frac{1}{2}(1 - E_0)\pi\right]}{\Gamma\left[E_0/2\right]} = -\frac{c}{\sqrt{2}}. \tag{2.20}$$

As shown in Figure 2.2 the appropriate solution of this equation gives E_0 as a smooth function of c with $E_0 \in [1, 2]$.

Substituting $N = 2$ into our perturbation formula (2.17) for the ground state energy leads to

$$E_0 = 2 - \frac{2}{c}\sqrt{\frac{2}{\pi}} + \mathcal{O}(1/c^2). \tag{2.21}$$

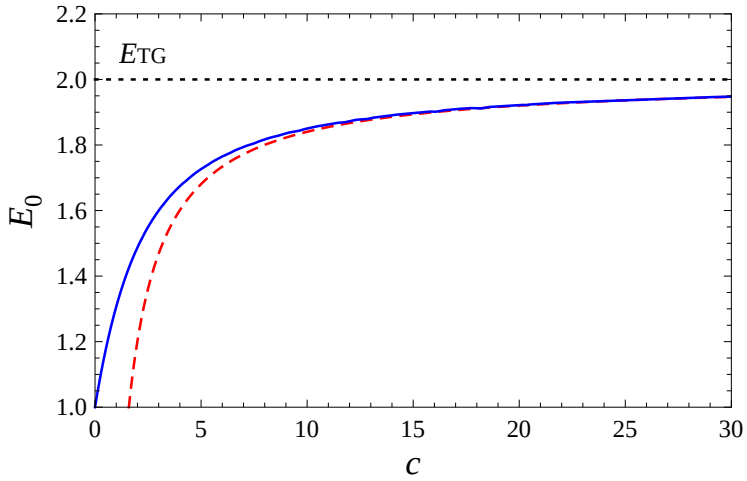

Figure 2.2: The first-order perturbation result (red dashed line) for the ground state energy of two delta-interacting bosons in a harmonic trap is compared to the exact solution (blue solid line). The ground state energy E_{TG} in the infinite repulsion limit is given by the horizontal dotted line.

This expression coincides with the leading terms of the $1/c$ series expansion of the exact solution (2.20) about the TG ground state energy $E_{\mathrm{TG}} = 2$. A comparison of the result from perturbation theory and the exact two-particle ground state energy is shown in Figure 2.2. We observe good agreement between the two results in the strongly interacting regime $c \gg 10$.

2.4.2 Large number of particles

Before discussing the situation of more than two particles, we restore energy units and rewrite the perturbed ground state energy as

$$E_0(N) = \frac{1}{2}\hbar\omega N^2\left[1 + \frac{2\alpha(N)}{c}\right] + \mathcal{O}(1/c^2). \tag{2.22}$$

Here $\alpha(N)$ is a dimensionless function of N. For values of N up to 10^3 the magnitude of the scaled first-order correction $-c\delta E(N)/N^2$ is plotted in Figure 2.3 as a function of N on a double logarithmic plot. Inspection of this graph suggests a simple power law scaling for the first-order correction with large N. In fact, the Thomas–Fermi approach leads to the conclusion that

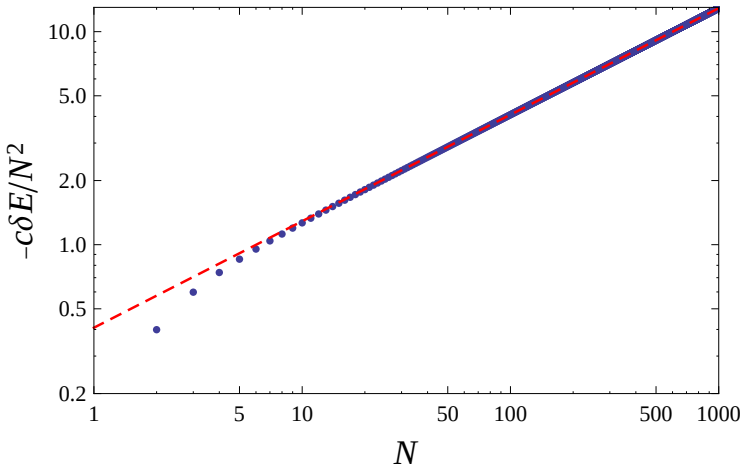

Figure 2.3: The scaled perturbation $-c\delta E/N^2$ (dots) grows as a power law $\sim \sqrt{N}$ in the thermodynamic limit $N \to \infty$. The dashed line is a regression fit $c\delta E \approx -0.408N^{5/2}$ that is calculated from values $N \in [100, 1000]$.

E_0/N^2 depends only on $\sqrt{N}/c$ as $N \to \infty$ [37]. Thus, for large $N \gg 1$ we must have $\alpha(N)/c \sim \sqrt{N}/c$ or

$$E_0(N) \approx \frac{1}{2}\hbar\omega N^2\left[1 + 2\alpha_0\frac{\sqrt{N}}{c}\right], \quad N \to \infty, \tag{2.23}$$

where α_0 is a constant number. Indeed, for as few as $N \gtrsim 15$ particles the factor $\alpha(N)$ is quite well approximated (within 1%) by the function $\alpha_0\sqrt{N}$ with $\alpha_0 \approx -0.408$. In other words, the correction factor $\alpha(N)$ reaches its asymptotic scaling behavior for systems with a small number of atoms $N > \mathcal{O}(10^1)$.

To obtain a thermodynamic limit with an extensive ground state energy (scaling linearly with N), we observe that we must require the trapping frequency ω to vanish as $1/N$ in addition to sending the number of particles to infinity. That is, imposing $\omega \sim 1/N$ as N tends to infinity implies that the ground state energy becomes proportional to the number of particles. This scaling requirement means that the quantity $\ell/\sqrt{N}$ approaches a constant in the thermodynamic limit ($\ell \sim \sqrt{N}$ as $N \to \infty$). This behavior is in contrast to the thermodynamic limit of a Lieb–Liniger gas confined in a flat-bottomed box, in which the linear dimension of the longitudinal trap is taken to scale propor-

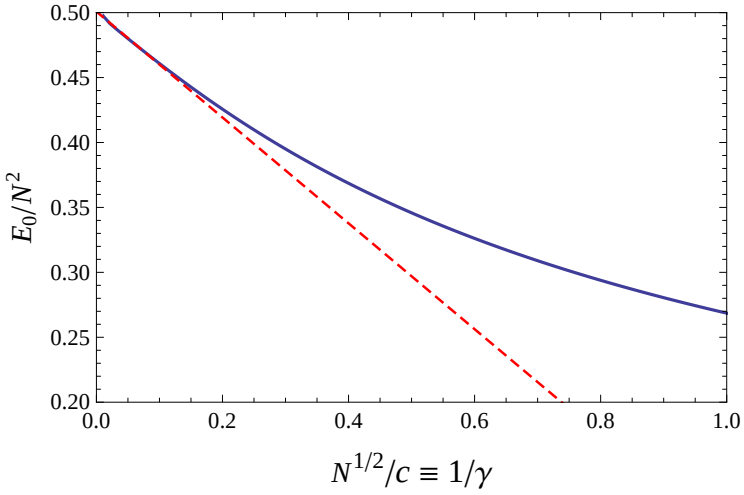

Figure 2.4: For large N the asymptotic formula $c\delta E \approx -0.408N^{5/2}$ (dashed line) reproduces numerical calculations in the Thomas–Fermi approximation (solid line) near the Tonks–Girardeau limit.

tionally with particle number [47]. Looking back at our asymptotic expression $\alpha(N) \approx \alpha_0\sqrt{N}$, we find that the quantity $\sqrt{N}/c$ approaches a constant value as $N \to \infty$ in our prescribed thermodynamic limit. This is precisely the condition used by Ma and Yang [36, 37] to obtain the ground state energy of the harmonically trapped interacting boson gas in the Thomas–Fermi formalism.

A comparison of our asymptotic perturbation formula (2.23) with the Thomas–Fermi result is given in Figure 2.4 (Section 2.6.2). Our formula essentially gives the leading order terms of the $\sqrt{N}/c$ power series expansion of the ground state energy of the trapped gas about the TG limit. We find that our first-order $1/c$ result is reliable for $\sqrt{N}/c \lesssim 0.1$. This means that for a typical experimental setup with hundreds of atoms first-order perturbation theory and the Thomas–Fermi result coincide only in the extreme repulsion limit $c \gtrsim 10^2$.

If we now define the chemical potential in the impenetrable Tonks–Girardeau limit as $\mu_{\mathrm{TG}} \equiv \lim_{N\to\infty,\,\omega\to 0} \hbar\omega N$ and the scaled interaction parameter as $\gamma \equiv \lim_{N\to\infty,\,\omega\to 0} c/\sqrt{N}$, we obtain the zero temperature chemical potential

$$\mu = \frac{\partial E_0}{\partial N} \approx \mu_{\mathrm{TG}}\left[1 + \frac{5}{2}\frac{\alpha_0}{\gamma}\right] = \mu_{\mathrm{TG}}\left[1 - \frac{5}{2}\frac{0.408}{\gamma}\right]. \tag{2.24}$$

The first term in this expression corresponds to the chemical potential of free fermions in a one-dimensional harmonic trap while the second term gives the reduction in the chemical potential due to the finite repulsion correction. It is a measure of the departure of the system from the Tonks–Girardeau limit.

2.5 Concluding remarks

In this chapter we have calculated the first-order finite repulsion correction to the ground state energy of harmonically trapped bosons having contact interactions for any finite number of particles N. For $N \gg \mathcal{O}(10^1)$ we found that this correction scales as a power law $N^{5/2}$ for any given interaction strength. In addition to this result, we describe a limiting procedure ($\omega \sim 1/N$ as $N \to \infty$) that enforces an extensive ground state energy. This extensivity condition is necessary for the thermodynamics assumptions of the Thomas–Fermi approach to hold. This procedure explains the importance of the parameter $\sqrt{N}/c$ in the Thomas–Fermi solution and why it is taken constant in the thermodynamic limit $N \to \infty$.

Additionally, our contribution clarifies the smooth transition of the ground state properties of a harmonically confined interacting boson system as the particle number goes from finite N to infinity near the Tonks–Girardeau limit. We have demonstrated that in this strongly interacting regime, to at least leading order in $1/c$, the effects of finite particle number are negligible when using the Thomas–Fermi approximation in experimental situations that have at least $\sim 10^2$ atoms.

A natural extension of this work would involve higher order corrections to the ground state energy and many-body wavefunction, as was done recently for a wedge-shaped trapping potential [48]. If we take the set of all fermionic Slater determinants as an expansion basis for ordinary perturbation theory about the TG limit, we discover that the perturbing pseudopotential couples the ground state to an infinite number of excited states. We therefore expect a complicated analytical result for the second order energy correction resulting in a numerical problem that may require a truncation of the corresponding Hilbert space. However, on the basis of the agreement between our asymptotic

results and the Thomas–Fermi calculation (Figure 2.4), we conjecture that the second order correction scales as $N^3/c^2 > 0$ in the thermodynamic limit. Mathematically, this statement amounts to a power series expansion of E_0/N^2 about $\sqrt{N}/c = 0^+$.

2.6 Derivations

2.6.1 Pair interactions

We calculate here the matrix element for the pair interaction

$$\tilde{v}_{mn} = v_{mnmn} = -\frac{4}{c}\int \lim_{r\to 0}\left\{\frac{\partial\big[\psi_m(x_1)\psi_n(x_2)\big]}{\partial r}\right\}^2 \mathrm{d}R, \quad m < n, \tag{2.25}$$

where $x_1 = R + \frac{1}{2}r$ and $x_2 = R - \frac{1}{2}r$. The condition $0 \le m < n$ is assumed throughout the derivation below. With the abbreviation for the integrand

$$I_{mn}(R) \equiv \lim_{r\to 0}\frac{\partial\big[\psi_m(x_1)\psi_n(x_2)\big]}{\partial r}, \tag{2.26}$$

we observe that

$$\begin{aligned} I_{mn} &= \lim_{r\to 0}\frac{\partial}{\partial r}\Big[\psi_m(R+\tfrac{1}{2}r)\psi_n(R-\tfrac{1}{2}r)\Big] \\ &= \frac{1}{2}\lim_{r=0}\big[\psi_m'(R+\tfrac{1}{2}r)\psi_n(R-\tfrac{1}{2}r) - \psi_m(R+\tfrac{1}{2}r)\psi_n'(R-\tfrac{1}{2}r)\big] \\ &= \frac{1}{2}\big[\psi_m'(R)\psi_n(R) - \psi_m(R)\psi_n'(R)\big] = -I_{nm}. \end{aligned} \tag{2.27}$$

We can calculate the necessary derivatives by using the identity

$$\psi_n' = \frac{1}{\sqrt{2}}\big[\sqrt{n}\psi_{n-1} - \sqrt{n+1}\psi_{n+1}\big], \tag{2.28}$$

to obtain

$$I_{mn} = \frac{\sqrt{2}}{4}\big[\big(\sqrt{m}\psi_{m-1} - \sqrt{m+1}\psi_{m+1}\big)\psi_n - \psi_m\big(\sqrt{n}\psi_{n-1} - \sqrt{n+1}\psi_{n+1}\big)\big]. \tag{2.29}$$

Each product of harmonic oscillator eigenfunctions may be written in the form

$$\begin{aligned}\psi_m(R)\psi_n(R) &= \frac{e^{-R^2}}{\sqrt{\pi 2^{m+n}m!n!}}\,H_m(R)H_n(R)\\ &= \frac{e^{-R^2}}{\sqrt{\pi 2^{m+n}m!n!}}\sum_{k=0}^{\min\{m,n\}} 2^k k!\binom{m}{k}\binom{n}{k}H_{m+n-2k}(R). \qquad (2.30)\end{aligned}$$

We make the abbreviation $C_{mn} = e^{-R^2}/\sqrt{\pi 2^{m+n}m!n!}$ for convenience and write

$$\sqrt{m}\psi_{m-1}\psi_n = \sqrt{2}C_{mn}m\sum_{k=0}^{m-1} 2^k k!\binom{m-1}{k}\binom{n}{k}H_{m+n-2k-1} \qquad (2.31)$$

$$\sqrt{m+1}\psi_{m+1}\psi_n = \frac{C_{mn}}{\sqrt{2}}\sum_{k=0}^{m+1} 2^k k!\binom{m+1}{k}\binom{n}{k}H_{m+n-2k+1} \qquad (2.32)$$

$$\sqrt{n}\psi_m\psi_{n-1} = \sqrt{2}C_{mn}n\sum_{k=0}^{m} 2^k k!\binom{m}{k}\binom{n-1}{k}H_{m+n-2k-1} \qquad (2.33)$$

$$\sqrt{n+1}\psi_m\psi_{n+1} = \frac{C_{mn}}{\sqrt{2}}\sum_{k=0}^{m} 2^k k!\binom{m}{k}\binom{n+1}{k}H_{m+n-2k+1}. \qquad (2.34)$$

Combining these terms gives, after some manipulation,

$$\sqrt{m}\psi_{m-1}\psi_n - \sqrt{n}\psi_m\psi_{n-1} = \sqrt{2}C_{mn}(m-n)\sum_{k=0}^{m} 2^k k!\binom{m}{k}\binom{n}{k}H_{m+n-2k-1}, \qquad (2.35)$$

and

$$\begin{aligned}\sqrt{n+1}\psi_m\psi_{n+1} - \sqrt{m+1}\psi_{m+1}\psi_n &= \frac{C_{mn}(m-n)}{\sqrt{2}}\sum_{k=1}^{m+1} 2^k k!\binom{m+1}{k}\binom{n+1}{k}\\ &\quad\times\frac{k}{(m+1)(n+1)}\,H_{m+n-2k+1}\\ &= \sqrt{2}C_{mn}(m-n)\\ &\quad\times\sum_{k=0}^{m} 2^k k!\binom{m}{k}\binom{n}{k}H_{m+n-2k-1}. \qquad (2.36)\end{aligned}$$

Thus,

$$I_{mn} = C_{mn}(m-n)\sum_{k=0}^{m} 2^k k! \binom{m}{k}\binom{n}{k} H_{m+n-2k-1}, \tag{2.37}$$

$$I_{mn}^2 = C_{mn}^2 (m-n)^2 \sum_{k,l=0}^{m} 2^{k+l} k!l! \binom{m}{k}\binom{n}{k}\binom{m}{l}\binom{n}{l} H_{m+n-2k-1} H_{m+n-2l-1}. \tag{2.38}$$

Evaluating the matrix element $\tilde{v}_{mn}$ therefore requires the integration of a product of Hermite polynomials and a Gaussian weighting factor. Using the formula 7.374.5 from Ref. [59] gives

$$\int_{-\infty}^{\infty} e^{-2R^2} H_p(R) H_q(R)\,\mathrm{d}R = (-1)^{(p+3q)/2} 2^{(p+q-1)/2} \Gamma\left(\frac{p+q+1}{2}\right), \tag{2.39}$$

where $p+q = 2, 4, \ldots$. Now, with $0 \le k, l \le m < n$,

$$\int_{-\infty}^{\infty} e^{-2R^2} H_{m+n-2k-1}(R) H_{m+n-2l-1}(R)\,\mathrm{d}R = \frac{(-1)^{k+l} 2^{m+n-k-l}}{2\sqrt{2}} \Gamma\big(m+n-k-l-\tfrac{1}{2}\big). \tag{2.40}$$

Making the necessary substitutions gives

$$\begin{aligned}\tilde{v}_{mn} &= -\frac{\sqrt{2}(m-n)^2}{c\pi m! n!} \sum_{k,l=0}^{m} (-1)^{k+l} k!l! \binom{m}{k}\binom{n}{k}\binom{m}{l}\binom{n}{l} \Gamma\big(m+n-k-l-\tfrac{1}{2}\big), \\ &= \frac{(m-n)^2}{2c} \sqrt{\frac{2}{\pi^3}} \frac{\Gamma\big(n-\frac{1}{2}\big)\Gamma\big(m-\frac{1}{2}\big)}{\Gamma(n+1)\Gamma(m+1)}\, {}_3F_2\left[\begin{matrix}\frac{3}{2}, -m, -n \\ \frac{3}{2}-m, \frac{3}{2}-n\end{matrix}; 1\right].\end{aligned} \tag{2.41}$$

The energy correction (2.17) follows immediately from this result through $\delta E = 2\sum_{m<n} \tilde{v}_{mn}$.

2.6.2 Thomas–Fermi approach

In this section we present the Thomas–Fermi (TF) result for the ground state energy of the harmonically confined Lieb–Liniger (LL) gas, following closely

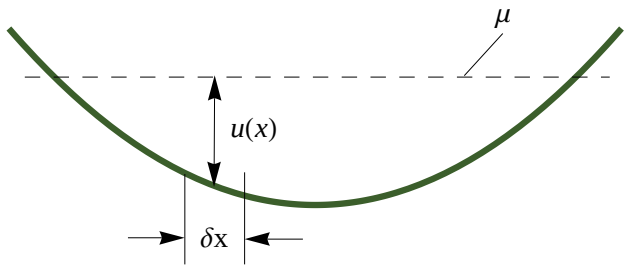

Figure 2.5: In the Thomas–Fermi approach, the external trapping potential modifies the local chemical potential of a homogeneous Lieb–Liniger gas of constant density.

the solution of Refs. [36, 37]. As the number of bosons tend to infinity $N \to \infty$ in the thermodynamic limit, the energy density $e(x)$ and number density $d(x)$ of the gas are described by continuous functions of the position coordinate x. In the TF approach, a small portion of the gas of width δx centered at the point x is thermodynamically described by a homogeneous LL gas with a uniform density $d(x)$ and at a constant local chemical potential $u(x)$ (Figure 2.5).

The ground state energy density $e(x)$ of a homogeneous LL gas of length δx and density $d(x) = \delta N/\delta x$ is [8, 36, 60]

$$e(x) = c^3 \beta \zeta(\beta), \quad \beta \equiv d(x)/c, \tag{2.42}$$

where the function $\zeta(\beta)$ is equal to

$$\zeta(\beta) = \frac{1}{\beta\sigma^3} \int_{-1}^{1} g(k) k^2 \, \mathrm{d}k. \tag{2.43}$$

Here, $g(k)$ is a quasimomentum distribution that solves the Lieb–Liniger integral equation

$$1 + 2\sigma \int_{-1}^{1} \frac{g(k') \, \mathrm{d}k'}{\sigma^2 + (k - k')^2} = 2\pi g(k), \tag{2.44}$$

subject to the normalization condition

$$\sigma = \frac{1}{\beta}\int_{-1}^{1} g(k)\,\mathrm{d}k. \tag{2.45}$$

The Lieb–Liniger equation (2.44) is the continuum analog of the Bethe equations (3.10) for the quasimomentum spectrum of the Lieb–Liniger ground state. This gas of width δx is assumed to be a thermodynamic system so that the fundamental equation holds:

$$\mathrm{d}\big(e(x)\delta x\big) = -p(x)\mathrm{d}(\delta x) + u(x)\mathrm{d}(\delta N). \tag{2.46}$$

The local equations of state are therefore

$$p(x) = cd(x)^2\zeta'(\beta), \qquad u(x) = c^2\zeta(\beta) + cd(x)\zeta'(\beta), \tag{2.47}$$

with $\zeta'(\beta) = \partial\zeta/\partial\beta$.

The Thomas–Fermi energy functional for the trapped gas is

$$E[d(x)] = \int_{-x_{\max}}^{x_{\max}} e(x) + \tfrac{1}{2}d(x)x^2\,\mathrm{d}x. \tag{2.48}$$

To obtain the equilibrium ground state energy, a variational calculation leads to the conditions $\mu = \frac{1}{2}x^2 + u_0(x)$ or

$$\mu = \tfrac{1}{2}x^2 + c^2\zeta(\beta_0) + cd_0(x)\zeta'(\beta_0), \tag{2.49}$$

where the global chemical potential μ is fixed by the constraint

$$N = \int_{-x_{\max}}^{x_{\max}} d_0(x)\,\mathrm{d}x. \tag{2.50}$$

The previous relations are sufficient to determine the ground state density function $d_0(x)$. The ground state energy of the harmonically trapped gas $E_0[d_0(x)]$ can then be calculated numerically from the definite integral (2.48). This Thomas–Fermi result is graphed alongside our perturbative result in Figure 2.4.

Chapter 3

Entanglement in pure state projections of the Lieb–Liniger gas

The contents of this chapter are based on the manuscript [**II**].

3.1 Entanglement

Entanglement refers to the inherently quantum correlations present in a quantum system. These quantum correlations are distinct from correlations between classical random variables. For example, two spin-1/2 particles in a singlet state $\big(|\uparrow\downarrow\rangle - |\downarrow\uparrow\rangle\big)/\sqrt{2}$ are entangled. This state is a superposition of orthogonal states where the particles have different spin projections. If the particles are separated in space and the spin projection of one is measured, the spin projection of the other particle is completely determined to be in the opposite direction. This kind of correlation between quantum observables is not present in a system described by classical random variables. This is so because joint classical probability distribution functions do not obey a superposition principle, whereas quantum mechanical wavefunctions do.

Studies of quantum entanglement and its measures are motivated by the idea that entanglement is a valuable resource for processing quantum informa-

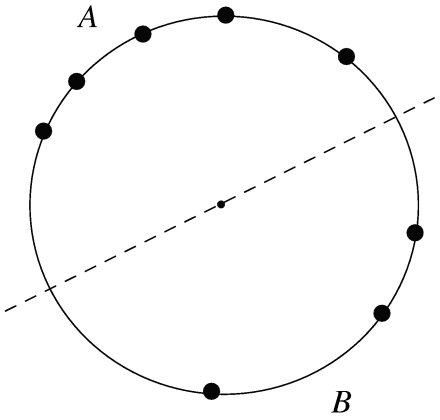

Figure 3.1: A coarse-grained measurement on region A determines the number of particles in A. The resulting pure state is spatially partitioned. The bipartite entanglement in this state may be measured by the entanglement entropy.

tion [61]. Additionally, there is much interest in the condensed matter community in the quantification of entanglement in many-body quantum systems [62, 63]. In addition to being a measure of quantum correlations, this interest also follows from the fact that certain signatures in the entanglement entropy are robust indicators of quantum phase transitions [64–68] and topological order [69, 70]. Furthermore, experimental protocols for the measurement of entanglement entropy have already been proposed using available techniques such as neutron scattering (for spin systems) and time-of-flight optical imaging (for cold atom systems) [71].

In this chapter we will study the entanglement that can be extracted from bipartite projections of the ground state of the homogeneous repulsive Lieb–Liniger model on a ring [8, 9]. As discussed in the previous chapter, the quasi one-dimensional gases modeled by the Lieb–Liniger interaction have been studied in atomic waveguides with tight axial (transverse) confinement [16, 18, 19]. However, the ring-shaped traps needed to reproduce periodic boundary conditions have only been recently developed [72, 73].

The main objective of our work here is to study the effects of the strength

of interactions on the entanglement in pure state projections of the ground state of this continuous many-body system. The specific type of projection we consider here is a coarse-grained measurement of the number of particles in a contiguous spatial partition (region A) of the ground state, which we respresent by the state vector $|\chi\rangle$. That is, if Π_k is a projector onto the state subspace having k particles in partition A, then we are interested in the entanglement present in the projected state $|\chi_{AB}(k)\rangle = \Pi_k|\chi\rangle$. As depicted in Figure 3.1, this measurement effectively fixes the number of particles in region A and its complement, region B. Thus, this measurement destroys the translational invariance of the ground state. Since the projected state $|\chi_{AB}(k)\rangle$ is a pure state, entanglement in this system may be quantified by the von Neumann entropy [62, 74–78]

$$S_A(k) \equiv -\operatorname{tr}[\rho_A(k)\log\rho_A(k)]. \tag{3.1}$$

Here $\rho_A(k)$ is the reduced density matrix

$$\rho_A(k) \equiv \operatorname{tr}_B \rho_{AB}(k) = \operatorname{tr}_B |\chi_{AB}(k)\rangle\langle\chi_{AB}(k)|, \tag{3.2}$$

which is obtained by tracing out the degrees of freedom (particle coordinates) in region B from the full density matrix of the projected state $\rho_{AB}(k)$. The von Neumann entropy (3.1) vanishes when the bipartite pure state ρ_{AB} is unentangled. That is, it is zero when the reduced density matrix ρ_A has only one non-zero eigenvalue (the reduced state is pure). On the other hand, the von Neumann entropy is maximum when ρ_{AB} is maximally entangled. This is the case when a rank D reduced density matrix ρ_A has all eigenvalues equal to $1/D$ (the reduced state is maximally mixed). Hence, the von Neumann entropy of a maximally entangled state is equal to $\log D$.

3.1.1 Partitioning schemes

For a system made up of indistinguishable particles, the choice of partitioning scheme has important consequences on the physical interpretation of the resulting entanglement entropy [79–81]. For example, in previous work the entanglement entropy in other continuous integrable systems, like the Calogero–

Sutherland (CS) model [82, 83] and the anyonic Lieb–Liniger (LL) model [84, 85], has been studied under the framework of particle partitioning. In this strategy, the reduced density matrix is obtained by integrating out one or more particle coordinates from the many-body wavefunction [86–90]. The entanglement entropy resulting from this type of partitioning may be interpreted as a measure of the distribution of occupation numbers of (quasi)momentum orbitals in the reduced state. For example, in the Calogero–Sutherland model the entanglement entropy as a function of the coupling parameter β was physically interpreted in terms of the fractional exclusion statistics [91] displayed by the model [92].[1] In the case of the anyonic Lieb–Liniger model, the entanglement entropy was obtained from the one-particle reduced density matrix (periodic boundaries)

$$\rho(x - x') = \int \cdots \int \chi^*(x, x_2, \ldots, x_N)\chi^*(x', x_2, \ldots, x_N)\, \mathrm{d}x_2 \cdots \mathrm{d}x_N, \qquad (3.3)$$

where integrations are done over the circumference of the ring. The entanglement entropy calculated from the eigenvalues of this matrix was interpreted as a measure of the uncertainty in assigning a momentum state to a single particle [93, 94]. The momentum distribution obtained from this one-particle reduced density matrix depends on the anyon statistics parameter, which reflects the breaking of parity symmetry in the anyonic LL model.

However, because the projective measurements described in the previous section divide the gas into spatially distinguished regions, we use a spatial partitioning scheme in this chapter. This scheme has been used to study entanglement in one-dimensional translationally invariant systems. For critical (gapless) systems, the entanglement entropy obtained under spatial partitioning has the same scaling behavior with partition size $\ell \to \infty$ as the particle number fluctuations within the partition [95–98]. The physical intuition behind this observation involves the critical role played by the boundary separating A and B in the definitions of the entanglement entropy [63, 99, 100] and the observation that particles enter and exit the partition through these bound-

[1] The N-particle ground state of the CS model has N occupied quasimomentum vacancies separated by $\beta - 1$ unoccupied vacancies.

aries. This idea has since been developed as an argument for using number fluctuations as an entanglement probe in continuous many-body systems like the non-interacting spin-polarized fermion gas [101–103] and various quantum spin models [104, 105]. For the continuous fermion gas, the entanglement entropy may also be obtained [102] as the appropriate limit of the corresponding lattice model results [106–112].

3.1.2 Projectively extractable entanglement

The projective measurements we consider here fix the particle number within each spatial partition. The resulting entanglement therefore does not include correlations that arise from the possible number distributions of particles between partitions (if there are k bosons in region A, there must be $(N-k)$ bosons in region B). That is, the projective measurements described here allow us to effectively isolate the quantum correlations that are due solely to interparticle interactions. We will show in this chapter that this measure of entanglement increases monotonically with increasing repulsion strength in the Lieb–Liniger gas.

Our objective is accomplished here by using the coordinate Bethe ansatz (Section 3.2) to obtain exact results for small particle numbers N. Some asymptotic results for large N are also calculated at the non-interacting boson limit ($c = 0$) and Tonks–Girardeau limit ($c \to \infty$). In particular, we are interested in measuring the entanglement in the Lieb–Liniger ground state after coarse-grained measurements reveal the number of particles in either partition A or B. Thus, the projected pure state is spatially partitioned (bipartite) and one can quantify the resulting entanglement by the von Neumann entropy (3.1). A similar procedure has been used to quantify the entanglement that is extractable from stationary and non-stationary states of impenetrable boson gases [113], supersinglet states, and several spin chains [114]. Entanglement in the ensemble of projected states is measured in these examples by the projectively extractable pure state entanglement $\mathcal{E}_{PP}$, which was introduced in these

works. It is defined by

$$\mathcal{E}_{PP} \equiv \max_k \{p(k)S_A(k)\} \equiv \max_k \{\mathcal{E}_k\}, \tag{3.4}$$

where $p(k)$ is the probability of projecting the ground state ket $|\chi\rangle$ into a state ket $|\chi_{AB}(k)\rangle$ having the fraction k/N of particles in region A. The entanglement measure above (3.4) gives the maximum weighted entanglement $\mathcal{E}_k \equiv p(k)S_A(k)$ over all possible projection outcomes and consequently captures the probabilistic nature of the preparatory projective measurements. It is identical in spirit to the entanglement of particles E_P introduced in Ref. [79] where the weighted sum over outcomes is used as an entanglement measure rather than the maximum weighted entanglement:

$$E_P = \sum_{k=0}^{N} p(k)S_A(k). \tag{3.5}$$

This quantity was proposed to reflect the maximum entanglement that can be extracted from a system of indistinguishable particles when local number conservation rules (superselection rules [115, 116]) restrict the possible operations that can be done on the subsystems. Imposing such a superselection rule is motivated experimentally. For a closed system of massive particles, any local measurement in region A can not change the particle number in region A without changing the particle number in region B.

3.1.3 Chapter outline

Our analysis begins in Section 3.2 with a brief introduction to the coordinate Bethe ansatz that forms the basis of our exact computations. The probability of obtaining each projection outcome is calculated in Section 3.3, while the von Neumann entropy of the projected states are given in Section 3.4. The corresponding weighted entanglement of these projections is discussed in Section 3.5. On the basis of these results, we argue that the projectively extractable pure state entanglement $\mathcal{E}_{PP}$ is equal to the weighted entanglement $\mathcal{E}_{N/2}$ of the balanced case in which exactly half of the bosons are present in

both partitions (the total number N is given to be even). Our main conclusion is that the extractable entanglement $\mathcal{E}_{PP}$ increases monotonically with interaction strength and saturates to its impenetrable boson value. We conclude with a summary and some remarks in Section 3.6.

3.2 Coordinate Bethe ansatz

We briefly review here some of the properties of the Bethe ansatz solution for the eigenfunctions of the Lieb–Liniger model (2.1). Written in dimensionless form (length is measured in units of the ring circumference L and energy in natural units $\hbar^2/2mL^2$), the Schrödinger equation for N delta-interacting bosons is

$$H\chi(\mathbf{x}) = \left[-\sum_{j=1}^{N}\frac{\partial^2}{\partial x_j^2} + 2c\sum_{1\le k<j\le N}\delta(x_j - x_k)\right]\chi(\mathbf{x}). \tag{3.6}$$

The dimensionless interaction constant is taken to be non-negative $c \geq 0$ so that the gas does not collapse into a macroscopic bound state involving all of the bosons. The stationary solutions of this hamiltonian are given by the normalized coordinate Bethe ansatz

$$\chi(\mathbf{x}) = \frac{1}{\mathcal{N}}\sum_{\{\mathcal{P}\}}^{N!}(-1)^{[\mathcal{P}]}F_{\mathcal{P}}(\mathbf{x})e^{i\boldsymbol{\lambda}_{\mathcal{P}}\cdot\mathbf{x}}, \tag{3.7}$$

$$F_{\mathcal{P}}(\mathbf{x}) \equiv \frac{\prod_{l<j}\lambda_{\mathcal{P}j} - \lambda_{\mathcal{P}l} - ic\,\mathrm{sgn}(x_j - x_l)}{\left\{N!\prod_{n<m}\left[(\lambda_m - \lambda_n)^2 + c^2\right]\right\}^{1/2}}. \tag{3.8}$$

The quantity $(-1)^{[\mathcal{P}]}$ is the signature of the permutation $\mathcal{P}$ and $\mathcal{N}$ is a normalization factor. The quasimomentum vector $\boldsymbol{\lambda}_{\mathcal{P}}$ has N components $\lambda_{\mathcal{P}j}$ that form a permutation $\mathcal{P}$ of the solutions λ_j of the Bethe equations

$$e^{i\lambda_j} = -\prod_{k=1}^{N}\frac{\lambda_j - \lambda_k + ic}{\lambda_j - \lambda_k - ic}. \tag{3.9}$$

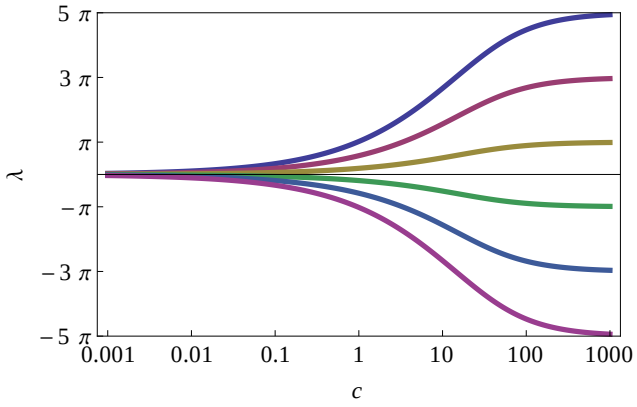

Figure 3.2: Ground state solution to the Bethe equations for six bosons as a function of interaction strength c.

With periodic boundary conditions, these equations are commonly expressed in the logarithmic form

$$L\lambda_j + i\sum_{k=1}^{N} \log \frac{ic + \lambda_j - \lambda_k}{ic - \lambda_j + \lambda_k} = 2\pi n_j, \tag{3.10}$$

where $\{n_j\}$ is a set of integers or half odd integers that completely parametrize the solutions $\{\lambda_j\}$. The set $\{\lambda_j\}$ consists of N quasimomenta (or spectral parameters). Such a set labels a given eigenstate of the hamiltonian (3.6). The total momentum of this eigenstate is $P = \sum_j \lambda_j$ and its energy eigenvalue is $E = \sum_j \lambda_j^2$. For example, the ground state of six interacting bosons is labeled by the quasimomenta given in Figure 3.2. There is a smooth transition from the Bose condensate spectrum at the non-interacting limit $c = 0$ to the free-fermionic spectrum at the Tonks–Girardeau limit $c \to \infty$. For any positive interaction strength $c > 0$ an exclusion principle holds [117], which means that the N quasimomenta labeling an eigenstate are distinct. As seen in Figure 3.2, the spacing between adjacent quasimomenta in the ground state increases monotonically with c until it saturates to the free-fermionic value of 2π.

The normalization factor $\mathcal{N}$ in the ansatz (3.7) may be obtained, for example, by the quantum inverse scattering method [118]. Explicitly, the absolute square $|\mathcal{N}|^2$ is the determinant of the second derivatives of the Yang action

[13]

$$\mathcal{S} = \frac{L}{2}\sum_{j=1}^{N}\lambda_j^2 - 2\pi\sum_{j=1}^{N}n_j\lambda_j + \frac{1}{2}\sum_{jk}^{N}\int_0^{\lambda_j-\lambda_k} i\log\frac{ic+\mu}{ic-\mu}\,\mathrm{d}\mu, \tag{3.11}$$

evaluated at the solutions of the Bethe equations (3.9):

$$\begin{aligned}|\mathcal{N}|^2 &= \det\left(\frac{\partial^2\mathcal{S}}{\partial\lambda_j\partial\lambda_k}\right)\\ &= \det\left(\delta_{jk} + \sum_{l=1}^{N}\frac{2c\delta_{jk}}{(\lambda_k-\lambda_l)^2+c^2} - \frac{2c}{(\lambda_j-\lambda_k)^2+c^2}\right).\end{aligned} \tag{3.12}$$

3.3 Projection probabilities

In this section we are interested in calculating the probability $p(k)$ of projecting the ground state χ into the pure state $\chi_{AB}(k)$ that has k bosons in partition A and $N-k$ bosons in partition B. We choose the partitions to be the same size so that the gas is divided into two contiguous regions of equal length. For convenience let us define the vectors $\mathbf{x}_A \equiv (x_1,\ldots,x_k)^\mathsf{T}$ and $\mathbf{x}_B \equiv (x_{k+1},\ldots,x_N)^\mathsf{T}$. Since the bosonic wavefunction $\chi(\mathbf{x})$ is unchanged by any permutation of coordinate indices, the desired projection probability is

$$p(k) = \binom{N}{k}\int_A\int_B |\chi(\mathbf{x})|^2\,\mathrm{d}\mathbf{x}_B\mathrm{d}\mathbf{x}_A. \tag{3.13}$$

Due to the periodicity of the ground state wavefunction we may choose the partitions to be $A = \{x|0 \le x \le \frac{1}{2}\}$ and $B = \{x|\frac{1}{2} \le x \le 1\}$ without loss of generality.

We first consider in Section 3.3.1 the probability of obtaining a projected state with an equal number of bosons in each partition (balanced case with $k = N/2$). It turns out that this balanced case is the most probable result of the local projective measurements of particle number for all interaction strengths c (Section 3.3.2).

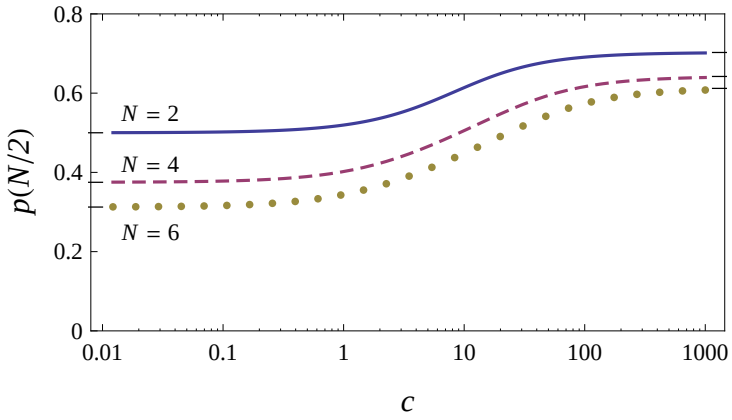

Figure 3.3: The probability of finding an equal number of particles in each half-ring A and B in the Lieb–Liniger ground state increases monotonically with repulsion strength and decreases with particle number. Black tick marks denote the free and impenetrable limit values.

3.3.1 Balanced projection

Figure 3.3 shows the probability of projection onto the balanced $k = N/2$ bipartite states for two, four, and six bosons at arbitrary repulsion strengths. For free bosons ($c = 0$) this probability is equal to

$$p^{\text{free}}(N/2) = \frac{N!}{2^N (N/2)!^2}. \tag{3.14}$$

The asymptotic Stirling approximation for $N!$ shows that this probability vanishes as $\sim\sqrt{2/(\pi N)}$ in the thermodynamic limit $N \to \infty$ (Figure 3.4). This is the expected result because each independent particle may be found in either half-ring with equal probability.

As the interparticle repulsion is turned on, however, correlations arise between the positions of the bosons and the corresponding success probability deviates from the free boson value. These quantum correlations give rise to fluctuations in the number of particles in each partition that result in the probability $p(N/2)$ increasing with repulsion strength c. In the limiting case $c \to \infty$ of impenetrable bosons (TG limit) this probability reduces to the analogous projection probability in a free spin-polarized fermion gas [49]. The charac-

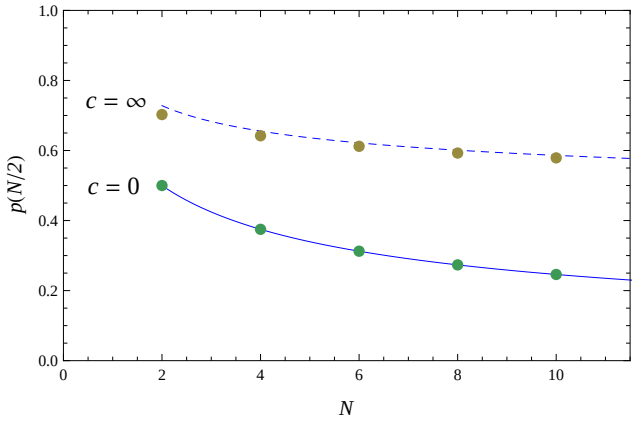

Figure 3.4: Balanced projection probabilities for the free boson ($c = 0$) and impenetrable boson ($c \to \infty$) cases. Our numerical values (dots) are compared to the exact result for free bosons (solid line) and the asymptotic result Eq. (3.15) for impenetrable bosons (dashed line).

teristic function of this probability distribution of particle numbers in finite regions of an infinite line [119, 120] and a ring [121] are known. We find that a Gaussian approximation (details are given in Section 3.7) to the probability distribution $p^{\mathrm{TG}}(k)$ asymptotically yields a balanced projection probability of

$$p^{\mathrm{TG}}(N/2) \sim \sqrt{\frac{\pi}{2\log(2Ne^{\gamma_{\mathrm{E}}+1})}}, \qquad (N \gg 1). \tag{3.15}$$

Here γ_{E} is Euler's constant. As shown in Figure 3.4, this projection probability decays to zero much slower (sublogarithmically) than the analogous probability in the free boson case in the limit of large particle number $N \to \infty$.

3.3.2 Unbalanced projections

For general values of k, the projection probabilities in the free boson limit are equal to

$$p^{\mathrm{free}}(k) = \frac{N!}{2^N k!(N-k)!}, \tag{3.16}$$

which is centered and peaked at $k = N/2$. For an arbitrary value of the interaction strength, the projection probability satisfies the property $p(k) = p(N-k)$ because the regions A and B are of the same size.

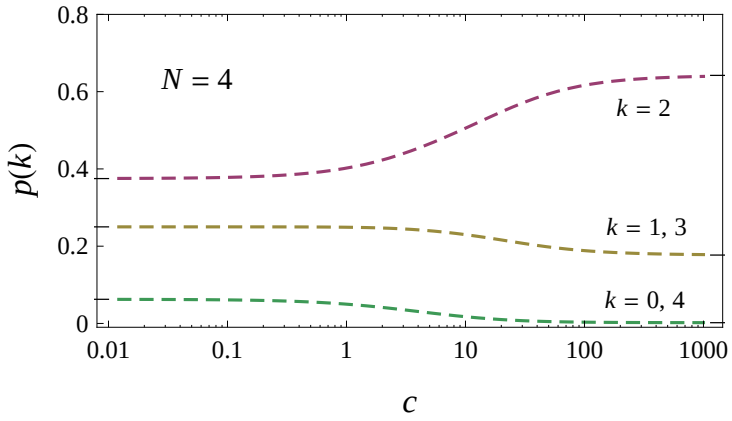

Figure 3.5: With $N = 4$ bosons the balanced case $k = 2$ is the most probable situation for all repulsion strengths. Black tick marks denote the free and impenetrable limit values.

In the impenetrable boson limit, a direct calculation from Eq. (3.13) gives the exact projection probabilities for small N. For two impenetrable bosons we have

$$p^{\mathrm{TG}}(1) = \frac{1}{2} + \frac{2}{\pi^2}, \tag{3.17}$$

$$p^{\mathrm{TG}}(0) = p^{\mathrm{TG}}_{AB}(2) = \frac{1}{4} - \frac{1}{\pi^2}, \qquad (N = 2) \tag{3.18}$$

while for four particles we have

$$p^{\mathrm{TG}}(2) = \frac{3}{8} + \frac{14}{9\pi^2} + \frac{32}{3\pi^4}, \tag{3.19}$$

$$p^{\mathrm{TG}}(1) = p^{\mathrm{TG}}(3) = \frac{1}{4} - \frac{64}{9\pi^4}, \tag{3.20}$$

$$p^{\mathrm{TG}}(0) = p^{\mathrm{TG}}(4) = \frac{1}{16} - \frac{7}{9\pi^2} + \frac{16}{9\pi^4}, \qquad (N = 4). \tag{3.21}$$

Finally, the corresponding probabilities for six particles are

$$p^{\mathrm{TG}}(3) = \frac{5}{16} + \frac{403}{300\pi^2} + \frac{5824}{675\pi^4} + \frac{262144}{3645\pi^6}, \tag{3.22}$$

$$p^{\mathrm{TG}}(2) = p^{\mathrm{TG}}(4) = \frac{15}{64} + \frac{403}{1200\pi^2} - \frac{1456}{675\pi^4} - \frac{65536}{1215\pi^6}, \tag{3.23}$$

$$p^{\mathrm{TG}}(1) = p^{\mathrm{TG}}(5) = \frac{3}{32} - \frac{403}{600\pi^2} - \frac{2912}{675\pi^4} + \frac{131072}{6075\pi^6}, \tag{3.24}$$

$$p^{\mathrm{TG}}(0) = p^{\mathrm{TG}}(6) = \frac{1}{64} - \frac{403}{1200\pi^2} + \frac{1456}{675\pi^4} - \frac{65536}{18225\pi^6}, \qquad (N = 6). \tag{3.25}$$

For a large number of impenetrable bosons, the probability distribution for a fixed large N becomes

$$p^{\mathrm{TG}}(k) \approx \frac{e^{-(k-N/2)^2/(2\sigma^2)}}{\sqrt{2\pi\sigma^2}}, \qquad (N \gg 1), \tag{3.26}$$

with $\sigma^2 = \pi^{-2}\log[2Ne^{\gamma_{\mathrm{E}}+1}]$ (Section 3.7). Therefore, at the two extreme limits of free and impenetrable bosons the most probable result of the projective measurement is the balanced bipartite state $\chi_{AB}(N/2)$. Since there are no critical values of $c \in (0, \infty)$, we expect this trend to hold for arbitrary finite repulsion strengths. Hence, we argue that the balanced projection is the most probable outcome for all non-negative values of c. We confirm this statement for $N = 4$ bosons and show in Figure 3.5 all possible projection probabilities for arbitrary repulsion strengths.

3.4 Entanglement entropy

We now quantify the entanglement between the partitions A and B in the projected state by calculating the von Neumann entropy $S_A(k)$ of region A. The full density matrix of the projected pure state is $\rho_{AB} = |\chi_{AB}\rangle\langle\chi_{AB}|$ and the relevant reduced density matrix is $\rho_A = \mathrm{tr}_B\, \rho_{AB}$. In the coordinate basis where $|\mathbf{x}\rangle \equiv \psi^\dagger(x_N)\cdots\psi^\dagger(x_1)|0\rangle$ with $\psi^\dagger(x)$ a bosonic field creation operator

and $|0\rangle$ the vacuum state ket, the projected state vector may be written as

$$|\chi_{AB}(k)\rangle = \sqrt{\binom{N}{k}\frac{1}{p(k)}}\int_A\int_B \chi(\mathbf{x})\,|\mathbf{x}\rangle\,\mathrm{d}\mathbf{x}_B\mathrm{d}\mathbf{x}_A. \tag{3.27}$$

The full density matrix $\rho_{AB}(k) = |\chi_{AB}(k)\rangle\langle\chi_{AB}(k)|$ of this projected state is therefore

$$\begin{aligned}\rho_{AB}(k) = &\binom{N}{k}\frac{1}{p(k)|\mathcal{N}|^2}\sum_{\{\mathcal{P}\}\{\mathcal{Q}\}}(-1)^{[\mathcal{P}]+[\mathcal{Q}]}\\ &\times\int_A\int_A\int_B\int_B F_{\mathcal{P}}(\mathbf{x})F^*_{\mathcal{Q}}(\mathbf{x}')e^{i(\boldsymbol{\lambda}_{\mathcal{P}}\cdot\mathbf{x}-\boldsymbol{\lambda}_{\mathcal{Q}}\cdot\mathbf{x}')}|\mathbf{x}\rangle\langle\mathbf{x}'|\,\mathrm{d}\mathbf{x}_B\mathrm{d}\mathbf{x}'_B\mathrm{d}\mathbf{x}_A\mathrm{d}\mathbf{x}'_A.\end{aligned} \tag{3.28}$$

The signum functions in the Bethe amplitudes $F_{\mathcal{P}}(\mathbf{x})$ evaluate trivially for each case $\mathrm{sgn}(x_{Bj}-x_{Ak}) = 1$ so that it factorizes as[2]

$$\sqrt{\binom{N}{k}}\,\frac{F_{\mathcal{P}}(\mathbf{x})}{\mathcal{N}} \equiv f_{\mathcal{P}}F_{\mathcal{P}A}(\mathbf{x}_A)F_{\mathcal{P}B}(\mathbf{x}_B), \tag{3.29}$$

with

$$f_{\mathcal{P}} = \frac{1}{\mathcal{N}}\frac{\prod_{l=1}^{k}\prod_{j=k+1}^{N}\lambda_{\mathcal{P}j}-\lambda_{\mathcal{P}l}-ic}{\left\{\prod_{n=1}^{k}\prod_{m=k+1}^{N}\left[(\lambda_{\mathcal{P}m}-\lambda_{\mathcal{P}n})^2+c^2\right]\right\}^{1/2}}, \tag{3.30}$$

$$F_{\mathcal{P}A} = \frac{\prod_{l<j}(\boldsymbol{\lambda}_{\mathcal{P}A})_j-(\boldsymbol{\lambda}_{\mathcal{P}A})_l-ic\,\mathrm{sgn}(x_{Aj}-x_{Al})}{\left\{k!\prod_{1\le n<m\le k}\left[(\lambda_{\mathcal{P}m}-\lambda_{\mathcal{P}n})^2+c^2\right]\right\}^{1/2}}, \tag{3.31}$$

$$F_{\mathcal{P}B} = \frac{\prod_{l<j}(\boldsymbol{\lambda}_{\mathcal{P}B})_j-(\boldsymbol{\lambda}_{\mathcal{P}B})_l-ic\,\mathrm{sgn}(x_{Bj}-x_{Bl})}{\left\{(N-k)!\prod_{k+1\le n<m\le N}\left[(\lambda_{\mathcal{P}m}-\lambda_{\mathcal{P}n})^2+c^2\right]\right\}^{1/2}}. \tag{3.32}$$

We introduce here the permuted momentum vectors $\boldsymbol{\lambda}_{\mathcal{P}A} \equiv (\lambda_{\mathcal{P}1},\ldots,\lambda_{\mathcal{P}k})^{\mathsf{T}}$ and $\boldsymbol{\lambda}_{\mathcal{P}B} \equiv (\lambda_{\mathcal{P}k+1},\ldots,\lambda_{\mathcal{P}N})^{\mathsf{T}}$.

Thus, the integrals over region B may be evaluated independently so that

[2]The definitions of $F_{\mathcal{P}A}$ and $F_{\mathcal{P}B}$ here are different from those used in manuscript [**II**].

tracing away the degrees of freedom in B gives the reduced density matrix

$$\rho_A(k) = \sum_{\{\mathcal{P}\}\{\mathcal{Q}\}} \int_A \int_A G_{\mathcal{P}\mathcal{Q}}(\mathbf{x}_A, \mathbf{x}'_A) e^{i(\boldsymbol{\lambda}_{\mathcal{P}A}\cdot\mathbf{x}_A - \boldsymbol{\lambda}_{\mathcal{Q}A}\cdot\mathbf{x}'_A)} |\mathbf{x}_A\rangle\langle\mathbf{x}'_A| \, \mathrm{d}\mathbf{x}_A \mathrm{d}\mathbf{x}'_A, \quad (3.33)$$

where the function $G_{\mathcal{P}\mathcal{Q}}(\mathbf{x}_A, \mathbf{x}'_A)$ is defined to be

$$G_{\mathcal{P}\mathcal{Q}}(\mathbf{x}_A, \mathbf{x}'_A) \equiv \frac{(-1)^{[\mathcal{P}]+[\mathcal{Q}]}}{p(k)} f_{\mathcal{P}} F_{\mathcal{P}A}(\mathbf{x}_A) f^*_{\mathcal{Q}} F^*_{\mathcal{Q}A}(\mathbf{x}'_A) \times \int_B F_{\mathcal{P}B}(\mathbf{x}_B) F^*_{\mathcal{Q}B}(\mathbf{x}_B) e^{i(\boldsymbol{\lambda}_{\mathcal{P}B} - \boldsymbol{\lambda}_{\mathcal{Q}B})\cdot\mathbf{x}_B} \, \mathrm{d}\mathbf{x}_B. \quad (3.34)$$

The eigenvalues a_i of the reduced density matrix ρ_A may be obtained by diagonalizing the associated homogeneous Fredholm integral equation

$$\int_A K(\mathbf{x}_A, \mathbf{x}'_A) \phi_i(\mathbf{x}'_A) \, \mathrm{d}\mathbf{x}'_A = a_i \phi_i(\mathbf{x}_A), \quad (3.35)$$

which has the kernel

$$K(\mathbf{x}_A, \mathbf{x}'_A) \equiv \sum_{\{\mathcal{P}\}\{\mathcal{Q}\}} G_{\mathcal{P}\mathcal{Q}}(\mathbf{x}_A, \mathbf{x}'_A) e^{i\boldsymbol{\lambda}_{\mathcal{P}A}\cdot\mathbf{x}_A} e^{-i\boldsymbol{\lambda}_{\mathcal{Q}A}\cdot\mathbf{x}'_A}. \quad (3.36)$$

The eigenvalue spectrum of the reduced density matrix is explicitly calculated for the case of two impenetrable bosons in Section 3.7.2.

Since free bosons condense in the ground state, the kernel reduces to a constant when there are no interactions and the only eigenvalue of the resulting reduced density matrix is unity. Thus, the von Neumann entropy vanishes when $c = 0$ and the projected states for any k are separable states with no entanglement.

For any non-zero contact repulsion between N bosons, however, there are $\binom{N}{k}$ distinct ways of choosing the components of the vectors $\boldsymbol{\lambda}_{\mathcal{P}A}$ and $\boldsymbol{\lambda}_{\mathcal{Q}A}$. Diagonalization of the reduced density matrix $\rho_A(k)$ reveals that it has at most $\binom{N}{k}$ non-zero eigenvalues (Section 3.7.3). Hence, the reduced density matrix $\rho_A(k)$ is a rank $\binom{N}{k}$ matrix and we may formulate an upper bound for

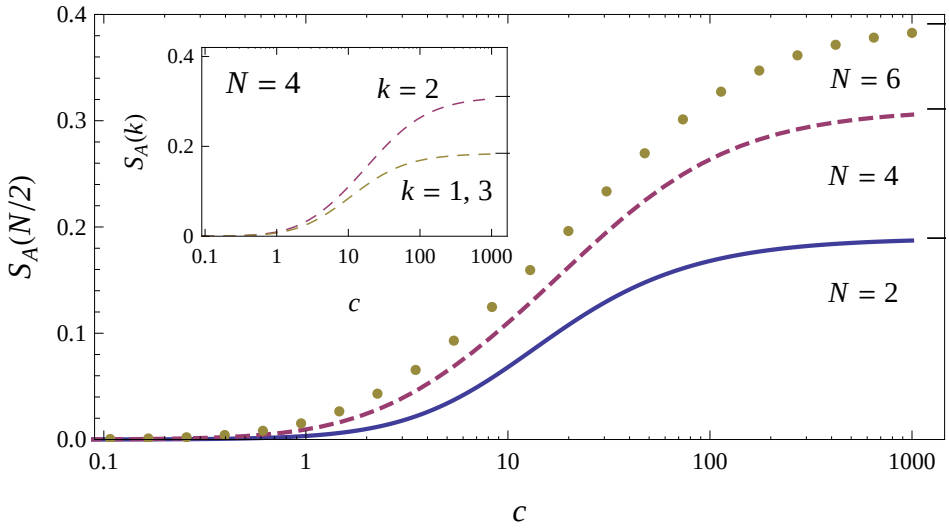

Figure 3.6: The von Neumann entropy between half-rings in the projected balanced pure state increases monotonically with the strength of repulsion. For the case of four bosons the balanced projection $k = N/2$ is more entangled than the unbalanced cases for all c (inset). Black tick marks denote the corresponding values in the impenetrable boson limit.

the entanglement entropy extractable from the projected state as

$$S_{\text{ub}}(k) \equiv \log \binom{N}{k} \geq S_A(k), \tag{3.37}$$

assuming a flat entanglement spectrum. For the balanced projection $k = N/2$ this upper bound scales asymptotically according to

$$S_{\text{ub}}(N/2) \sim N \log 2 - \tfrac{1}{2} \log N, \quad N \to \infty. \tag{3.38}$$

The eigenvalue problem (3.35) can be solved analytically by linear algebra methods for small values of N, but becomes increasingly cumbersome for large N. This difficulty arises because the projected many-particle wavefunction is no longer an eigenfunction of the system hamiltonian. That is, the projected state is excited and diagonalization of the reduced density matrix requires the calculation of a large number of overlap matrix elements (Section 3.7.3). A numerically exact evaluation of the von Neumann entropy is

shown in Figure 3.6 for two, four, and six bosons. For the balanced cases we find that more entanglement is present in the projected states as the repulsion strength is increased, with significant entanglement produced above the scale set by $c = 1$. In the inset of Figure 3.6 we show that we can extract more entanglement from the balanced projection than from any of the unbalanced cases for $N = 4$ and any c. For arbitrary N, we can expect the same behavior to hold based on the calculated upper bound (3.37) for the von Neumann entropy: $S_{\rm ub}(k \neq N/2) < S_{\rm ub}(N/2)$ or, equivalently, $\operatorname{rank}\rho_A(k \neq N/2) < \operatorname{rank}\rho_A(N/2)$. However, for the cases we have considered above the projected states χ_{AB} are not maximally entangled, that is, $S_A < S_{\rm ub}$. Nevertheless, because the rank of the reduced density matrix is maximum when $k = N/2$ and the symmetry $S_A(k) = S_A(N-k)$, we conjecture that the balanced projections have more entanglement entropy than the unbalanced ones: $S_A(k \neq N/2) < S_A(N/2)$ for all c.

3.5 Extractable entanglement

So far we have argued that the projection probabilities and von Neumann entropies are largest for the balanced projections $k = N/2$ at any given value of the repulsion strength. Thus, according to the definition (3.4), the projectively extractable pure state entanglement from the Lieb–Liniger ground state is given by the weighted entanglement of the balanced fixed number projection:

$$\mathcal{E}_{PP} = p(N/2)S_A(N/2) = \mathcal{E}_{k=N/2}, \quad \forall c \geq 0. \tag{3.39}$$

This statement is trivial for free bosons as we have already proven that the von Neumann entropy vanishes in all possible projections for any even N. In the opposite limit of impenetrable bosons this assertion is verified in Figure 3.7 where we give numerically exact results for all possible cases of up to six bosons. Also apparent in this graph is a slower than linear increase in the extractable entropy $\mathcal{E}_{PP}$ with respect to the boson number N.

We further observe that although the probability of successful projection becomes smaller with increasing boson number, the von Neumann entropy

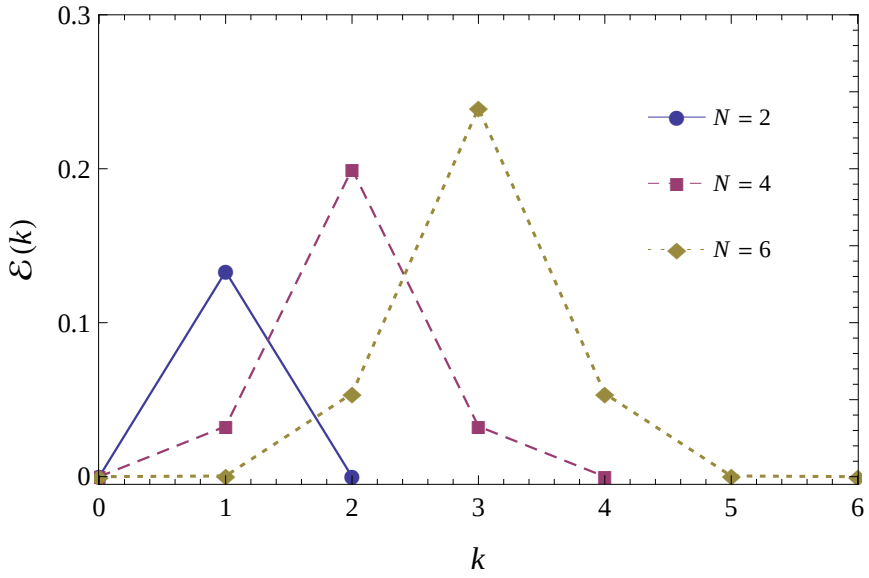

Figure 3.7: In the impenetrable boson limit the weighted entanglement $\mathcal{E}(k)$ is a maximum for the balanced case $k = N/2$. This maximum $\mathcal{E}(N/2)$ gives the extractable entanglement $\mathcal{E}_{PP}$. Connecting lines serve to guide the eye.

S_A increases faster with N so that the extractable entanglement $\mathcal{E}_{PP}$ increases with both repulsion strength and the number of bosons in the ring (Figure 3.8). Furthermore, for the few boson cases we have analyzed here, this increase is monotonic with respect to both N and c. Hence, more entanglement can be extracted from these projections of the Lieb–Liniger gas in the TG limit of impenetrable bosons and we may regard the quantity $\mathcal{E}_{PP}$ as a probe of both quantum correlations and interparticle interactions in the ensemble of fixed number projections of the type we considered here.

3.6 Concluding remarks

We have used the projectively extractable pure state entanglement $\mathcal{E}_{PP}$ to quantify the entanglement in coarse-grained fixed number projections of the Lieb–Liniger ground state. This entanglement measure quantifies the entanglement present in the set of all projection outcomes by giving the largest von Neumann entropy weighted by the projection probability of a particular mea-

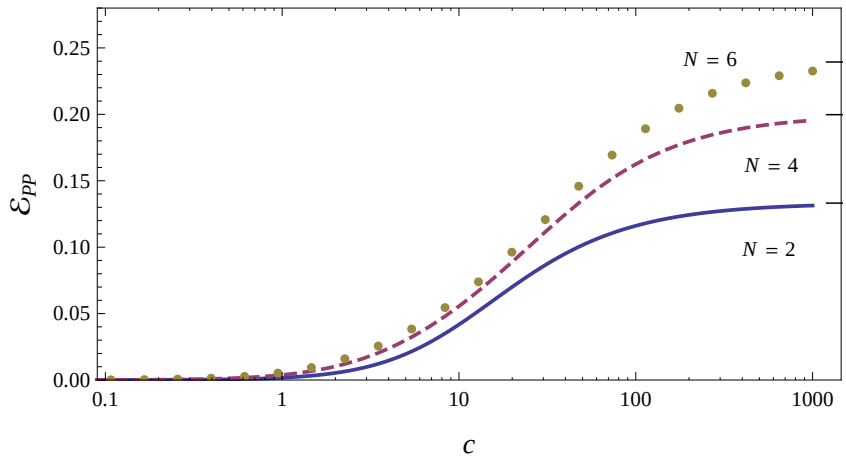

Figure 3.8: The projectively extractable pure state entanglement monotonically increases with repulsion strength, smoothly transitioning from the free and impenetrable boson limits (black ticks).

surement result. In our case, this maximum corresponds to the most probable and most entangled projection having an equal number of particles in each half of the ring. In our numerically exact few-particle results, we have seen indications that the extractable entanglement increases monotonically with the strength of repulsion and with particle number. We have also observed that significant amounts of entanglement can be extracted by this projection procedure only in the strongly repulsive regime $c \gg 1$. This increase and subsequent saturation of entanglement with interaction strength c has also been previously observed numerically in a few-particle Lieb–Liniger gas under the framework of single-particle partioning of the ground state [94].

Since the impenetrable TG limit displays free-fermionic characteristics, our work reveals a fundamental difference in the entanglement extractable from one-dimensional bosonic and fermionic systems. When appropriate projective measurements eliminate the uncertainty in partition occupancies, the entanglement vanishes for free bosons, whereas it is non-zero for impenetrable bosons. Based on an analytic upper bound for the von Neumann entropy (3.37), we see that entanglement in a projected pure state having k out of N bosons in region A depends on the number of ways of choosing k quasimomenta from a set of N

distinct ones. In other words, the extractable entanglement $\mathcal{E}_{PP}$ is a measure of quantum correlations due to an exclusion principle arising from interparticle interactions (parametrized by c). As seen from Figures 3.6 and 3.8, more entanglement is present in the system as the exclusion effect approaches its maximum at the pseudofermionic TG limit. Thus, this work reveals the crucial role of particle interactions on the entanglement in a spatially partitioned many-body system of indistinguishable particles. We expect this feature to be preserved at larger particle numbers N, which may be viewed as an essential difference between a free-boson and a free-fermion gas from the perspective of quantum information. In fact, a similar observation was made regarding the entanglement of particles (3.5) in the ground state of two non-interacting bosons and two non-interacting fermions in small lattices [80]. The fact that the free boson system has zero entanglement while the free fermion system has non-zero entanglement was mathematically attributed to the difference in particle statistics. In our example of a boson gas, however, we attribute this difference to a dynamically generated exclusion principle.

It is important to remark that the projected states we have described here are not eigenstates of the original Lieb–Liniger hamiltonian (3.6) and will therefore evolve non-trivially in time. The results we present here are therefore only valid immediately after measurement while the spatial partitioning of particles is meaningful; the number of particles in each partition will change in time. However, one can also adopt the perspective of treating the projective measurement as an operational part of the theoretical definition of extractable entanglement. This point of view has been adopted in studies of systems of indistinguishable particles where superselection rules [115, 116] fix certain local observables like the number of massive particles [79, 80]. In this case, projective measurements form part of the definition of the entanglement of particles (3.5).

3.7 Derivations

3.7.1 Projection probabilities for impenetrable bosons

We restore length units in this derivation.

We seek an asymptotic approximation to the characteristic function $f(\alpha) \equiv \langle e^{i\alpha \int_0^\ell \psi^\dagger(x)\psi(x)\,dx} \rangle$ for the probability distribution $p(k)$ of finding k impenetrable bosons in an arc ℓ of a ring of circumference L. In the thermodynamic limit $N \to \infty$ with finite particle density N/L, the characteristic function is equal to the Fredholm determinant [10]

$$f(\alpha) = \det\bigl(\hat{\mathbb{1}} - (1 - e^{i\alpha})\hat{V}\bigr), \tag{3.40}$$

where the linear integral operator $\hat{V}$ acts on the interval $[-q, q]$ with $q = (N-1)\pi/L$ and possesses the kernel

$$V(\lambda, \mu) = \frac{1}{\pi(\lambda - \mu)} \sin\bigl[\tfrac{1}{2}(\lambda - \mu)\ell\bigr]. \tag{3.41}$$

Let us make a discrete approximation to the integral $\hat{V}[F(\mu)](\lambda)$ by transforming $\lambda \to \lambda_m = (2m-1)\pi/L$ and $\mu \to \mu_n = (2n-1)\pi/L$ to obtain

$$\int_{-q}^{q} V(\lambda_i, \mu) F(\mu)\, d\mu \approx \sum_{j=1}^{N} \Gamma_{ij}\, F\left[\frac{2\pi}{L}\left(j - \frac{N+1}{2}\right)\right], \tag{3.42}$$

Here, the elements Γ_{ij} of the matrix $\mathbf{\Gamma}$ are

$$\Gamma_{ij} = \delta_{ij}\frac{\ell}{L} + (1 - \delta_{ij})\frac{\sin[\pi(i-j)\ell/L]}{\pi(i-j)}. \tag{3.43}$$

The characteristic function may therefore be approximated by the $N \times N$ Toeplitz determinant when $N \gg 1$:

$$f(\alpha) \approx \det\bigl(\mathbb{1}_N - (1 - e^{i\alpha})\mathbf{\Gamma}\bigr). \tag{3.44}$$

The matrix $\mathbf{\Gamma}$ is identical to the single-particle correlation matrix of free

fermions on an infinite one-dimensional lattice upon making the replacement $\pi\ell/L \to k_F a$ with k_F the Fermi wavevector and a the lattice spacing [120].

For $|\alpha| < \pi$ the Fisher–Hartwig formulas [122, 123] may be used to obtain the asymptotic $N \to \infty$ result [120, 121]

$$f(\alpha) \sim \frac{e^{i\alpha N\ell/L}\big[G\big(1+\alpha/(2\pi)\big)G\big(1-\alpha/(2\pi)\big)\big]^2}{\big[2N\sin(\pi\ell/L)\big]^{\alpha^2/(2\pi^2)}}, \tag{3.45}$$

where $G(z)$ is the Barnes G-function defined functionally through $G(1+z) = \Gamma(z)G(z)$ and $G(1) = 1$, with $\Gamma(z)$ the usual gamma function. Using a small $\alpha \ll \pi$ expansion [120] gives

$$\log f(\alpha) \sim \frac{iN\ell}{L}\alpha - \frac{\log[2Ne^{\gamma_{\mathrm{E}}+1}\sin(\pi\ell/L)]}{2\pi^2}\alpha^2 + 0\alpha^3 - \frac{\zeta(3)}{(2\pi)^4}\alpha^4, \quad 0 < \alpha \ll \pi, \tag{3.46}$$

where γ_{E} is Euler's constant. We extract the first two cumulants of the probability distribution $p(k)$ from this expression and make a Gaussian approximation for the case of interest $\ell = L/2$ about the central peak $k = N/2$ to obtain

$$p(k) \approx \frac{e^{-(k-N/2)^2/(2\sigma^2)}}{\sqrt{2\pi\sigma^2}}, \tag{3.47}$$

with variance $\sigma^2 = \pi^{-2}\log[2Ne^{\gamma_{\mathrm{E}}+1}]$. Physically, the variance σ^2 is the fluctuation of particle number in the half-ring $\ell = L/2$ about the mean value $N/2$. The probability of finding exactly $N/2$ impenetrable bosons (or free fermions) in a half-ring is therefore

$$p(N/2) \sim \sqrt{\frac{\pi}{2\log(2Ne^{\gamma_{\mathrm{E}}+1})}}, \qquad (N \gg 1). \tag{3.48}$$

3.7.2 Entanglement entropy for impenetrable bosons

In this section, we present an explicit calculation for the entanglement entropy in a balanced projection of a two-particle Lieb–Liniger gas in the Tonks–

Girardeau limit. The normalized ground state wavefunction is

$$\chi(x_1, x_2) = \frac{\operatorname{sgn}(x_1 - x_2)}{\sqrt{2}} \left[e^{i(\lambda_1 x_1 + \lambda_2 x_2)} - e^{i(\lambda_2 x_1 + \lambda_1 x_2)} \right], \tag{3.49}$$

with $\lambda_1 = -\pi$ and $\lambda_2 = \pi$. The probability p of finding one particle each in region A and B is

$$p = 2 \int_0^{1/2} \int_{1/2}^{1} \chi^*(x_1, x_2) \chi(x_1, x_2) \, \mathrm{d}x_2 \mathrm{d}x_1 = \frac{1}{2} + \frac{2}{\pi^2}. \tag{3.50}$$

The eigenvalues of the reduced density matrix $\{a_i\}$ are therefore given by the spectrum of the integral equation (3.36)

$$\int_0^{1/2} K(x, x') \phi(x') \, \mathrm{d}x' = a \phi(x), \tag{3.51}$$

with kernel

$$\begin{aligned} K(x, x') = G_{11}(x, x') e^{-i\pi(x - x')} + G_{12}(x, x') e^{-i\pi(x + x')} \\ + G_{21}(x, x') e^{i\pi(x + x')} + G_{22}(x, x') e^{i\pi(x - x')}. \end{aligned} \tag{3.52}$$

In this example the functions $G_{\mathcal{P},\mathcal{Q}}(x, x')$ reduce to constants

$$G_{11}(x, x') = G_{22}(x, x') = \frac{\pi^2}{4 + \pi^2} \equiv g, \tag{3.53}$$

$$G_{12}(x, x') = G_{21}^*(x, x') = \frac{2\pi i}{4 + \pi^2} \equiv \frac{2gi}{\pi}. \tag{3.54}$$

We then rearrange terms in the sum for the integral kernel (3.52) to get

$$K(x, x') = \frac{g}{\pi} \left[e^{-i\pi x} (\pi e^{i\pi x'} + 2i e^{-i\pi x'}) + e^{i\pi x} (\pi e^{-i\pi x'} - 2i e^{i\pi x'}) \right]. \tag{3.55}$$

Defining the constants

$$c_1 = \int_0^{1/2} e^{i\pi x'} \phi(x')\, \mathrm{d}x', \tag{3.56}$$

$$c_2 = \int_0^{1/2} e^{-i\pi x'} \phi(x')\, \mathrm{d}x', \tag{3.57}$$

and multiplying the integral equation (3.51) by $e^{\pm i\pi x}$ and then integrating over region A gives the following matrix equation

$$\begin{pmatrix} 1/2 & 2\pi i/(4+\pi^2) \\ -2\pi i/(4+\pi^2) & 1/2 \end{pmatrix} \begin{pmatrix} c_1 \\ c_2 \end{pmatrix} = a \begin{pmatrix} c_1 \\ c_2 \end{pmatrix}. \tag{3.58}$$

The eigenvalues of the reduced density matrix are therefore

$$a_\pm = \frac{1}{2} \pm \frac{2\pi}{4+\pi^2}, \tag{3.59}$$

and the von Neumann entropy is $S_A = -(a_+ \log a_+ + a_- \log a_-)$.

3.7.3 Reduced density matrix

The state vector of the projected pure state having k bosons in region A is

$$|\chi_{AB}(k)\rangle = \sqrt{\binom{N}{k} \frac{1}{p(k)}}\, \frac{1}{\mathcal{N}} \sum_{\{\mathcal{P}\}} (-1)^{[\mathcal{P}]} \int_A \int_B F_{\mathcal{P}}(\mathbf{x}) e^{i\boldsymbol{\lambda}_{\mathcal{P}}\cdot\mathbf{x}} |\mathbf{x}\rangle\, \mathrm{d}\mathbf{x}_B \mathrm{d}\mathbf{x}_A. \tag{3.60}$$

Let us decompose the sum over permutations $\{\mathcal{P}\}$ into three different sums. First, we consider an ordered subset $\{\mathcal{C}'\}$ of these permutations. Each member of $\{\mathcal{C}'\}$ has a signature $+1$, that is they are even permutations. Furthermore, the first k elements of each permutation is a distinct way (combination) of choosing k items from N. Thus, $\{\mathcal{C}'\}$ has $\binom{N}{k}$ elements. For example, given the ordered set (1234), one way of choosing the six members of $\{\mathcal{C}'\}$ is

$$\{\mathcal{C}'\} = \{(1234), (1342), (1423), (2314), (4213), (3412)\}. \tag{3.61}$$

Now, let $\{\mathcal{C}_A\}$ be the set of $k!$ permutations of the first k elements of $\mathcal{C}'$ and

$\{\mathcal{C}_B\}$ be the set of $(N-k)!$ permutations of the remaining elements. The full sum over permutations $\{\mathcal{P}\}$ is thus equivalent to

$$\sum_{\{\mathcal{P}\}} = \sum_{\{\mathcal{C}'\}} \sum_{\{\mathcal{C}_A\}} \sum_{\{\mathcal{C}_B\}}. \tag{3.62}$$

The reduced density matrix (3.33) can therefore be written as

$$\rho_A(k) = \sum_{\{\mathcal{C}'\}\{\mathcal{D}'\}} \sum_{\{\mathcal{C}_A\}\{\mathcal{D}_A\}} \int_A \int_A G_{\mathcal{C}'\mathcal{D}'}(\mathbf{x}_A, \mathbf{x}'_A) e^{i(\boldsymbol{\lambda}_{\mathcal{C}A}\cdot\mathbf{x}_A - \boldsymbol{\lambda}_{\mathcal{D}A}\cdot\mathbf{x}'_A)} |\mathbf{x}_A\rangle\langle\mathbf{x}'_A| \, \mathrm{d}\mathbf{x}_A \mathrm{d}\mathbf{x}'_A, \tag{3.63}$$

where the function $G_{\mathcal{C}'\mathcal{D}'}(\mathbf{x}_A, \mathbf{x}'_A)$ is

$$\begin{aligned} G_{\mathcal{C}'\mathcal{D}'}(\mathbf{x}_A, \mathbf{x}'_A) \equiv{}& \frac{(-1)^{[\mathcal{C}_A]+[\mathcal{D}_A]}}{p(k)} f_{\mathcal{C}'} F_{\mathcal{C}A}(\mathbf{x}_A) f^*_{\mathcal{D}'} F^*_{\mathcal{D}A}(\mathbf{x}'_A) \\ &\times \sum_{\{\mathcal{C}_B\}\{\mathcal{D}_B\}} (-1)^{[\mathcal{C}_B]+[\mathcal{D}_B]} \int_B F_{\mathcal{C}B}(\mathbf{x}_B) F^*_{\mathcal{D}B}(\mathbf{x}_B) e^{i(\boldsymbol{\lambda}_{\mathcal{C}B} - \boldsymbol{\lambda}_{\mathcal{D}B})\cdot\mathbf{x}_B} \, \mathrm{d}\mathbf{x}_B. \end{aligned} \tag{3.64}$$

Let us construct the following state vectors

$$|\boldsymbol{\lambda}^A_{\mathcal{C}'}\rangle = f_{\mathcal{C}'} \int_A \sum_{\{\mathcal{C}_A\}} (-1)^{[\mathcal{C}_A]} F_{\mathcal{C}A}(\mathbf{x}_A) e^{i\boldsymbol{\lambda}_{\mathcal{C}A}\cdot\mathbf{x}_A} |\mathbf{x}_A\rangle \, \mathrm{d}\mathbf{x}_A, \tag{3.65}$$

$$|\boldsymbol{\lambda}^B_{\mathcal{C}'}\rangle = \int_B \sum_{\{\mathcal{C}_B\}} (-1)^{[\mathcal{C}_B]} F_{\mathcal{C}B}(\mathbf{x}_B) e^{i\boldsymbol{\lambda}_{\mathcal{C}B}\cdot\mathbf{x}_B} |\mathbf{x}_B\rangle \, \mathrm{d}\mathbf{x}_B, \tag{3.66}$$

and their corresponding dual vectors

$$\langle\boldsymbol{\lambda}^A_{\mathcal{D}'}| = f^*_{\mathcal{D}'} \int_A \sum_{\{\mathcal{D}_A\}} (-1)^{[\mathcal{D}_A]} F^*_{\mathcal{D}A}(\mathbf{x}_A) e^{-i\boldsymbol{\lambda}_{\mathcal{D}A}\cdot\mathbf{x}_A} \langle\mathbf{x}_A| \, \mathrm{d}\mathbf{x}_A, \tag{3.67}$$

$$\langle\boldsymbol{\lambda}^B_{\mathcal{D}'}| = \int_B \sum_{\{\mathcal{D}_B\}} (-1)^{[\mathcal{D}_B]} F^*_{\mathcal{D}B}(\mathbf{x}_B) e^{-i\boldsymbol{\lambda}_{\mathcal{D}B}\cdot\mathbf{x}_B} \langle\mathbf{x}_B| \, \mathrm{d}\mathbf{x}_B. \tag{3.68}$$

These vectors have similarities with the Bethe state vectors, but it must be emphasized that they do not form an orthonormal basis within their respective Hilbert spaces. Still, the $\binom{N}{k}$ vectors in $\{|\boldsymbol{\lambda}^A_{\mathcal{C}'}\rangle\}$ are linearly independent so that the reduced density matrix has rank $\binom{N}{k}$. Writing the reduced density matrix

in terms of these vectors leads to the compact expression

$$\rho_A(k) = \frac{1}{p(k)} \sum_{\{\mathcal{C}'\}\{\mathcal{D}'\}} |\boldsymbol{\lambda}^A_{\mathcal{C}'}\rangle\langle\boldsymbol{\lambda}^B_{\mathcal{D}'}|\boldsymbol{\lambda}^B_{\mathcal{C}'}\rangle\langle\boldsymbol{\lambda}^A_{\mathcal{D}'}|. \tag{3.69}$$

We now express the reduced density matrix in terms of an orthonormal basis for the vector space spanned by $\{|\boldsymbol{\lambda}^A_{\mathcal{C}}\rangle\}$. Let $A_{\mathcal{C}\mathcal{D}} \equiv \langle\boldsymbol{\lambda}^A_{\mathcal{C}}|\boldsymbol{\lambda}^A_{\mathcal{D}}\rangle$ and $B_{\mathcal{D}\mathcal{C}} \equiv \langle\boldsymbol{\lambda}^B_{\mathcal{D}}|\boldsymbol{\lambda}^B_{\mathcal{C}}\rangle$ be the elements of the hermitian overlap matrices $\mathbf{A}$ and $\mathbf{B}$, respectively. Further, let $U_{i\mathcal{C}}$ be the elements of an arbitrary orthogonal matrix $\mathbf{U}$. Let us construct the desired orthonormal basis $\{|i\rangle\}$ by letting

$$|i\rangle = \sum_{\{\mathcal{C}\}} U_{i\mathcal{C}}|\boldsymbol{\lambda}^A_{\mathcal{C}}\rangle, \qquad \langle j| = \sum_{\{\mathcal{D}\}} \langle\boldsymbol{\lambda}^A_{\mathcal{D}}|V_{\mathcal{D}j}, \tag{3.70}$$

and choosing the matrix elements $V_{\mathcal{D}j}$ of $\mathbf{V}$ to satisfy

$$\langle j|i\rangle = \sum_{\{\mathcal{C}\}\{\mathcal{D}\}} V_{\mathcal{D}j} A_{\mathcal{D}\mathcal{C}} U_{i\mathcal{C}} \equiv \delta_{ji}. \tag{3.71}$$

In matrix notation we have $\mathbf{V}^\mathsf{T}\mathbf{A}\mathbf{U}^\mathsf{T} = \mathbb{1}$ or $\mathbf{V} = (\mathbf{U}\mathbf{A}^\mathsf{T})^{-1}$. From these relations we obtain the overlaps

$$\langle i|\boldsymbol{\lambda}^A_{\mathcal{C}}\rangle = U^{-1}_{\mathcal{C}i}, \tag{3.72}$$

$$\langle\boldsymbol{\lambda}^A_{\mathcal{D}}|j\rangle = V^{-1}_{j\mathcal{D}} = (\mathbf{U}\mathbf{A}^\mathsf{T})_{j\mathcal{D}}. \tag{3.73}$$

The reduced density matrix (3.69) becomes

$$\rho_A(k) = \frac{1}{p(k)} \sum_{ij} |i\rangle\langle j| \sum_{\{\mathcal{C}'\}\{\mathcal{D}'\}} U^{-1}_{\mathcal{C}'i} B_{\mathcal{D}'\mathcal{C}'} (\mathbf{U}\mathbf{A}^\mathsf{T})_{j\mathcal{D}}, \tag{3.74}$$

$$= \frac{1}{p(k)} \sum_{ij} |i\rangle\langle j| \, (\mathbf{U}\mathbf{A}^\mathsf{T}\mathbf{B}\mathbf{U}^{-1})^\mathsf{T}_{ij}. \tag{3.75}$$

In the $\{|i\rangle\}$ basis we may therefore write $\rho_A(k) = \mathbf{U}\mathbf{B}^\mathsf{T}\mathbf{A}\mathbf{U}^{-1}/p(k)$. Thus, the eigenvalue spectrum of the reduced density matrix $\rho_A(k)$ is the same as that of $\tilde{\rho}_A(k) \equiv \mathbf{B}^\mathsf{T}\mathbf{A}/p(k)$. Furthermore, since $\operatorname{tr}\rho_A(k) = \operatorname{tr}\tilde{\rho}_A(k) = 1$, the projection probability is simply $p(k) = \operatorname{tr}(\mathbf{B}^\mathsf{T}\mathbf{A})$. This result implies that the extractable

entanglement is completely determined by the overlap matrices $\mathbf{A}$ and $\mathbf{B}$.

The preceding construction is a general result that is related to the Schmidt decomposition of the bipartite pure state [124]. For example, consider a pure state represented by a state vector $|\Psi\rangle$ in the partitioned Hilbert space $\mathscr{H} = \mathscr{H}_A \otimes \mathscr{H}_B$. Its Schmidt decomposition is $|\Psi\rangle = \sum_i a_i \, |i^A\rangle \otimes |i^B\rangle$, where $\{|i^U\rangle\}$ is an orthonormal basis in the Hilbert space $\mathscr{H}_U$. In practice, such in our case above, the decomposition is conveniently expressed in terms of the nonorthogonal bases $\{|\mu^A\rangle\}$ and $\{|\mu^B\rangle\}$. The partitioned state vector and full density matrix are

$$|\Psi\rangle = \frac{1}{\mathcal{N}} \sum_{\mu} |\mu^A\rangle \otimes |\mu^B\rangle, \tag{3.76}$$

$$|\Psi\rangle\langle\Psi| = \frac{1}{|\mathcal{N}|^2} \sum_{\mu\nu} |\mu^A\rangle\langle\nu^A| \otimes |\mu^B\rangle\langle\nu^B|, \tag{3.77}$$

where $\langle\mu^U|\nu^U\rangle \neq \delta_{\mu\nu}$. This is the situation encountered for spatially partitioned models that are solvable by the Bethe ansatz having factorable Bethe amplitudes $F(\mathbf{x}) = g(\mathbf{x}_A) \times h(\mathbf{x}_B)$, as in (3.29). Taking the partial trace over the Hilbert space $\mathscr{H}_B$ gives the reduced density matrix

$$\rho_A = \frac{1}{|\mathcal{N}|^2} \sum_{\mu\nu} |\mu^A\rangle\langle\nu^B|\mu^B\rangle\langle\nu^A|. \tag{3.78}$$

As above, we construct the overlap matrix elements $A_{\mu\nu} \equiv \langle\mu^A|\nu^A\rangle$ and $B_{\nu\mu} \equiv \langle\nu^B|\mu^B\rangle$ to obtain

$$\tilde{\rho}_A = \frac{\mathbf{B}^{\mathsf{T}}\mathbf{A}}{\mathrm{tr}(\mathbf{B}^{\mathsf{T}}\mathbf{A})}, \tag{3.79}$$

which has the same eigenvalue spectrum as ρ_A. This formula is independent of the specific hamiltonian governing the system under consideration. Its utility depends on two important factors. First is the ease with which the pure state can be decomposed into the partitioned form (3.76) and second is the computational effort needed to evaluate the overlap matrix elements.

Chapter 4

Entanglement in q-deformed valence-bond-solid states

The contents of this chapter are based on the manuscripts [**III**] and [**IV**].

4.1 Affleck–Kennedy–Lieb–Tasaki model

The Affleck–Kennedy–Lieb–Tasaki (AKLT) model is a one-dimensional antiferromagnetic model of interacting Heisenberg spins [125, 126]. The main motivation for the construction and investigation of this model was the search for a novel antiferromagnetic system possessing a unique ground state that is protected by a Haldane gap [127, 128]. The gapped ground state of this model is known exactly and referred to as a valence-bond-solid or VBS state. In general, the existence and uniqueness of this VBS state is guaranteed by construction when a specific condition between the valency and magnitude of each spin is imposed. Hence, the AKLT model may be generalized to arbitrary connected graphs [129]. Currently, interest in VBS states also includes physical applications, especially following the suggestion that these states may function as platforms for measurement-based quantum computation [130, 131]. Indeed, single-qubit logic gates have already been constructed using photonic VBS states [4–6] and it has been demonstrated that the two-dimensional AKLT VBS state is a universal computational resource [132]. Also, there is further

interest in AKLT models among condensed matter physicists because of their connection to the fractional quantum hall effect (FQHE) through the similarity between the Schwinger boson representation of the VBS ground state and the Laughlin wavefunction (Jastrow forms) [133].

In its general formulation [129, 134], the AKLT model consists of a collection of spin operators $\mathbf{S}_k$ associated with a vertex k of a connected graph. The spin magnitude $s_k = z_k/2$ is half the coordination number z_k (number of edges or valence bonds connecting vertex k). The antiferromagnetic interactions between connected spins are then described by the hamiltonian

$$H_{\mathrm{AKLT}} = \sum_{\langle kl \rangle} h_{kl} = \sum_{\langle kl \rangle} \sum_{J=s_k+s_l-M_{kl}+1}^{s_k+s_l} C_J \pi_J(k,l), \tag{4.1}$$

where M_{kl} is the number of valence bonds connecting the vertex pair $\langle kl \rangle$ and $C_J > 0$ are parameters of the model. The $\pi_J(k,l)$ are projection operators for the state of the total spin $\mathbf{J}_{kl} = \mathbf{S}_k + \mathbf{S}_l$ onto the subspace with a fixed spin magnitude J:

$$\pi_J(k,l) \equiv \prod_{\substack{j=|s_k-s_l| \\ j \neq J}}^{s_k+s_l} \frac{(\mathbf{S}_k + \mathbf{S}_l)^2 - j(j+1)}{J(J+1) - j(j+1)}. \tag{4.2}$$

That is, the hamiltonian density h_{kl} per pair of connected spins $\langle kl \rangle$ is a mapping onto the subspace spanned by the $(s_k + s_l - M_{kl} + 1)$, $(s_k + s_l - M_{kl} + 2), \ldots,$ and $(s_k + s_l)$-multiplets formed by spins at sites k and l. The AKLT hamiltonian is therefore manifestly SU(2) symmetric.

4.1.1 Valence-bond-solid state

For our purposes, we consider a translationally invariant (homogeneous) spin-s AKLT chain with nearest-neighbor interactions so that $s \equiv s_k = M_{k,k+1} = z_k/2$ for all k [125, 126]. The VBS state $|\mathrm{VBS}\rangle$ is then constructed by requiring $h_{k,k+1}|\mathrm{VBS}\rangle = 0$ for all neighboring pairs of interacting spins. Due to this property, the VBS state is referred to as frustration-free. Since the the projector $\pi_J(k, k+1)$ has eigenvalues $\{0, 1\}$ and $C_J > 0$, the hamiltonian H_{AKLT} is positive semidefinite. It therefore follows that $|\mathrm{VBS}\rangle$ is the ground state of

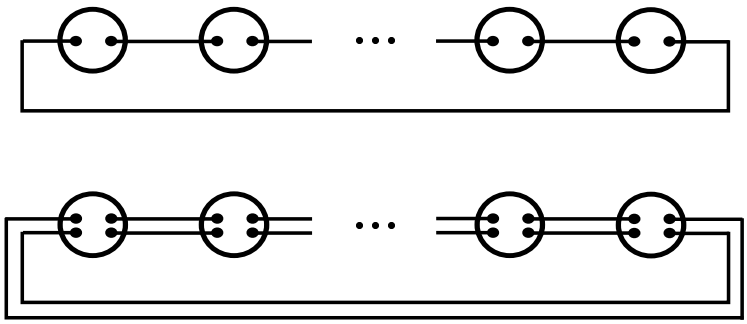

Figure 4.1: Schematic diagrams of spin-1 (top) and spin-2 (bottom) valence-bond-solid states with periodic boundaries. The lines (valence bonds) denote the antisymmetric singlet state of two auxiliary spin-1/2's (solid dots). Circles denote projections onto the respective spin-1 and spin-2 subspaces and represent physical spins.

the AKLT model. A pictorial representation of a homogeneous spin-1 VBS state with periodic boundaries is given in Figure 4.1. It is the unique ground state for the special case

$$H_{\mathrm{AKLT}} = \sum_{k=1}^{L} \pi_2(k, k+1) = \sum_{k=1}^{L} \frac{1}{6}\big[(\mathbf{S}_k \cdot \mathbf{S}_{k+1})^2 + 3\mathbf{S}_k \cdot \mathbf{S}_{k+1} + 2\big], \tag{4.3}$$

with the spin $\mathbf{S}_{L+1}$ identified with $\mathbf{S}_1$. For a homogeneous spin-s AKLT chain, the VBS ground state depicted in Figure 4.1 generalizes to one with s valence bonds connecting neighboring spins. The AKLT hamiltonian in this case is

$$H^s_{\mathrm{AKLT}} = \sum_{k=1}^{L} \sum_{J=s+1}^{2s} C_J \pi_J(k, k+1), \quad C_J > 0. \tag{4.4}$$

4.1.2 Matrix product states

The translationally invariant VBS state is conveniently represented in the form of a matrix product state $|\mathrm{MPS}\rangle$ [135–138]. For a periodic chain of L identical spins the matrix product state is written as

$$|\mathrm{MPS}\rangle = \mathrm{tr}\big(\mathbf{g}_1 \cdot \mathbf{g}_2 \cdot \ldots \mathbf{g}_L\big), \tag{4.5}$$

where the $\mathbf{g}_j$ are $D \times D$ matrices with elements that are state vectors and the trace operation is done over the auxiliary matrix space. The elements of $\mathbf{g}_j$ are

$$(\mathbf{g}_j)_{\alpha\beta} = \sum_m A_{\alpha\beta}(m)|m\rangle_j. \tag{4.6}$$

The set $\{|m\rangle_j\}$ is a complete orthonormal basis for the Hilbert space of the spin at site j and the coefficients $A_{\alpha\beta}(m)$ are independent of the site index. Due to translational invariance, we omit the site label j whenever possible. We denote the matrix dual to $\mathbf{g}$ as $\bar{\mathbf{g}}$ with elements $(\bar{\mathbf{g}})_{\alpha\beta} = \sum_m A^*_{\alpha\beta}(m)\langle m|$. Here, the coefficients are replaced by their complex conjugates and the kets are replaced by the corresponding bras. In the MPS construction (4.5) the matrix multiplication ($\cdot$) involves tensor products of vector matrix elements, that is,

$$(\mathbf{g}_j \cdot \mathbf{g}_{j+1})_{\alpha\gamma} = \sum_{\beta mn} A_{\alpha\beta}(m)A_{\beta\gamma}(n)\,|m\rangle_j \otimes |n\rangle_{j+1}. \tag{4.7}$$

The dual $(\bar{\mathbf{g}}_j \cdot \bar{\mathbf{g}}_{j+1})_{\alpha\gamma}$ is defined analogously:

$$(\bar{\mathbf{g}}_j \cdot \bar{\mathbf{g}}_{j+1})_{\alpha\gamma} = \sum_{\beta mn} A^*_{\alpha\beta}(m)A^*_{\beta\gamma}(n)\,\langle m|_j \otimes \langle n|_{j+1}. \tag{4.8}$$

For products of $\mathbf{g}$ matrices denoting a block of sequential spins we introduce an abbreviation

$$(\mathbf{g}_j \cdot \mathbf{g}_{j+1} \cdot \ldots \cdot \mathbf{g}_{j'})_{\alpha\alpha'} = |\alpha\alpha'; j, j'\rangle. \tag{4.9}$$

These vectors span the Hilbert space of the block of spins from j to j' and we refer to them as block state vectors.

For the spin-1 AKLT model, we denote the ground state vector as $|\mathrm{VBS}^1_1\rangle$. Its matrix product form may be generated from the $\mathbf{g}_j$ matrix

$$\mathbf{g}_j = \begin{pmatrix} |0\rangle_j & -\sqrt{2}|+\rangle_j \\ \sqrt{2}|-\rangle_j & -|0\rangle_j \end{pmatrix}, \tag{4.10}$$

where $\{|-\rangle_j, |0\rangle_j, |+\rangle_j\}$ are eigenvectors of the spin-1 operator S^z_j at site j [136, 139]. In Section 4.2.2 we derive this matrix for the more general case of a q-deformed AKLT model.

The matrix product formulation allows for the calculation of important quantities such as correlation functions and the reduced density matrix by transfer matrix methods. A transfer matrix $\mathbf{G}$ is constructed from the MPS matrix $\mathbf{g}$ through the definition $\mathbf{G} \equiv \bar{\mathbf{g}} \otimes \mathbf{g}$. The (scalar) elements of the transfer matrix are thus

$$(\mathbf{G})_{\alpha\gamma,\beta\delta} \equiv (\bar{\mathbf{g}})_{\alpha\beta}(\mathbf{g})_{\gamma\delta} = \sum_m A^*_{\alpha\beta}(m)A_{\gamma\delta}(m). \tag{4.11}$$

In terms of this transfer matrix, the norm of a translationally invariant MPS is

$$\langle \mathrm{MPS}|\mathrm{MPS}\rangle = \mathrm{tr}\,\mathbf{G}^L. \tag{4.12}$$

The expectation value of a local operator A_j at site j is therefore

$$\langle A_j\rangle = \frac{\mathrm{tr}\big(\mathbf{G}_A\mathbf{G}^{L-1}\big)}{\mathrm{tr}\,\mathbf{G}^L}, \tag{4.13}$$

where $\mathbf{G}_A \equiv \bar{\mathbf{g}} \otimes A\mathbf{g}$. In like fashion, two-point correlation functions are given by

$$\langle A_1 B_r\rangle = \frac{\mathrm{tr}\big(\mathbf{G}_A\mathbf{G}^{r-2}\mathbf{G}_B\mathbf{G}^{L-r}\big)}{\mathrm{tr}\,\mathbf{G}^L}. \tag{4.14}$$

In the double scaling limit of $r \to \infty$ and $L - r \to \infty$, the leading asymptotic behavior of the correlation functions can be obtained from power methods by considering the dominant eigenvalues of the transfer matrix and their corresponding eigenvectors.

Additionally, the reduced density matrix can be written in terms of the transfer matrix. The full density matrix of the MPS is

$$\rho = \frac{\mathrm{tr}[\mathbf{g}_1 \bullet \ldots \bullet \mathbf{g}_L]\,\mathrm{tr}[\bar{\mathbf{g}}_1 \bullet \ldots \bullet \bar{\mathbf{g}}_L]}{\mathrm{tr}\,\mathbf{G}^L}. \tag{4.15}$$

Taking the partial trace over the Hilbert spaces of the spins in region B (sites

$j = \ell + 1$ to $j = L$) yields

$$\rho_\ell = \mathrm{tr}_B\, \rho = \sum_{\alpha\alpha'\beta\beta'} \frac{|\alpha\alpha'; 1, \ell\rangle \big(\mathbf{G}^{L-\ell}\big)_{\alpha'\beta',\alpha\beta} \langle\beta\beta'; 1, \ell|}{\mathrm{tr}\, \mathbf{G}^L}. \tag{4.16}$$

We find that ρ_ℓ acts in the subspace spanned by the block state vectors $\{|\alpha\alpha'; 1, \ell\rangle\}$. The dimension of this subspace is at most D^2. This result highlights an important feature of matrix product states: the dimension of the relevant Hilbert space spanned by the block state vectors does not increase exponentially with block length. Furthermore, due to the frustration-free property of the VBS_q^s state, this subspace corresponds to the ground state space of the block hamiltonian $H_{\mathrm{block}} = \sum_{i=1}^{\ell-1} h_{i,i+1}$ [140, 141].

We construct an overlap matrix $\mathbf{K}(n)$ that is related to the n^{th} power of $\mathbf{G}$ by

$$\big(\mathbf{K}(n)\big)_{\alpha\alpha',\beta\beta'} \equiv (\mathbf{G}^n)_{\alpha\beta,\alpha'\beta'} = \langle\alpha\alpha'; 1, n|\beta\beta'; 1, n\rangle. \tag{4.17}$$

This matrix contains all scalar products (overlaps) between block state vectors and is identical to the overlap matrices defined in Section 3.7.3. For the AKLT models described here, $\langle\alpha\alpha'; 1, n|\beta\beta'; 1, n\rangle = \langle\alpha'\alpha; 1, n|\beta'\beta; 1, n\rangle$ and the matrix $\mathbf{K}(n)$ is symmetric. We can therefore express the reduced density matrix in terms of overlap matrices according to:

$$\rho_\ell = \sum_{\alpha\alpha'\beta\beta'} \frac{|\alpha\alpha'; 1, \ell\rangle \big(\mathbf{K}(L-\ell)\big)_{\alpha\alpha',\beta\beta'} \langle\beta\beta'; 1, \ell|}{\mathrm{tr}\, \mathbf{G}^L}. \tag{4.18}$$

The indices are now matched so that we can express ρ_ℓ as a product of matrices. Suitable similarity transformations within the space spanned by $\{|\alpha\alpha'; 1, \ell\rangle\}$ gives the matrix

$$\tilde{\rho}_\ell = \frac{\mathbf{K}(L-\ell)\mathbf{K}(\ell)}{\mathrm{tr}[\mathbf{K}(L-\ell)\mathbf{K}(\ell)]}, \tag{4.19}$$

which has the same spectrum as ρ_ℓ. Thus, for an MPS the reduced density matrix ρ_ℓ has a small number of nonzero eigenvalues, $\mathrm{rank}\, \rho_\ell \leq D^2$ [142, 143]. That is, the dimensions of the $D \times D$ MPS matrix $\mathbf{g}$ gives an upper bound $S_{\mathrm{ub}} = 2 \log D$ for the entanglement entropy of a matrix product state.

4.1.3 Chapter outline

In this chapter, we investigate the entanglement present in the ground state of an $\mathrm{SU}_q(2)$ generalization of the integer spin-s AKLT model (Section 4.2). This ground state is a q-deformed VBS state and we denote its state vector as $|\mathrm{VBS}_q^s\rangle$. The spatially partitioned reduced density matrix is calculated and diagonalized in Section 4.3. The eigenvalues of this matrix are then used to measure entanglement in the system through the entanglement entropies and entanglement spectrum (Section 4.4). Concluding remarks are given in Section 4.5. Finally, a similar analysis of the entanglement in another anisotropic quantum spin chain is given in Section 4.7.

4.2 q-deformed AKLT model

The q-deformed AKLT (AKLT_q) model is an $\mathrm{SU}_q(2)$ [144, 145] invariant generalization of the isotropic SU(2) model described in the previous section. This continuous one parameter (q) generalization of the underlying symmetry group introduces anisotropy into the model by a continuous deformation of the usual SU(2) symmetry. For example, this q-deformation of SU(2) symmetry appears naturally in the anisotropic spin-1/2 XXZ Heisenberg model [146]. Hence, this study aims to determine how entanglement in a VBS state is affected by anisotropy. There have been previous studies of the effects of anistropy on the entanglement in VBS states [147–149], but here we still maintain the symmetry of the $\mathrm{SU}_q(2)$ quantum group. This allows us to obtain exact and compact results through the matrix product formalism and by use of q-deformed Clebsch–Gordan coefficients and $6j$ symbols.

The anisotropic q-deformed generalization of the spin-1 AKLT chain was first considered in Refs. [136, 150, 151]. The ground state of this model has been constructed in the matrix product state formalism [136, 151] and in terms of q-deformed Schwinger bosons [152]. It is separated from excited states by a Haldane gap and the spin-spin correlation functions decay exponentially. The higher integer spin-s generalization of the q-deformed AKLT model was first proposed in Refs. [152, 153], where the spin-spin correlation functions

were obtained. Later, the geometric entanglement and higher order finite-size correction terms for the entanglement entropy were calculated for the spin-s AKLT$_q$ model [154].

In Section 4.2.1 we present the algebra for the SU$_q$(2) quantum group and discuss angular momentum addition for the q-deformed spin states. We continue with the explicit matrix product construction of the ground state of a spin-s AKLT$_q$ model (Section 4.2.2) and the corresponding reduced density matrix.

4.2.1 Quantum algebra

Let us denote states of a spin-s at site j by $|s, m\rangle_j$. Here $m \in \{-s, -s+1, \ldots, s\}$ is the magnetic quantum number denoting the z-component of the spin. The spin quantum number s is unchanged by the action of the q-deformed angular momentum operators $\mathbb{S}_j^{\pm}$ and $\mathbb{S}_j^z$. These operators satisfy the SU$_q$(2) quantum algebra

$$[\mathbb{S}_j^z, \mathbb{S}_j^{\pm}] = \pm \mathbb{S}_j^{\pm}, \qquad [\mathbb{S}_j^+, \mathbb{S}_j^-] = [2\mathbb{S}_j^z], \tag{4.20}$$

where the q-number $[x]$ is defined as

$$[x] \equiv \frac{q^{x/2} - q^{-x/2}}{q^{1/2} - q^{-1/2}}. \tag{4.21}$$

This algebra has a unitary representation for positive real $q \in \mathbb{R}^+$ [155]. It is invariant under the transformation $q \to q^{-1}$ so that we consider further $q \in (0, 1]$. The usual SU(2) algebra is recovered at the isotropic point $q = 1$, while full deformation occurs in the limit $q \to 0^+$.

The actions of these angular momentum operators on the states $|s, m\rangle_j$ are given by

$$\mathbb{S}_j^{\pm}|s, m\rangle_j = \sqrt{[s \mp m][s \pm m + 1]}\,|s, m \pm 1\rangle_j, \tag{4.22}$$

$$\mathbb{S}_j^z|s, m\rangle_j = m\,|s, m\rangle_j. \tag{4.23}$$

The rules of angular momentum addition $\mathbb{J}_{\text{tot}}^{z,\pm} = \mathbb{S}_1^{z,\pm} + \mathbb{S}_2^{z,\pm}$ follow from the

definition of the coproduct

$$\mathbb{J}^{\pm}_{\text{tot}} \equiv \mathbb{S}^{\pm}_1 \otimes q^{\mathbb{S}^z_2/2} + q^{-\mathbb{S}^z_1/2} \otimes \mathbb{S}^{\pm}_2, \tag{4.24}$$

$$\mathbb{J}^{z}_{\text{tot}} \equiv \mathbb{S}^{z}_1 \otimes \mathbb{1}_2 + \mathbb{1}_1 \otimes \mathbb{S}^{z}_2. \tag{4.25}$$

A $(2J+1)$-dimensional irreducible representation for $\mathbb{J}_{\text{tot}}$ is therefore spanned by the states

$$|J, m\rangle \equiv \sum_{m_1, m_2} \begin{bmatrix} s_1 & s_2 & J \\ m_1 & m_2 & m \end{bmatrix}_q |s_1, m_1\rangle \otimes |s_2, m_2\rangle. \tag{4.26}$$

The decomposition coefficients $\left[\begin{smallmatrix} J & K & L \\ m_j & m_k & m_l \end{smallmatrix}\right]_q$ are the q-deformed Clebsch-Gordan (q-CG) coefficients and may be chosen to be real [155–157]. These coefficients vanish if the triangle relation $|s_1 - s_2| \leq J \leq s_1 + s_2$ and selection rule $m_1 + m_2 = m$ are not satisfied (angular momentum conservation). Throughout this chapter, the summation indices m_i (lower row of q-CG symbols) are understood to run over all values compatible with the corresponding quantum number s_i (upper row of q-CG symbols). That is, in Eq. (4.26) we sum over $m_i \in \{-s_i, -s_i+1, \ldots, s_i\}$. For example, the decompositions of the total spin $J = 0, 1, 2$ basis states in terms of tensor products of two spin-1 states are given in Table 4.1 (modulo a normalization factor). Some identities involving the q-CG coefficients that we use in this chapter are collected in Section 4.6.1.

4.2.2 Model and ground state

The q-deformed spin-s AKLT^s_q hamiltonian is given by [136, 153]

$$\mathcal{H}^s_q = \sum_{i=1}^{L} h_{i,i+1} \equiv \sum_{i=1}^{L} \sum_{J=s+1}^{2s} C_J \Pi_J(i, i+1), \quad C_J > 0, \tag{4.27}$$

where $\Pi_J(i, i+1)$ is a projector onto the subspace spanned by the q-deformed total spin-J multiplet formed by the spins at i and $i+1$. This hamiltonian is positive semi-definite like the undeformed AKLT hamiltonian (4.4). The site $L+1$ is identified with site 1 (periodic boundaries). In the basis of physical

$J=0$	$q^{1/2}\|+-\rangle - \|00\rangle + q^{-1/2}\|-+\rangle$
$J=1$	$q\|+0\rangle - \|0+\rangle$ $\|+-\rangle + \left(q^{1/2}-q^{-1/2}\right)\|00\rangle - \|-+\rangle$ $q\|0-\rangle - \|-0\rangle$
$J=2$	$\|++\rangle$ $\|+0\rangle + q\|0+\rangle$ $q^{-1}\|+-\rangle + \left(q^{1/2}+q^{-1/2}\right)\|00\rangle + q\|-+\rangle$ $\|0-\rangle + q\|-0\rangle$ $\|--\rangle$

Table 4.1: Unnormalized q-deformed basis vectors arising from the coupling of two spin-1's.

spin states $\{|s,m_i\rangle_i\}$ we have

$$\begin{aligned}\mathcal{H}_q^s &\equiv \sum_{i=1}^{L}\sum_{J=s+1}^{2s}\sum_{M_i=-J}^{J}|J,M_i\rangle\langle J,M_i|,\\ &= \sum_{i=1}^{L}\sum_{J=s+1}^{2s}\sum_{\substack{m_i,m_{i+1}\\ m_i',m_{i+1}'}}\begin{bmatrix} s & s & J\\ m_i & m_{i+1} & M_i\end{bmatrix}_q\begin{bmatrix} s & s & J\\ m_i' & m_{i+1}' & M_i\end{bmatrix}_q\\ &\qquad\times|s,m_i\rangle_i\langle s,m_i'|_i\otimes|s,m_{i+1}\rangle_{i+1}\langle s,m_{i+1}'|_{i+1}. \end{aligned}\tag{4.28}$$

where $M_i = m_i + m_{i+1}$ (selection rule for longitudinal component of angular momentum) and we have set $C_J = 1$ for all J. Here we have used the decomposition

$$|J,M_i\rangle \equiv \sum_{m_i m_{i+1}}\begin{bmatrix} s & s & J\\ m_i & m_{i+1} & M_i\end{bmatrix}_q |s,m_i\rangle_i\otimes|s,m_{i+1}\rangle_{i+1}.\tag{4.29}$$

In terms of the undeformed SU(2) spin operators $\mathbf{S}_i$, the AKLT$_q$ Hamiltonian for the spin-1 case is

$$\begin{aligned}\mathcal{H}_q^1 = b\sum_j \big\{ & c\,\mathbf{S}_j\cdot\mathbf{S}_{j+1} + \tfrac{1}{2}\,c\,(q-q^{-1})(S^z_{j+1}-S^z_j) + (c-1) \\ & + \big[\mathbf{S}_j\cdot\mathbf{S}_{j+1} + \tfrac{1}{2}(1-c)(q^{1/2}+q^{-1/2}-2)S^z_jS^z_{j+1} \\ & \quad + \tfrac{1}{4}(1+c)(q^{1/2}-q^{-1/2})(S^z_{j+1}-S^z_j)\big]^2 \\ & + \tfrac{1}{4}\,c\,(1+c)(q^{1/2}-q^{-1/2})(q^{1/2}+q^{-1/2}-2)S^z_jS^z_{j+1}(S^z_{j+1}-S^z_j) \\ & + \tfrac{1}{4}\,c\,(1-c)(q^{1/2}+q^{-1/2}-2)^2(S^z_jS^z_{j+1})^2 \\ & + \tfrac{1}{4}(c-3)\big[\big(c-1+\tfrac{1}{2}(1+c)^2\big)S^z_jS^z_{j+1} \\ & \quad + 2\big(c-\tfrac{1}{8}(1+c)^2\big)\big((S^z_{j+1})^2+(S^z_j)^2\big)\big]\big\},\end{aligned} \tag{4.30}$$

with $c = 1+q+q^{-1}$ and $b = [c\,(c-1)]^{-1}$ [150, 151]. When $q = 1$, we recover the isotropic AKLT hamiltonian. In the limit $q \to 0^+$, the AKLT$_q$ Hamiltonian is dominated by Ising-type interactions. In this case the $\mathbf{g}$ matrix has only one non-zero element $|0\rangle$, which is on the diagonal. The resulting ground state is therefore a product state $\bigotimes_j |0\rangle_j$ describing a magnet polarized in the transverse direction. In this limit all spins are in the $S^z_j = 0$ state. Hence, any block in the chain has zero entropy and we shall sometimes refer to the limit $q \to 0^+$ as the classical limit.

Let us denote the frustration-free ground state vector of the AKLT^s_q model by $|\mathrm{VBS}^s_q\rangle$. This ground state may be constructed by the matrix product formalism (Section 4.1.2):

$$|\mathrm{VBS}^s_q\rangle = \mathrm{tr}\big(\mathbf{g}_1\cdot\mathbf{g}_2\cdot\ldots\mathbf{g}_L\big), \tag{4.31}$$

where $\mathbf{g}_i$ are $(s+1)\times(s+1)$ matrices. The elements of $\mathbf{g}_i$ and its dual $\bar{\mathbf{g}}_i$ are given by the state vectors:

$$(\mathbf{g}_i)_{ab} = \sum_m \begin{bmatrix} s & s/2 & s/2 \\ m & b & a \end{bmatrix}_q |s,m\rangle_i, \tag{4.32}$$

$$(\bar{\mathbf{g}}_i)_{ab} = \sum_m \begin{bmatrix} s & s/2 & s/2 \\ m & b & a \end{bmatrix}_q \langle s,m|_i. \tag{4.33}$$

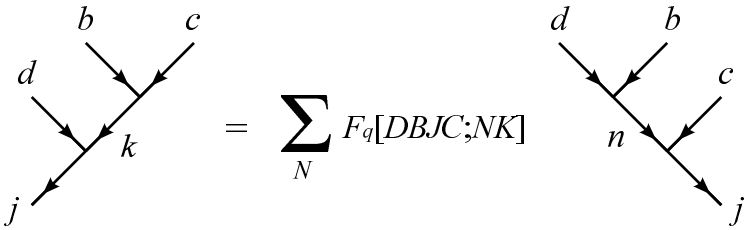

Figure 4.2: The q-deformed F-matrix relates the linearly dependent bases that result from the different orders in which three angular momenta are coupled.

As in the undeformed model, this ground state is annihilated by the local hamiltonian density $h_{i,i+1}$. To prove this, we look at the overlap between the two states $|J, M_i\rangle$ (4.29) and

$$(\mathbf{g}_i \cdot \mathbf{g}_{i+1})_{ac} = \sum_{bm_i m_{i+1}} \begin{bmatrix} s & s/2 & s/2 \\ m_{i+1} & c & b \end{bmatrix}_q \begin{bmatrix} s & s/2 & s/2 \\ m_i & b & a \end{bmatrix}_q |s, m_i\rangle_i \otimes |s, m_{i+1}\rangle_{i+1}. \quad (4.34)$$

Since the states $\{|s, m_i\rangle_i\}$ are orthonormal to each other, we obtain

$$\langle J, M_i|(\mathbf{g}_i \cdot \mathbf{g}_{i+1})_{ac} = \sum_{bm'm} \begin{bmatrix} s & s & J \\ m & m' & M_i \end{bmatrix}_q \begin{bmatrix} s & s/2 & s/2 \\ m' & c & b \end{bmatrix}_q \begin{bmatrix} s & s/2 & s/2 \\ m & b & a \end{bmatrix}_q . \quad (4.35)$$

Applying an identity (4.100) derived in Section 4.6.2 gives

$$\langle J, M_i|(\mathbf{g}_i \cdot \mathbf{g}_{i+1})_{ac} = F_q\left[ss\tfrac{s}{2}\tfrac{s}{2}; J\tfrac{s}{2}\right] \begin{bmatrix} J & s/2 & s/2 \\ M_i & c & a \end{bmatrix}_q . \quad (4.36)$$

The elements $F_q[DBJC; NK]$ of the q-deformed F-matrix are defined diagrammatically in Figure 4.2 and calculated in Section 4.6.2. Due to the triangle relation, the q-CG coefficient in the overlap (4.36) vanishes whenever $J > \frac{s}{2} + \frac{s}{2}$, so that $h_{i,i+1}|\mathrm{VBS}_q^s\rangle = 0$. Since $h_{i,i+1}$ is a sum of projectors (times positive constants) it has nonnegative eigenvalues. Thus, $|\mathrm{VBS}_q^s\rangle$ is the ground state of the AKLT_q^s hamiltonian (4.27).

4.3 Reduced density matrix

To calculate the reduced density matrix for the AKLT$_q^s$ model, we use the matrix product formalism mentioned in Section 4.1.2. Let us construct the transfer matrix $\mathbf{G}$, which is defined in terms of $\mathbf{g}$ and $\bar{\mathbf{g}}$ by $(\mathbf{G})_{ab;cd} = (\bar{\mathbf{g}})_{ac}(\mathbf{g})_{bd}$. Explicitly, its elements are

$$(\mathbf{G})_{ab;cd} = \sum_{m'} \begin{bmatrix} s & s/2 & s/2 \\ m' & c & a \end{bmatrix}_q \begin{bmatrix} s & s/2 & s/2 \\ m' & d & b \end{bmatrix}_q . \tag{4.37}$$

Let us diagonalize this matrix through an approach based on the q-deformed F-matrix (Section 4.6.2). As depicted in Figure 4.3, we use the q-CG coefficients as an ansatz for the elements of the eigenvector e_{cd} for the eigenvalue equation $(\mathbf{G})_{ab;cd}e_{cd} = \lambda e_{ab}$. The resulting equation is

$$\begin{aligned} (\mathbf{G})_{ab;cd}e_{cd} &= \sum_{cdm'} \begin{bmatrix} s & s/2 & s/2 \\ m' & c & a \end{bmatrix}_q \begin{bmatrix} s/2 & j & s/2 \\ c & m & d \end{bmatrix}_q \begin{bmatrix} s & s/2 & s/2 \\ m' & d & b \end{bmatrix}_q , \\ &= \lambda_{jm} \begin{bmatrix} s/2 & j & s/2 \\ a & m & b \end{bmatrix}_q . \end{aligned} \tag{4.38}$$

This expression may be summed by using the identity (4.100), which gives

$$(\mathbf{G})_{ab;cd}e_{cd} = F_q\left[s\tfrac{s}{2}\tfrac{s}{2}j;\tfrac{s}{2}\tfrac{s}{2}\right] \begin{bmatrix} s/2 & j & s/2 \\ a & m & b \end{bmatrix}_q \equiv \lambda_{jm} \begin{bmatrix} s/2 & j & s/2 \\ a & m & b \end{bmatrix}_q . \tag{4.39}$$

We find that the elements of the eigenvectors of the transfer matrix $\mathbf{G}$ are $e_{ab} = (\mathbf{e}_{jm})_{ab} = \left[\begin{smallmatrix} s/2 & j & s/2 \\ a & m & b \end{smallmatrix}\right]_q$. These eigenvectors are labeled by the quantum numbers $j \in \{0, 1, \ldots, s\}$ and $m \in \{-j, -j+1, \ldots, j\}$. They correspond to the eigenvalues

$$\lambda_{jm} = F_q\left[s\tfrac{s}{2}\tfrac{s}{2}j;\tfrac{s}{2}\tfrac{s}{2}\right] = (-1)^j[s+1] \begin{Bmatrix} s & s/2 & s/2 \\ j & s/2 & s/2 \end{Bmatrix}_q , \tag{4.40}$$

where the q-deformed $6j$ symbol $\left\{\begin{smallmatrix} A & B & E \\ D & C & F \end{smallmatrix}\right\}_q$ is defined in Eq. (4.102). The eigenvalue λ_{jm} is $(2j+1)$-fold degenerate, which corresponds to the $2j+1$

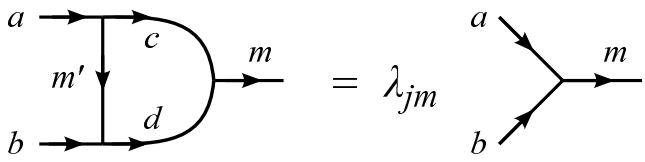

Figure 4.3: Diagonalization of the transfer matrix.

possible values of m. Thus, we can label the eigenvalue $\lambda_{jm} \to \lambda_j$ for brevity. The absolute value of λ_j decreases with increasing j so that the dominant (nondegenerate) eigenvalue is λ_0.

With the column transposition identities in Section 4.6.1 we are able to contruct the vectors $\bar{\mathbf{e}}_{jm}$ dual to the eigenvectors $\mathbf{e}_{jm}$:

$$(\bar{\mathbf{e}}_{jm})_{ab} = (-1)^{a+j-s/2} q^{-a/2} \sqrt{\frac{[2j+1]}{[s+1]}} \begin{bmatrix} s/2 & s/2 & j \\ -a & b & m \end{bmatrix}_q . \tag{4.41}$$

These pairs of eigenvectors satisfy orthonormality $\bar{\mathbf{e}}_{j'm'} \cdot \mathbf{e}_{jm} = \delta_{jj'}\delta_{mm'}$ and completeness $\sum_{jm} (\mathbf{e}_{jm})_{ab} (\bar{\mathbf{e}}_{jm})_{cd} = \delta_{ac}\delta_{bd}$. Using the column transposition identities(4.95), a suitable similarity transformation on $\mathbf{G}$ allows us to construct the projection matrix

$$(\mathbf{P}_j)_{ab;cd} = \sum_{m=-j}^{j} \begin{bmatrix} s/2 & s/2 & j \\ -a & b & m \end{bmatrix}_q \begin{bmatrix} s/2 & s/2 & j \\ -c & d & m \end{bmatrix}_q . \tag{4.42}$$

This matrix projects a state vector onto the subspace spanned by the eigenvectors corresponding to the eigenvalue λ_j. The elements of the projection matrix onto the dominant eigenspace ($j = 0$) simplifies to

$$(\mathbf{P}_0)_{ab;cd} = \begin{bmatrix} s/2 & s/2 & 0 \\ -a & b & 0 \end{bmatrix}_q \begin{bmatrix} s/2 & s/2 & 0 \\ -c & d & 0 \end{bmatrix}_q = \frac{(-1)^{a+c+S} q^{-(a+c)/2}}{[s+1]} \delta_{ab}\delta_{cd}. \tag{4.43}$$

We now use the general formula (4.19) for the reduced density matrix (up to a similarity transformation) of a matrix product state to obtain

$$(\rho_\ell)_{ab;cd} = \frac{1}{\operatorname{tr} \mathbf{G}^L} \sum_{a'b'} \left(\mathbf{G}^{L-\ell}\right)_{aa';bb'} \left(\mathbf{G}^{\ell}\right)_{a'c;b'd}. \tag{4.44}$$

Integer powers of the transfer matrix $\mathbf{G}$ may be written in terms of the projection matrices (4.42) as

$$\mathbf{G}^n = \sum_j \lambda_j^n \mathbf{P}_j. \tag{4.45}$$

Since the dominant eigenvalue of $\mathbf{G}$ is λ_0, large integer powers of $\mathbf{G}$ simplify to $\mathbf{G}^n \to \lambda_0^n \mathbf{P}_0$ as $n \to \infty$. Thus, in the limit of infinite chains $L \to \infty$ the reduced density matrix (4.44) simplifies to

$$(\rho_\ell)_{ab;cd} = \frac{(-1)^{a+b+s} q^{-(a+b)/2}}{[s+1]} \sum_{j=0}^{s} \frac{\lambda_j^\ell}{\lambda_0^\ell} \sum_{m=-j}^{j} \begin{bmatrix} s/2 & s/2 & j \\ -a & c & m \end{bmatrix}_q \begin{bmatrix} s/2 & s/2 & j \\ -b & d & m \end{bmatrix}_q. \tag{4.46}$$

We can further express the reduced density matrix as a sum of matrix outer products by defining the $(s+1) \times (s+1)$ matrix

$$\left(\mathbf{Q}_{jm}\right)_{ac} \equiv \frac{(-1)^{a+s/2} q^{-a/2}}{\sqrt{[s+1]}} \begin{bmatrix} s/2 & s/2 & j \\ -a & c & m \end{bmatrix}_q \delta_{m,c-a}. \tag{4.47}$$

Making the necessary substitutions gives the compact form

$$\rho_\ell = \sum_{j=0}^{s} \frac{\lambda_j^\ell}{\lambda_0^\ell} \sum_{m=-j}^{j} \mathbf{Q}_{jm} \otimes \mathbf{Q}_{jm}. \tag{4.48}$$

Let us express the reduced density matrix in the basis of the following vectors:

$$(\mathbf{v}_{JM})_{ab} = \frac{(-1)^{-(J+b)} q^{b/2}}{\sqrt{[2J+1]}} \begin{bmatrix} s/2 & s/2 & J \\ a & -b & M \end{bmatrix}_q, \tag{4.49}$$

with corresponding dual

$$(\bar{\mathbf{v}}_{JM})_{ab} = (-1)^{J+b} q^{-b/2} \sqrt{[2J+1]} \begin{bmatrix} s/2 & s/2 & J \\ a & -b & M \end{bmatrix}_q. \tag{4.50}$$

This choice of basis allows us to use identity (4.100) and get

$$(\rho_\ell)_{J'M',JM} = \frac{(-1)^{J'-J}}{[s+1]^2}\sqrt{\frac{[2J'+1]}{[2J+1]}}\left(1+\sum_{j=1}^{s}[2j+1]\frac{\lambda_j^\ell}{\lambda_0^\ell}F_q\left[j\,\tfrac{s}{2}\,\tfrac{s}{2}J;\,\tfrac{s}{2}\,\tfrac{s}{2}\right]\right) \times \delta_{M'M}\sum_{ab} q^{-(a+b)}\begin{bmatrix} s/2 & s/2 & J' \\ a & -b & M\end{bmatrix}_q\begin{bmatrix} s/2 & s/2 & J \\ a & -b & M\end{bmatrix}_q. \quad (4.51)$$

We find that the reduced density matrix can be decomposed into sectors labeled by the quantum number $M \in [-s, s]$. Each sector is represented by an $(s+1-|M|)\times(s+1-|M|)$ matrix.

The reduced density matrix can be diagonalized analytically for the following special cases: The double scaling limit of long blocks $\ell \to \infty$ (Section 4.3.1), the spin-1 case (Section 4.3.2), and the isotropic limit $q = 1$ (Section 4.3.3). For higher integer spin $s > 1$ and finite blocks we give a perturbation solution about the double scaling limit (Section 4.3.4).

4.3.1 Double scaling limit

In the double scaling limit, we consider infinitely long blocks and take $\ell \to \infty$. The reduced density matrix ρ_∞ (4.48) simplifies to a Kronecker product of diagonal matrices $\rho_\infty = \mathbf{Q}_{00} \otimes \mathbf{Q}_{00}$. Explicitly, we have:

$$(\rho_\infty)_{ab;cd} = \frac{(-1)^{a+b+S}q^{-(a+b)/2}}{[s+1]}\begin{bmatrix} s/2 & s/2 & 0 \\ -a & a & 0\end{bmatrix}_q\begin{bmatrix} s/2 & s/2 & 0 \\ -b & b & 0\end{bmatrix}_q\delta_{ac}\delta_{bd}. \quad (4.52)$$

The eigenvalues of the reduced density matrix are therefore

$$(\rho_\infty)_{ab;cd} = \frac{q^{-(a+b)}}{[s+1]^2}\delta_{ac}\delta_{bd}. \quad (4.53)$$

For example, in the case of a q-deformed spin-2 VBS state we have

$$\rho_\infty = \frac{1}{(1+q+q^{-1})^2}\begin{pmatrix} q^{-1} & 0 & 0 \\ 0 & 1 & 0 \\ 0 & 0 & q\end{pmatrix}\otimes\begin{pmatrix} q^{-1} & 0 & 0 \\ 0 & 1 & 0 \\ 0 & 0 & q\end{pmatrix}. \quad (4.54)$$

The eigenvalues of this matrix are proportional to $\{q^2, q, q, 1, 1, 1, q^{-1}, q^{-1}, q^{-2}\}$ (the proportionality constant is $1/(1+q+q^{-1})^2$).

4.3.2 Spin-1 case

For the spin-1 case, the reduced density matrix in the $\mathbf{v}_{JM}$ basis (4.51) is block diagonal in three sectors. The sector labeled by $M = 0$ is 2×2 dimensional, while the sectors $M = \pm 1$ are 1×1. An exact diagonalization is therefore possible. A direct calculation gives the following eigenvalues of ρ_ℓ:

$$\begin{aligned} p_{\pm,0} &= \frac{q + q^{-1} + 2(-\Lambda)^{-\ell}}{2(2+q+q^{-1})} \pm \sqrt{\frac{1}{4} - \frac{1-(-\Lambda)^{-2\ell}}{2+q+q^{-1}}}, \\ p_{1,\pm 1} &= \frac{1-(-\Lambda)^{-\ell}}{2+q+q^{-1}}, \end{aligned} \tag{4.55}$$

where $\Lambda = 1 + q + q^{-1}$. The finite-size corrections decay exponentially as expected for a gapped system. At $q = 1$ we recover the eigenvalues

$$p_{+,0} = \frac{1+3(-3)^{-\ell}}{4}, \quad p_{1,\pm 1} = p_{-,0} = \frac{1-(-3)^{-\ell}}{4}, \tag{4.56}$$

that were obtained for the isotropic AKLT chain [158].

4.3.3 Isotropic case

When $q = 1$ the vectors $\mathbf{v}_{JM}$ (4.49) are eigenvectors of the reduced density matrix. The exact $(2J+1)$-fold degenerate eigenvalues are

$$\begin{aligned} p_{JM} &= \frac{1}{(s+1)^2}\left(1 + \sum_{j=1}^{s}(2j+1)\frac{\lambda_j^\ell}{\lambda_0^\ell}\, F_1\left[j\,\tfrac{s}{2}\,\tfrac{s}{2}\,J;\,\tfrac{s}{2}\,\tfrac{s}{2}\right]\right), \\ &= \frac{1}{(s+1)^2} + \frac{(-1)^{J+s}}{s+1}\sum_{j=1}^{s}(-1)^j(2j+1)\,\frac{\lambda_j^\ell}{\lambda_0^\ell}\begin{Bmatrix} j & s/2 & s/2 \\ J & s/2 & s/2 \end{Bmatrix}_1. \end{aligned} \tag{4.57}$$

For instance, taking $s = 2$ gives the exact eigenvalues

$$p_{00} = \tfrac{1}{9}\left(1 + 3(-2)^{-\ell} + 5(10)^{-\ell}\right), \qquad \text{(degeneracy 1)}, \tag{4.58}$$

$$p_{1M} = \tfrac{1}{9}\left(1 + \tfrac{3}{2}(-2)^{-\ell} - \tfrac{5}{2}(10)^{-\ell}\right), \qquad \text{(degeneracy 3)}, \tag{4.59}$$

$$p_{2M} = \tfrac{1}{9}\left(1 - \tfrac{3}{2}(-2)^{-\ell} + \tfrac{1}{2}(10)^{-\ell}\right), \qquad \text{(degeneracy 5)}. \tag{4.60}$$

The formula (4.57) reproduces the previous results [140, 159] for undeformed spin-s AKLT chains obtained from the Schwinger boson representation of the VBS state. Our approach, however, emphasizes the role of the $6j$ symbols in determining the finite-size corrections to the entanglement in isotropic VBS states. Furthermore, this result solves a recursive formula [140, 159] for the coefficients in the sums for the eigenvalues p_{JM}.

4.3.4 Anisotropic case

The magnitude of the eigenvalues $|\lambda_j|$ of the reduced density matrix decreases with increasing j. Thus, the leading order finite-size correction to ρ_ℓ depends on $|\lambda_1/\lambda_0| = [s]/[s+2] < 1$. We may therefore approximate the reduced density matrix as

$$\rho_\ell \approx \mathbf{Q}_{00} \otimes \mathbf{Q}_{00} + \frac{\lambda_1^\ell}{\lambda_0^\ell} \sum_{m=-1}^{1} \mathbf{Q}_{1m} \otimes \mathbf{Q}_{1m}. \tag{4.61}$$

We have already determined that $\mathbf{Q}_{00}$ is diagonal with nondegenerate eigenvalues (4.47). This means that first-order perturbation theory within each sector of the preceding equation involves only the diagonal elements of $\mathbf{Q}_{1m}$. From Eq. (4.47) we know that only $\mathbf{Q}_{10}$ has nonzero diagonal elements and hence we obtain the approximate eigenvalues

$$p_{ab} = p_{ba} \approx \frac{q^{-(a+b)}}{[s+1]^2}\left(1 + [3]\,\frac{\lambda_1^\ell}{\lambda_0^\ell}\begin{bmatrix} s/2 & 1 & s/2 \\ a & 0 & a \end{bmatrix}_q \begin{bmatrix} s/2 & 1 & s/2 \\ b & 0 & b \end{bmatrix}_q\right). \tag{4.62}$$

The labels a and b are eigenvalue labels that run from $-s/2$ to $s/2$ with integer steps. The second term in (4.62) involving the q-CG coefficients may

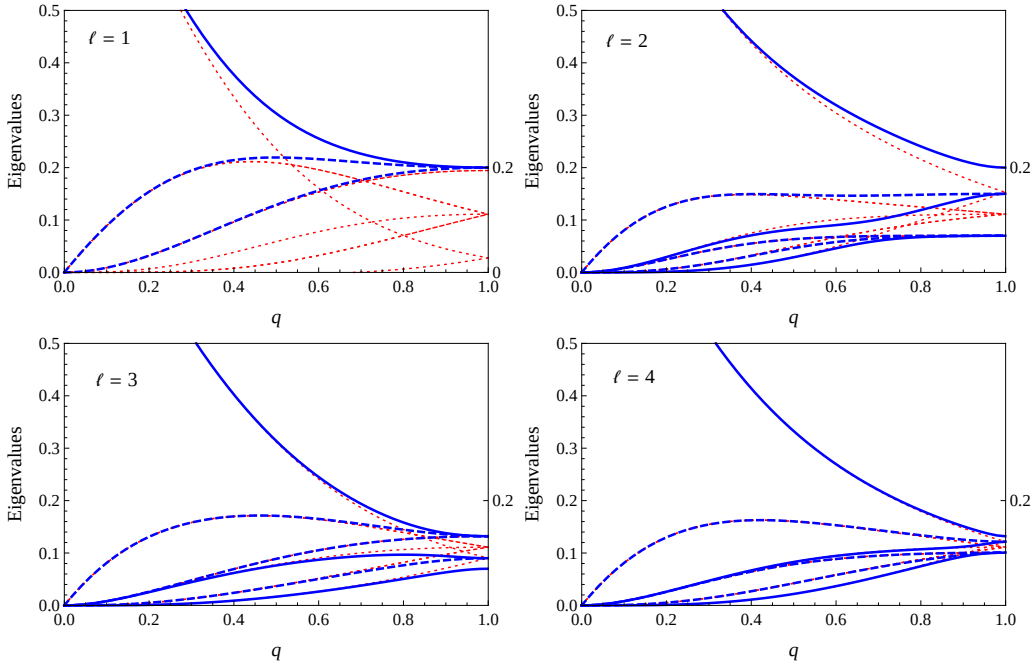

Figure 4.4: The eigenvalues of the reduced density matrix of a block of ℓ spins in a spin-2 VBS_q state (solid and dashed blue lines) are compared to the perturbation result (red dotted lines). Solid blue lines denote nondegenerate eigenvalues while dashed blue lines denote doubly degenerate ones. The dominant eigenvalue approaches unity as $q \to 0$. For $\ell = 1$ four eigenvalues are zero for all q.

be evaluated explicitly with the identity [155]

$$\begin{bmatrix} s/2 & 1 & s/2 \\ a & 0 & a \end{bmatrix}_q = \frac{q^{-a/2}}{\sqrt{[s][s+2]}} \left\{ q^{\frac{1}{2}(1+s/2)} \left[\tfrac{s}{2}+a\right] - q^{-\frac{1}{2}(1+s/2)} \left[\tfrac{s}{2}-a\right] \right\}. \tag{4.63}$$

These approximate eigenvalues are compared to exact numerical results for the spin-2 case in Figure 4.4. We observe a rapid improvement in the accuracy of the perturbation result with increasing block length ℓ. Furthermore, these numerical results reveal how q-deformation modifies the degeneracy of the entanglement spectrum by breaking the multiplet structure present in the isotropic case.

4.4 Entanglement entropies and spectrum

Entanglement in the ground states of isotropic AKLT models has been studied in the literature [140, 141, 158–164]. In this section we give quantitative measures of the entanglement in the VBS_q^s ground state of the anisotropic AKLT model. From the reduced density matrix ρ_ℓ of blocks of length ℓ obtained in the previous section, we evaluate the the Rényi and von Neumann entanglement entropies

$$S_{\mathrm{R}}(\alpha) \equiv \frac{\log \operatorname{tr} \rho_\ell^\alpha}{1-\alpha}, \tag{4.64}$$

$$S_{\mathrm{vN}} \equiv -\operatorname{tr}(\rho_\ell \log \rho_\ell) = \lim_{\alpha \to 1} S_{\mathrm{R}}(\alpha). \tag{4.65}$$

As discussed in Section 3.1, these quantities are frequently used measures of entanglement in pure states [62, 74–78]. Additionally, we use the full set of eigenvalues of the reduced density matrix to obtain the entanglement spectrum of the block [165]. This entanglement spectrum describes the mixed state of the block that results from tracing over the environmental degrees of freedom. That is, we write $\rho_\ell = e^{-\beta H_{\mathrm{eff}}} / \operatorname{tr} e^{-\beta H_{\mathrm{eff}}}$, where H_{eff} is an effective Hamiltonian and $1/\beta$ an effective temperature. The eigenvalue spectrum of this effective Hamiltonian constitutes the entanglement spectrum of the block. As we see below, the entanglement spectrum allows one to interpret block entanglement in terms of interacting boundary degrees of freedom.

4.4.1 Double scaling limit

In the double scaling limit of an infinite block $\ell \to \infty$ in an infinite chain $(L-\ell) \to \infty$, the reduced density matrix becomes diagonal. Thus, the block states $|\alpha\beta; 1, \ell\rangle$ (4.9) are orthogonal to each other. The eigenvalues of the reduced density matrix are proportional to powers of the deformation parameter (4.53):

$$p_\mu = \frac{q^\mu}{[s+1]^2}, \quad \mu \in \{-s, -s+1, \ldots, s\}. \tag{4.66}$$

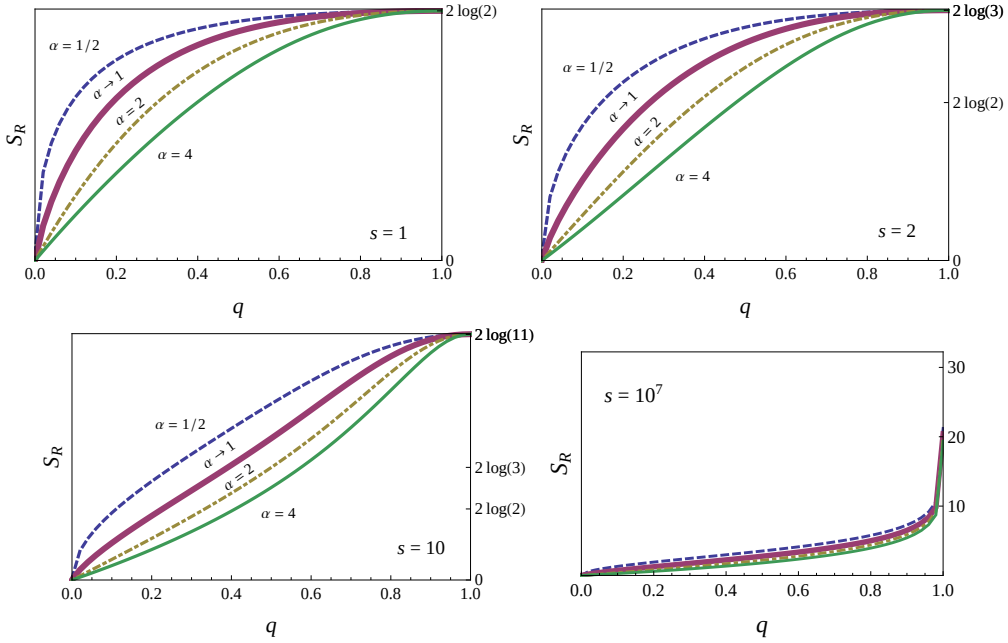

Figure 4.5: The Rényi entropy $S_{\rm R}(\alpha)$ of a q-deformed spin-s VBS state vanishes in the limit $q \to 0^+$. In the double scaling limit, long blocks are maximally entangled $S_{\rm R}(\alpha) = 2\log(s+1)$ at the isotropic point $q = 1$. The von Neumann entropy is obtained in the limit $\alpha \to 1$ (bold line).

The degeneracy of the eigenvalue p_μ is $s + 1 - |\mu|$. We can therefore compute the Rényi entropy exactly

$$\begin{aligned} S_{\rm R}(\alpha) &= \frac{\log \operatorname{tr} \rho^\alpha}{1-\alpha} = \frac{2}{1-\alpha} \log \left\{ \frac{q^{\alpha(s+1)/2} - q^{-\alpha(s+1)/2}}{q^{\alpha/2} - q^{-\alpha/2}} \, \frac{1}{[s+1]^\alpha} \right\}, \\ &= \frac{2}{1-\alpha} \log \left\{ \frac{q^{\alpha(s+1)/2} - q^{-\alpha(s+1)/2}}{q^{\alpha/2} - q^{-\alpha/2}} \left(\frac{q^{\frac{1}{2}} - q^{-\frac{1}{2}}}{q^{(s+1)/2} - q^{-(s+1)/2}} \right)^\alpha \right\}. \end{aligned} \tag{4.67}$$

Taking the limit $\alpha \to 1$ gives the von Neumann entropy

$$\begin{aligned} S_{\text{vN}} &= 2\log\big([s+1]\big) + \left\{ \frac{q^{\frac{1}{2}} + q^{-\frac{1}{2}}}{q^{\frac{1}{2}} - q^{-\frac{1}{2}}} - (s+1)\frac{q^{(s+1)/2} + q^{-(s+1)/2}}{q^{(s+1)/2} - q^{-(s+1)/2}} \right\} \log q, \\ &= 2\log\left\{ \frac{q^{(s+1)/2} - q^{-(s+1)/2}}{q^{\frac{1}{2}} - q^{-\frac{1}{2}}} \right\} \\ &\quad + \left\{ \frac{q^{\frac{1}{2}} + q^{-\frac{1}{2}}}{q^{\frac{1}{2}} - q^{-\frac{1}{2}}} - (s+1)\frac{q^{(s+1)/2} + q^{-(s+1)/2}}{q^{(s+1)/2} - q^{-(s+1)/2}} \right\} \log q. \end{aligned} \tag{4.68}$$

These entanglement entropies are graphed in Figure 4.5 as functions of the parameter q for different values of the spin s. We see that quantum correlations in the system decrease monotonically as the degree of anisotropy in the model increases. This effect persists even in the limit of long blocks. At the isotropic point $q = 1$, the entanglement entropy is a maximum for any spin s. It simplifies to

$$S_{\text{R}}(\alpha) = S_{\text{vN}} = 2\log(s+1), \qquad q = 1. \tag{4.69}$$

We thus recover previous results [140, 158, 159] for isotropic spin-s VBS states. Meanwhile, in the opposite limit of full deformation $q \to 0^+$ the entanglement entropy vanishes and there are no quantum correlations in the system.

Now, let us consider the case of very high spin at fixed $0 < q < 1$. Taking the limit $s \to \infty$ in (4.67) and (4.68) gives

$$S_{\text{R}}(\alpha) = \frac{2}{1-\alpha}\log\left\{ \frac{\left(q^{-1/2} - q^{1/2}\right)^{\alpha}}{q^{-\alpha/2} - q^{\alpha/2}} \right\}, \tag{4.70}$$

$$S_{\text{vN}} = 2\log\left(\frac{1}{q^{-1/2} - q^{1/2}} \right) + \left(\frac{q^{1/2} + q^{-1/2}}{q^{1/2} - q^{-1/2}} \right) \log q, \qquad s \to \infty. \tag{4.71}$$

We find that the entanglement entropy is bounded for any q-deformed AKLT chain of arbitrary spin s. It diverges only at the isotropic point $q = 1$. This behavior is shown in Figure 4.5 for the high spin case $s = 10^7$.

Finally, let us calculate the entanglement spectrum of the block by writing $\rho_\infty = e^{-\beta H_{\text{eff}}} / \operatorname{tr} e^{-\beta H_{\text{eff}}}$. The tensor product form of ρ_∞ (4.53) yields the simple

paramagnetic model

$$-\beta H_{\text{eff}} = -\beta\big(H_{\text{eff}}^{(1)} + H_{\text{eff}}^{(2)}\big) \equiv \beta h(S_1^z + S_2^z\big), \qquad \mathbf{S}_i^2 = \tfrac{s}{2}\big(\tfrac{s}{2}+1\big), \tag{4.72}$$

$$\beta h = |\log q|\,. \tag{4.73}$$

Here h is the magnitude of an effective magnetic field along the z-axis, while $\mathbf{S}_i$ are spin-$s/2$ operators of the undeformed SU(2) algebra. We can thus identify $|\log q|$ as the ratio h/T_{eff} between the magnitude of the magnetic field and effective temperature T_{eff}. We observe that the spectrum of $H_{\text{eff}}^{(i)}$ consists of $s+1$ equidistant energy levels. Thus, in the limit $s \to \infty$ the entanglement spectrum of the block is equal to the energy spectrum of two harmonic oscillators with frequency ω (with an s-dependent energy shift). This frequency is related to the deformation parameter through $|\log q| = \omega/T_{\text{eff}}$.

In this effective picture, the isotropic case $q = 1$ corresponds to infinite temperature or zero field strength. The reduced density matrix ρ_∞ has $(s+1)^2$ nonzero identical eigenvalues. Therefore, the block is maximally mixed. In the opposite limit $q \to 0^+$ the effective model corresponds to zero temperature or infinite field magnitude. Hence, the block is in a pure state with zero entanglement.

4.4.2 Spin-1 case

The spin-1 case is important because we can obtain exact results for the entanglement entropy at arbitrary anisotropy q and arbitrary block lengths ℓ. We can therefore analytically study the effect of finite block lengths on the entanglement present in the system. Let us first consider the extreme case of a block consisting of only one spin $\ell = 1$. The eigenvalues of the reduced density matrix become

$$p_{+,0} = 1 - \frac{2}{1+q+q^{-1}} = 1 - \frac{2}{\Lambda}, \tag{4.74}$$

$$p_{1,\pm1} = \frac{1}{1+q+q^{-1}} = \frac{1}{\Lambda}, \tag{4.75}$$

$$p_{-,0} = 0, \qquad \ell = 1. \tag{4.76}$$

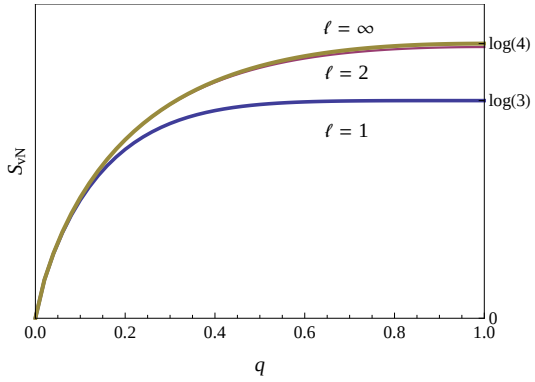

Figure 4.6: The double scaling limit is already approached by a block of two spins in the VBS_q^1 state. For any value of the anisotropy parameter q, the entanglement entropy is bounded by its value in the double scaling limit.

The single-site entanglement entropies are therefore

$$S_{\mathrm{R}}^{\ell=1} = \frac{\log\big((\Lambda-2)^\alpha + 2^\alpha\big) - \alpha\log\Lambda}{1-\alpha}, \tag{4.77}$$

$$S_{\mathrm{vN}}^{\ell=1} = \log\Lambda - \left(1-\frac{2}{\Lambda}\right)\log(\Lambda-2), \quad \Lambda = 1+q+q^{-1}. \tag{4.78}$$

These entropies are zero at the classical limit $q \to 0^+$ and increase monotonically to the saturation value $S_{\mathrm{R}}^{\ell=1} = S_{\mathrm{vN}}^{\ell=1} = \log 3$ at the isotropic point $q = 1$. That is, at the isotropic point the block is in a uniform mixture of the three spin-1 S_z states. For longer blocks, the entanglement entropy reaches its value at the double scaling limit exponentially fast. It is reached when the block length ℓ exceeds the characteristic length $\xi_q = 1/\log\Lambda$. This behavior is shown in Figure 4.6 where the von Neumann entropy of a block of length $\ell = 2$ is nearly indistinguishable from the infinite block entropy for all values of the anisotropy parameter q.

In addition to the effective paramagnetic model (4.72) discussed in the previous section, an alternative model may be constructed for the spin-1 case in the double scaling limit $\ell \to \infty$. We can define the effective temperature

$1/\beta \equiv 1/|\log q|$ and effective Hamiltonian

$$H_{\text{eff}} \equiv \tfrac{1}{2}\big(\sigma_1^x \sigma_\ell^x + \sigma_1^y \sigma_\ell^y\big), \tag{4.79}$$

where σ_j^i are Pauli operators at site j. Thus, $\rho_{\ell\to\infty}$ also describes a thermal ensemble of two spin-1/2's at the block boundaries with Heisenberg (XX) interaction. The anisotropy parameter q determines the effective boundary temperature $T_{\text{eff}} = 1/|\log q|$. For the isotropic AKLT model $q = 1$ the effective boundary spins are in a maximally mixed state ($T_{\text{eff}} \to \infty$), while in the classical limit $q \to 0^+$ they are in a pure state ($T_{\text{eff}} = 0$). This result for the effective Hamiltonian is consistent with the area law for gapped models [63, 166]. It is similar to the effective boundary spin chain proposed for two-dimensional AKLT models [167, 168]. However, in the AKLT$_q^1$ chain the effective boundary spin interaction is long-ranged and exists for arbitrarily long blocks.

4.4.3 Isotropic case

For arbitrary integer spins, the reduced density matrix is diagonalizable analytically at the isotropic limit. When $q = 1$, the eigenvalues p_{JM} are arranged into $(2J+1)$-multiplets (4.57). The leading finite-size correction to the eigenvalue p_{JM} is proportional to the exponential factor $(\lambda_1/\lambda_0)^\ell \equiv (-1)^\ell e^{-\ell/\xi}$. Using the formula

$$\begin{Bmatrix} s & s/2 & s/2 \\ j & s/2 & s/2 \end{Bmatrix}_1 = \frac{(s!)^2}{(s-j)!(s+j+1)!}, \tag{4.80}$$

gives the characteristic length of decay $\xi = 1/\log\big((s+2)/s\big)$. This length is equal to the correlation length of the spin-spin correlation functions in the isotropic spin-s VBS state [153].

A simple result for the entanglement entropy of a block consisting of a single spin $\ell = 1$ can be obtained at the isotropic point. The eigenvalues of

the reduced density matrix may be written as

$$p_{JM}^{\ell=1} = \frac{1}{(s+1)^2} + \frac{(-1)^{J+s}}{\begin{Bmatrix} s & \frac{s}{2} & \frac{s}{2} \\ 0 & \frac{s}{2} & \frac{s}{2} \end{Bmatrix}_1} \sum_{j=1}^{s} \frac{2j+1}{s+1} \begin{Bmatrix} s & \frac{s}{2} & \frac{s}{2} \\ j & \frac{s}{2} & \frac{s}{2} \end{Bmatrix}_1 \begin{Bmatrix} j & \frac{s}{2} & \frac{s}{2} \\ J & \frac{s}{2} & \frac{s}{2} \end{Bmatrix}_1 . \quad (4.81)$$

Making use of the identity (4.80) and

$$\begin{Bmatrix} s & s/2 & s/2 \\ 0 & s/2 & s/2 \end{Bmatrix}_1 \begin{Bmatrix} J & s/2 & s/2 \\ 0 & s/2 & s/2 \end{Bmatrix}_1 = \frac{(-1)^{J+s}}{(s+1)^2}, \quad (4.82)$$

$$\sum_{j=0}^{s} (2j+1) \begin{Bmatrix} s & s/2 & s/2 \\ j & s/2 & s/2 \end{Bmatrix}_1 \begin{Bmatrix} j & s/2 & s/2 \\ J & s/2 & s/2 \end{Bmatrix}_1 = \frac{\delta_{sJ}}{2s+1}, \quad (4.83)$$

gives the desired result

$$p_{JM}^{\ell=1} = \frac{\delta_{sJ}}{2s+1}, \qquad q = 1. \quad (4.84)$$

Thus, the single-site reduced density matrix has $(2s+1)$ nonzero identical eigenvalues. This result proves that the block is a uniform mixture of the $(2s+1)$ states of a single spin-s as expected. The entanglement entropy in this case is $S_{\mathrm{R}}^{\ell=1}(\alpha) = S_{\mathrm{vN}}^{\ell=1} = \log(2s+1)$.

For long blocks satisfying $\ell \gg \xi$, the leading nonvanishing correction to the entanglement entropy is proportional to $(\lambda_1/\lambda_0)^{2\ell}$. The approximate Rényi entropy in this case is

$$S_{\mathrm{R}}(\alpha) \approx 2\log(s+1) - \frac{3\alpha}{2} \left(\frac{s}{s+2}\right)^{2\ell} s(s+1)(s+2). \quad (4.85)$$

Finite-size corrections to the von Neumann entropy can be obtained from this result by taking the limit $\alpha \to 1$. We find that the entanglement entropy exponentially approaches its double scaling limit value $S_{\mathrm{R}}^{\infty}(\alpha) = S_{\mathrm{vN}}^{\infty} = 2\log(s+1)$.

Let us construct an effective Hamiltonian for long blocks $\xi \ll \ell < \infty$ in the isotropic case. Considering only the leading-order correction to the eigenvalues

(4.57) gives

$$p_{JM} \approx \frac{1}{(s+1)^2}\left\{1 - \frac{3}{s(s+2)}\left(\frac{-s}{s+2}\right)^{\ell}\big(2J(J+1) - s(s+2)\big)\right\}. \quad (4.86)$$

Since the reduced density matrix is diagonal in the $\{\mathbf{v}_{JM}\}$ basis, we can write the effective Hamiltonian H_{eff} as

$$\begin{aligned} -\beta H_{\text{eff}} &\approx \log\left\{1 - \frac{3}{s(s+2)}\left(\frac{-s}{s+2}\right)^{\ell}\big(2J(J+1) - s(s+2)\big)\right\}, \\ &\approx -\frac{12}{s(s+2)}\left(\frac{-s}{s+2}\right)^{\ell} \times \tfrac{1}{2}\big\{J(J+1) - s(\tfrac{s}{2}+1)\big\}. \end{aligned} \quad (4.87)$$

This expression is valid for $3s^{\ell}(s+2)^{-\ell} \ll 1$. If we define an undeformed spin-S operator $\mathbf{J} \equiv \mathbf{S}_1 + \mathbf{S}_{\ell}$ as the sum of two spin-$\frac{s}{2}$ operators $\mathbf{S}_1$ and $\mathbf{S}_{\ell}$ on the block boundaries, we obtain the Heisenberg model

$$\beta H_{\text{eff}} = \gamma(s,\ell)\,(-1)^{\ell}\,\mathbf{S}_1 \cdot \mathbf{S}_{\ell}, \qquad \gamma(s,\ell) = \frac{12}{s(s+2)}\left(\frac{s}{s+2}\right)^{\ell}. \quad (4.88)$$

We can identify $T_{\text{eff}} = 1/\gamma(s,\ell)$ as an effective temperature that depends on the length of the block. The double scaling limit $\ell \to \infty$ therefore corresponds to a maximally mixed state (infinite temperature). In this interpretation, we observe that the sign of the coupling strength changes with block length (alternation between ferromagnetic and antiferromagnetic interactions). This implies that the dominant eigenvalue of the reduced density matrix alternates between the p_{00} singlet (even ℓ) and p_{sM} multiplet (odd ℓ).

4.4.4 Anisotropic case

In the general case of arbitrary q, the dominant characteristic length of finite-size corrections generalizes to $\xi_q = 1/\log\big([s+2]/[s]\big)$:

$$\frac{1}{\xi_q} = \log\left(\frac{1-q^{2+s}}{q(1-q^s)}\right). \quad (4.89)$$

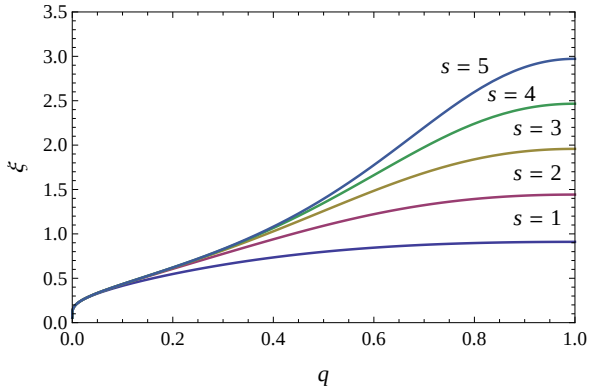

Figure 4.7: The characteristic length ξ_q of finite-size effects increases monotonically with spin s and anisotropy q. Its maximum value occurs at the isotropic point $q = 1$.

As depicted in Figure 4.7, this characteristic length is a maximum at the isotropic limit $\xi_{\max} \equiv 1/\log\big((s+2)/s\big)$ for any value of the spin s. This means that the condition $\ell \gg \xi_q$ for the double scaling limit to apply is reached by shorter blocks with increasing anisotropy and longer blocks by increasing spin.

As seen from the block decomposition of the reduced density matrix (4.51), obtaining the eigenvalue spectrum of ρ_ℓ generally requires finding the roots of polynomials of degree 1 to $s+1$. Thus, numerical methods are necessary to calculate the entanglement entropy in higher integer spin VBS_q states. We present numerical results for the von Neumann entropy for the spin-5 case in Figure 4.8. We compare these results with those obtained from the approximate eigenvalue spectrum (4.62) of the reduced density matrix. Good agreement between the two results is obtained near the double scaling limit (large ℓ) and near the completely deformed limit ($q \to 0^+$).

4.5 Concluding remarks

In this chapter we studied entanglement in the ground state of the anisotropic AKLT_q^s model. We contructed the VBS_q^s ground state model in the matrix product formulation. From this representation, we derived a compact formula for the reduced density matrix in terms of the q-deformed Clebsch-Gordan co-

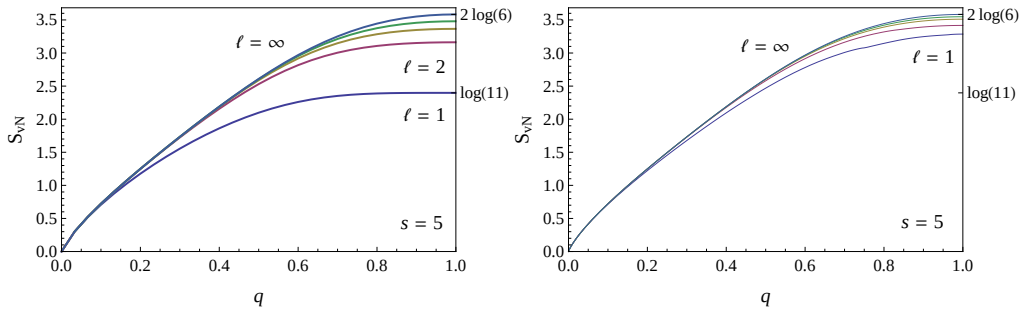

(a) Numerically exact (b) Approximate

Figure 4.8: A numerical evaluation of the von Neumann entropy (a) of a spin-5 VBS_q^5 state for block lengths $\ell = 1, 2, 3, 4$, and $\ell \to \infty$ is compared to the results of perturbation theory (b). The perturbation approximation is good when the block length ℓ is much greater than the characteristic length ξ_q.

efficients and q-deformed F-matrix elements. The eigenvalue spectrum of this reduced density matrix was obtained analytically in some important parameter regimes that include the isotropic ($q = 1$) and double scaling ($\ell \to \infty$) limits. For arbitrary deformations and block lengths, the reduced density matrix is decomposed into $(2s + 1)$ sectors so that its eigenvalues are grouped into multiplets. This decomposition is such that the diagonalization of each sector requires a numerical search for the roots of (at most) an $(s + 1)$-degree polynomial. The leading finite-size correction to the eigenvalue spectrum of the reduced density matrix is proven to decay exponentially with a characteristic length ξ_q. This result allowed us to obtain a first-order perturbative approximation to the eigenvalues in the long block regime $\ell \gg \xi_q$. From this approximation we discovered that q-deformation partially breaks the degeneracy of eigenvalues within each multiplet of the isotropic result.

With these results we calculated the entanglement entropies on continuous parameter spaces connecting the isotropic VBS state ($q = 1$) with product states ($q \to 0^+$) with zero entanglement. We demonstrated that the introduction of anisotropy by q-deformation decreases the entanglement present in the VBS_q^s ground state. This decrease in entanglement with q-deformation is observed even in the double scaling limit of infinitely long blocks.

Additionally, we constructed effective thermal models for the mixed state of

the block from the entanglement spectrum of the system. In the double scaling limit, we showed how the deformation parameter $|\log q|$ may be interpreted as an external magnetic field acting on two spin-$s/2$'s at the boundaries of a long block. At the isotropic point, the proposed effective picture consists of two spin-$s/2$'s having a Heisenberg-type interaction. The coupling constant in this case depends on the block length ℓ in such a way that a uniform mixture is obtained as $\ell \to \infty$.

The analytic approach presented in this chapter may be applied to other systems that may be represented as a matrix product state. These MPS include other one-dimensional valence-bond-solid (VBS) states [125, 126, 129, 139, 169] and anisotropic spin chains [136, 151, 170]. We demonstrate this generality in Section 4.7 where we study entanglement in a spin chain with broken SU(2) symmetry. Furthermore, the formalism given here will be useful in the analysis of entanglement in other states that may be approximated as MPS [137].

4.6 Derivations

4.6.1 Identities for q-CG coefficients

The q-CG coefficients enter the decomposition transformation

$$|J,m\rangle = \sum_{m_1,m_2} \begin{bmatrix} j_1 & j_2 & J \\ m_1 & m_2 & m \end{bmatrix}_q |j_1,m_1\rangle \otimes |j_2,m_2\rangle, \tag{4.90}$$

as well as the inverse transformation

$$|j_1,m_1\rangle \otimes |j_2,m_2\rangle = \sum_{J,m} \begin{bmatrix} j_1 & j_2 & J \\ m_1 & m_2 & m \end{bmatrix}_q |J,m\rangle, \tag{4.91}$$

where the triangle relation $\left|j_1 - j_2\right| \leq J \leq j_1 + j_2$ is implied to hold. A set of real q-CG coefficients may be evaluated numerically through the definition

[155]:

$$\begin{bmatrix} j_1 & j_2 & J \\ m_1 & m_2 & m \end{bmatrix}_q \equiv \delta_{m_1+m_2,m} q^{\frac{1}{4}(j_1+j_2-j)(j_1+j_2+j+1)+\frac{1}{2}(j_1m_1-j_2m_1)} \triangle(j_1j_2j)$$
$$\times \big([j_1+m_1]![j_1-m_1]![j_2+m_2]![j_2-m_2]![j+m]![j-m]![2j+1]\big)^{1/2}$$
$$\times \sum_n \Bigg(\frac{(-1)^n q^{-n(j_1+j_2+j+1)/2}}{[n]![j_1+j_2-j-n]![j_1-m_1-n]![j_2+m_2-n]!}$$
$$\times \frac{1}{[j-j_2+m_1+n]![j-j_1-m_2+n]!} \Bigg). \quad (4.92)$$

The triangle function $\triangle(abc)$ appearing here is equal to

$$\triangle(abc) \equiv \sqrt{\frac{[a+b-c]![a-b+c]![-a+b+c]!}{[a+b+c+1]!}}. \quad (4.93)$$

For integer arguments, the q-factorial is $[n]! \equiv [n][n-1]\cdots[1]$ with $[0]! \equiv 1$.

Among the key properties of the q-CG coefficients that we use in this chapter are the orthogonality relations

$$\sum_{Jm} \begin{bmatrix} j_1 & j_2 & J \\ m_1 & m_2 & m \end{bmatrix}_q \begin{bmatrix} j_1 & j_2 & J \\ m_1' & m_2' & m \end{bmatrix}_q = \delta_{m_1m_1'}\delta_{m_2m_2'}, \quad \text{(columns)},$$
$$\sum_{m_1m_2} \begin{bmatrix} j_1 & j_2 & J \\ m_1 & m_2 & m \end{bmatrix}_q \begin{bmatrix} j_1 & j_2 & J' \\ m_1 & m_2 & m' \end{bmatrix}_q = \delta_{JJ'}\delta_{mm'}\varepsilon_{j_1j_2J}, \quad \text{(rows)}. \quad (4.94)$$

The number $\varepsilon_{j_1j_2J}$ enforces the triangle relation: It is equal to unity when $|j_1 - j_2| \le J \le j_1 + j_2$ and zero otherwise. We also make much use of the

following identities involving column transpositions [155, 156]:

$$\begin{bmatrix} j_1 & j_2 & J \\ m_1 & m_2 & m \end{bmatrix}_q = (-1)^{j_1-J+m_2} q^{-m_2/2} \sqrt{\frac{[2J+1]}{[2j_1+1]}} \begin{bmatrix} J & j_2 & j_1 \\ m & -m_2 & m_1 \end{bmatrix}_q , \tag{4.95}$$

$$\begin{bmatrix} j_1 & j_2 & J \\ m_1 & m_2 & m \end{bmatrix}_q = \begin{bmatrix} j_2 & j_1 & J \\ -m_2 & -m_1 & -m \end{bmatrix}_q , \tag{4.96}$$

$$\begin{bmatrix} j_1 & j_2 & J \\ m_1 & m_2 & m \end{bmatrix}_q = (-1)^{J-j_2-m_1} q^{m_1/2} \sqrt{\frac{[2J+1]}{[2j_2+1]}} \begin{bmatrix} j_1 & J & j_2 \\ -m_1 & m & m_2 \end{bmatrix}_q . \tag{4.97}$$

4.6.2 q-deformed F-matrix and $6j$ symbols

The elements of the q-deformed F-matrix are shown diagrammatically in Figure 4.2. This diagram corresponds to the equation

$$\sum_{bcdk} \begin{bmatrix} D & K & J \\ d & k & j \end{bmatrix}_q \begin{bmatrix} B & C & K \\ b & c & k \end{bmatrix}_q |D,d\rangle \otimes |B,b\rangle \otimes |C,c\rangle = \sum_{\substack{bcdn \\ N}} F_q[DBJC;NK] \begin{bmatrix} N & C & J \\ n & c & j \end{bmatrix}_q \begin{bmatrix} D & B & N \\ d & b & n \end{bmatrix}_q |D,d\rangle \otimes |B,b\rangle \otimes |C,c\rangle . \tag{4.98}$$

Using the composition transformation (4.91)

$$|D,d\rangle \otimes |B,b\rangle = \sum_{Aa} \begin{bmatrix} D & B & A \\ d & b & a \end{bmatrix}_q |A,a\rangle \tag{4.99}$$

and applying the orthogonality relation (4.94) leads to the identity

$$\sum_{\substack{acbdk \\ A}} \begin{bmatrix} D & B & A \\ d & b & a \end{bmatrix}_q \begin{bmatrix} B & C & K \\ b & c & k \end{bmatrix}_q \begin{bmatrix} D & K & J \\ d & k & j \end{bmatrix}_q |A,a\rangle \otimes |C,c\rangle = \sum_{\substack{ac \\ A}} F_q[DBJC;AK] \begin{bmatrix} A & C & J \\ a & c & j \end{bmatrix}_q |A,a\rangle \otimes |C,c\rangle . \tag{4.100}$$

Repeating this procedure finally gives

$$\delta_{JJ'} F_q[DBJC;AK] = \sum_{bcj} \begin{bmatrix} D & B & A \\ j-c-b & b & j-c \end{bmatrix}_q \begin{bmatrix} B & C & K \\ b & c & b+c \end{bmatrix}_q \begin{bmatrix} D & K & J' \\ j-b-c & b+c & j \end{bmatrix}_q \begin{bmatrix} A & C & J \\ j-c & c & j \end{bmatrix}_q . \quad (4.101)$$

The q-deformed $6j$ symbol $\left\{ \begin{smallmatrix} A & B & E \\ D & C & F \end{smallmatrix} \right\}_q$ is related to the elements of the q-deformed F-matrix by [155]

$$\begin{Bmatrix} A & B & E \\ D & C & F \end{Bmatrix}_q = \frac{(-1)^{A+B+C+D}}{\sqrt{[2E+1][2F+1]}} F_q[ABCD;EF] . \quad (4.102)$$

For numerical calculations we use the sum

$$\begin{aligned} \begin{Bmatrix} A & B & E \\ D & C & F \end{Bmatrix}_q &= \triangle(ABE)\triangle(CDE)\triangle(ACF)\triangle(BDF) \\ &\times \sum_n \Bigg\{ \frac{(-1)^n [n+1]!}{[n-A-B-E]![n-A-C-F]!} \\ &\times \frac{1}{[n-B-D-F]![n-D-C-E]!} \\ &\times \frac{1}{[A+B+C+D-n]![A+D+E+F-n]!} \\ &\times \frac{1}{[B+C+E+F-n]!} \Bigg\}, \end{aligned} \quad (4.103)$$

where the sum is over all integers n so that the arguments of all q-factorials $[m]!$ are nonnegative $m \geq 0$.

4.7 Other matrix product states

In this section we apply the previous analysis to another anisotropic spin-1 quantum chain proposed by Klümper, Schadschneider, and Zittartz (KSZ model) [170]. The KSZ hamiltonian has partially broken SU(2) symmetry. By

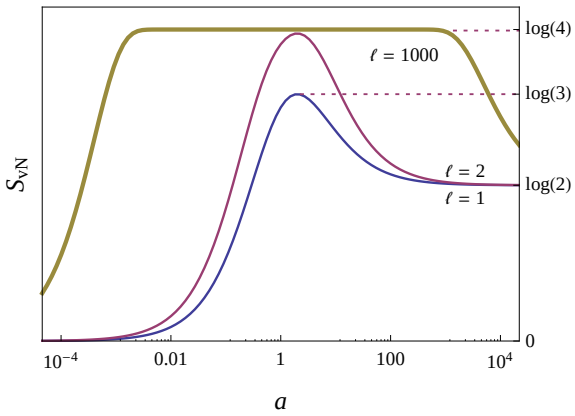

Figure 4.9: The von Neumann entropy decreases away from the isotropic AKLT points $a = 2$ for the KSZ_a state. Finite-size corrections are smallest at the isotropic point.

construction, it is invariant under lattice translations and reflections; spin rotations about the longitudinal z-axis; and spin reflections about the transverse plane $S_i^z \to -S_i^z$. It may be written as $H_{\mathrm{KSZ}} = \sum_j h_{j,j+1}$, where $h_{j,j+1}$ is the KSZ hamiltonian density given by

$$h_{j,j+1} = \alpha_0 A_j^2 + \alpha_1 (A_j B_j + B_j A_j) + \alpha_2 B_j^2 + \alpha_3 A_j + \alpha_4 B_j (1 + B_j) + \alpha_5 \left[(S_j^z)^2 + (S_{j+1}^z)^2 \right] + \alpha_6. \quad (4.104)$$

Here we have a transverse interaction term $A_j = S_j^x S_{j+1}^x + S_j^y S_{j+1}^y$, longitudinal interaction term $B_j = S_j^z S_{j+1}^z$, and constants α_i. Requiring $h_{j,j+1}$ to have nonnegative eigenvalues and annihilate an MPS ground state $|\mathrm{KSZ}_a\rangle$ leads to a family of hamiltonians with restrictions on the constants α_i [170]. The correlation functions and low-lying excitations of this model have been studied [170, 171], and here we present its entanglement properties.

We obtain the MPS form of $|\mathrm{KSZ}_a\rangle$ from the $\mathbf{g}$ matrix

$$\mathbf{g} = \begin{pmatrix} |0\rangle & -\sqrt{a}|+\rangle \\ \sqrt{a}|-\rangle & -\sigma|0\rangle \end{pmatrix}, \quad (4.105)$$

where $a > 0$ is an anisotropy parameter and $\sigma = \operatorname{sgn} \alpha_3$. The corresponding

transfer matrix is

$$\mathbf{G} = \begin{pmatrix} 1 & 0 & 0 & a \\ 0 & -\sigma & 0 & 0 \\ 0 & 0 & -\sigma & 0 \\ a & 0 & 0 & 1 \end{pmatrix}. \tag{4.106}$$

The unique ground state is $|\mathrm{KSZ}_a\rangle = \mathrm{tr}[\mathbf{g}_1 \cdot \mathbf{g}_2 \cdot \ldots \cdot \mathbf{g}_L]$ (periodic boundary conditions). It reduces to the isotropic VBS state at $a = 2$ and $\sigma = 1$.

The eigenvalues of ρ_ℓ for an infinite chain $L \to \infty$ are

$$\begin{aligned} p_{1,4} &= \frac{1}{4}\left[1 + \left(\frac{1-a}{1+a}\right)^\ell \pm 2\left(\frac{-\sigma}{1+a}\right)^\ell\right], \\ p_2 = p_3 &= \frac{1}{4}\left[1 - \left(\frac{1-a}{1+a}\right)^\ell\right]. \end{aligned} \tag{4.107}$$

We observe that the entanglement spectrum is the same for $\sigma = \pm 1$.

In the double scaling limit the eigenvalues of $\rho_{\ell\to\infty}$ become equal to each other $p_i^{\ell\to\infty} = \frac{1}{4}$. The block is maximally entangled with $S_\mathrm{R} = \log 4$. The entanglement spectrum therefore corresponds to a four-level system at infinite temperature. For blocks of finite length, the von Neumann entropy is a maximum at the isotropic point $a = 2$. This property is depicted in Figure 4.9. For a block of one spin ($\ell = 1$) one eigenvalue of ρ_ℓ vanishes and the entanglement entropy is a maximum at the isotropic point, $S_\mathrm{R}^{\ell=1} = \log 3$ at $a = 2$.

In the limit $a \to 0^+$, the $|\mathrm{KSZ}_a\rangle$ ground state approaches the transverse ferromagnet $\bigotimes_j |0\rangle_j$. This is a (classical) product state with no entanglement. In the opposite limit $a \to \infty$ the reduced density matrix represents a uniform mixture of two degenerate Néel ordered states. In this limit the von Neumann entropy approaches $\log 2$.

As in the case of the q-deformed AKLT model, finite-size corrections to the eigenvalues (4.107) decay exponentially with block length ℓ. The characteristic lengths of these corrections are $\xi_\parallel = 1/\log|(1+a)/(1-a)|$ and $\xi_\perp = 1/\log(1+a)$. These quantities are equal to the longitudinal ($\xi_\parallel$) and

transverse ($\xi_\perp$) correlation lengths of the spin-spin correlation functions [170]:

$$\langle S_1^z S_\ell^z \rangle = -\frac{a^2}{(1-a)^2}[\mathrm{sgn}(1-a)]^\ell \times \mathrm{e}^{-\ell/\xi_\parallel}, \tag{4.108}$$

$$\langle S_1^x S_\ell^x \rangle = -a(\sigma+1)[\mathrm{sgn}(-\sigma)]^\ell \times \mathrm{e}^{-\ell/\xi_\perp}, \quad \ell \geq 2. \tag{4.109}$$

Anisotropy in the KSZ model also reduces entanglement in the $|\mathrm{KSZ}_a\rangle$ state for blocks of finite length. But unlike the $|\mathrm{VBS}_q\rangle$ state, the boundary spins of infinitely long blocks are maximally entangled at fixed anisotropy $0 < a < \infty$. Thus, the effective boundary spins in the double scaling limit are at infinite temperature.

Chapter 5

Conclusions and outlook

In this thesis we calculated some exact and approximate physical quantities in one-dimensional models with broken and deformed symmetries.

For a Lieb–Liniger gas in an external longitudinal harmonic potential, we obtained the first-order correction to the ground state energy and chemical potential near the limit of infinite repulsion $c \to \infty$. After applying a fermion-boson mapping to transform the bosonic wavefunction into a fermionic one, we obtained a hamiltonian with a pseudopotential term proportional to $1/c$. Thus, we were able to use ordinary perturbation theory to obtain the first-order $1/c$ correction to the ground state energy. Our main result (2.17) was obtained for any number of bosons N. This correction was demonstrated to coincide with the Thomas–Fermi result when $\sqrt{N}/c \ll 1$ for $N \gtrsim 10$. Additionally, we remarked that the ground state energy E_0/N^2 is a function of $\sqrt{N}/c$ in the Thomas–Fermi approach as a consequence of energy being an extensive quantity at thermodynamic equilibrium. In principle, this perturbation-based method can also be applied to other trapping potentials for the strongly repulsive Lieb–Liniger gas. The practicality of such an approach depends on two considerations. First is the solvability of the corresponding free-fermionic model. Second is the ease of calculating the necessary matrix elements.

Next, we quantified the entanglement that can be extracted from the ground state of the periodic Lieb–Liniger model after the particle number in half the length of the gas is measured. This entanglement arises from quan-

tum correlations due to the interaction between particles. Among the possible measurement results with k bosons in partition A and $(N-k)$ in partition B, the balanced state with $N/2$ in each partition is the most probable. This balanced state also has more entanglement entropy than the other unbalanced states. For a given number of bosons, entanglement in the system increases with repulsion strength until it saturates at the impenetrable limit. In addition, we obtained a formula for the reduced density matrix of the projected state in terms of overlap matrices of linearly independent block state vectors (3.75). This expression leads to an upper bound for the von Neumann entropy in the projected state, $S_{\mathrm{vN}} \leq \log \binom{N}{k}$. This analysis applies to other many-body states that are represented by a class of Bethe ansätze with factorable Bethe amplitudes.

Finally, we evaluated the entanglement entropy and entanglement spectrum in blocks of the VBS_q^s ground state of the q-deformed spin-s Affleck–Kennedy–Lieb–Tasaki model. We were able to obtain exact analytic results in the double scaling limit, spin-1 case, and isotropic limit $q = 1$. There is no entanglement in the fully deformed classical limit $q \to 0^+$. The entanglement entropy decreases monotonically as the anisotropy parameter q decreases from 1 to 0^+, while it increases monotonically with block length ℓ. Hence, the entanglement entropy in a spin-s VBS_q^s state is a maximum $S_{\mathrm{vn}} = S_{\mathrm{R}}(\alpha) = 2\log(s+1)$ at the isotropic and double scaling limit ($q = 1$ and $\ell \to \infty$). These behaviors were interpreted in terms of effective models with interacting spin-$s/2$'s at the boundaries of the block. The quantity $1/|\log q|$ is the rescaled temperature of the effective thermal model describing the block. In this picture, the isotropic limit corresponds to infinite temperature and the classical limit corresponds to zero temperature. To obtain these results, we used a formula (4.19) for the reduced density matrix that we derived in terms of the $D^2 \times D^2$ transfer matrix of a matrix product state. This approach can therefore be used to study entanglement in other translationally invariant matrix product states.

Bibliography

[1] M. Lewenstein, A. Sanpera, V. Ahufinger, B. Damski, A. Sen(De), and U. Sen, "Ultracold atomic gases in optical lattices: mimicking condensed matter physics and beyond," Adv. Phys. **56**, 243 (2007).

[2] I. Bloch, J. Dalibard, and W. Zwerger, "Many-body physics with ultracold gases," Rev. Mod. Phys. **80**, 885 (2008).

[3] M. A. Cazalilla, R. Citro, T. Giamarchi, E. Orignac, and M. Rigol, "One dimensional bosons: From condensed matter systems to ultracold gases," Rev. Mod. Phys. **83**, 1405 (2011).

[4] A. S. Darmawan and S. D. Bartlett, "Optical spin-1 chain and its use as a quantum-computational wire," Phys. Rev. A **82**, 012328 (2010).

[5] R. Kaltenbaek, J. Lavoie, B. Zeng, S. D. Bartlett, and K. J. Resch, "Optical one-way quantum computing with a simulated valence-bond solid," Nature Phys. **6**, 850 (2010).

[6] R. Raussendorf, "Quantum computing: Shaking up ground states," Nature Phys. **6**, 840 (2010).

[7] M. Hagiwara, K. Katsumata, I. Affleck, B. I. Halperin, and J. P. Renard, "Observation of $S = 1/2$ degrees of freedom in an $S = 1$ linear-chain Heisenberg antiferromagnet," Phys. Rev. Lett. **65**, 3181 (1990).

[8] E. H. Lieb and W. Liniger, "Exact analysis of an interacting Bose gas. I. The general solution and the ground state," Phys. Rev. **130**, 1605 (1963).

[9] E. H. Lieb, "Exact analysis of an interacting Bose gas. II. The excitation spectrum," Phys. Rev. **130**, 1616 (1963).

[10] V. E. Korepin, N. M. Bogoliubov, and A. G. Azergin, *Quantum Inverse Scattering Method and Correlation Functions* (Cambridge University Press, Cambridge, 1993).

[11] B. Davies and V. E. Korepin, "Higher conservation laws for the quantum non-linear Schrödinger equation," (1989), preprint CMA-R33-89 (Centre for Mathematical Analysis, Australian National University), arXiv:1109.6604.

[12] C. N. Yang, "Some exact results for the many-body problem in one dimension with repulsive delta-function interaction," Phys. Rev. Lett. **19**, 1312 (1967).

[13] C. N. Yang and C. P. Yang, "Thermodynamics of a one-dimensional system of bosons with repulsive delta-function interaction," J. Math. Phys. **10**, 1115 (1969).

[14] M. Takahashi, *Thermodynamics of One-dimensional Solvable Models* (Cambridge University Press, Cambridge, 1999).

[15] B. Sutherland, *Beautiful Models: 70 Years of Exactly Solved Quantum Many-Body Problems* (World Scientific Co. Pte. Ltd., Singapore, 2004).

[16] A. Görlitz, J. M. Vogels, A. E. Leanhardt, C. Raman, T. L. Gustavson, J. R. Abo-Shaeer, A. P. Chikkatur, S. Gupta, S. Inouye, T. Rosenband, et al., "Realization of Bose-Einstein condensates in lower dimensions," Phys. Rev. Lett. **87**, 130402 (2001).

[17] H. Moritz, T. Stöferle, M. Köhl, and T. Esslinger, "Exciting collective oscillations in a trapped 1D gas," Phys. Rev. Lett. **91**, 250402 (2003).

[18] B. Paredes, A. Widera, V. Murg, O. Mandel, S. Fölling, I. Cirac, G. V. Shlyapnikov, T. W. Hänsch, and I. Bloch, "Tonks-Girardeau gas of ultracold atoms in an optical lattice," Nature **429**, 277 (2004).

[19] T. Kinoshita, T. Wenger, and D. S. Weiss, "Observation of a one-dimensional Tonks-Girardeau gas," Science **305**, 1125 (2004).

[20] M. Horikoshi and K. Nakagawa, "Atom chip based fast production of Bose-Einstein condensate," Appl. Phys. B **82**, 363 (2006).

[21] L. Della Pietra, S. Aigner, C. vom Hagen, S. Groth, I. Bar-Joseph, H. J. Lezec, and J. Schmiedmayer, "Designing potentials by sculpturing wires," Phys. Rev. A **75**, 063604 (2007).

[22] A. H. van Amerongen, J. J. P. van Es, P. Wicke, K. V. Kheruntsyan, and N. J. van Druten, "Yang-Yang thermodynamics on an atom chip," Phys. Rev. Lett. **100**, 090402 (2008).

[23] J. J. P. van Es, P. Wicke, A. H. van Amerongen, C. Rétif, S. Whitlock, and N. J. van Druten, "Box traps on an atom chip for one-dimensional quantum gases," J. Phys. B: At. Mol. Opt. Phys. **43**, 155002 (2010).

[24] M. Greiner, O. Mandel, T. Esslinger, T. Hänsch, and I. Bloch, "Quantum phase transition from a superfluid to a Mott insulator in a gas of ultracold atoms," Nature **415**, 39 (2002).

[25] T. Stöferle, H. Moritz, C. Schori, M. Köhl, and T. Esslinger, "Transition from a strongly interacting 1D superfluid to a Mott insulator," Phys. Rev. Lett. **92**, 130403 (2004).

[26] E. Haller, M. Gustavsson, M. J. Mark, J. G. Danzl, R. Hart, G. Pupillo, and H.-C. Nägerl, "Realization of an excited, strongly correlated quantum gas phase," Science **325**, 1224 (2009).

[27] T. Kinoshita, T. Wenger, and D. Weiss, "A quantum Newton's cradle," Nature **440**, 900 (2006).

[28] S. Palzer, C. Zipkes, C. Sias, and M. Köhl, "Quantum transport through a Tonks-Girardeau gas," Phys. Rev. Lett. **103**, 150601 (2009).

[29] B. Gadway, D. Pertot, J. Reeves, and D. Schneble, "Probing an ultracold-atom crystal with matter waves," Nature Phys. **8**, 544 (2012).

[30] M. Olshanii, "Atomic scattering in the presence of an external confinement and a gas of impenetrable bosons," Phys. Rev. Lett. **81**, 938 (1998).

[31] T. Bergeman, M. G. Moore, and M. Olshanii, "Atom-atom scattering under cylindrical harmonic confinement: Numerical and analytic studies of the confinement induced resonance," Phys. Rev. Lett. **91**, 163201 (2003).

[32] K. Huang, *Statistical Mechanics* (John Wiley & Sons, Inc., New York, 1987).

[33] S. Inouye, M. R. Andrews, J. Stenger, H. Miesner, D. M. Stamper-Kurn, and W. Ketterle, "Observation of Feshbach resonances in a Bose–Einstein condensate," Nature **392**, 151 (1998).

[34] C. Chin, R. Grimm, P. Julienne, and E. Tiesinga, "Feshbach resonances in ultracold gases," Rev. Mod. Phys. **82**, 1225 (2010).

[35] V. Dunjko, V. Lorent, and M. Olshanii, "Bosons in cigar-shaped traps: Thomas-Fermi regime, Tonks-Girardeau regime, and in between," Phys. Rev. Lett. **86**, 5413 (2001).

[36] Z.-Q. Ma and C. N. Yang, "Spinless bosons in a 1D harmonic trap with repulsive delta function interparticle interaction I: General theory," Chin. Phys. Lett. **26**, 120506 (2009).

[37] Z.-Q. Ma and C. N. Yang, "Spinless bosons in a 1D harmonic trap with repulsive delta function interparticle interaction II: Numerical solutions," Chin. Phys. Lett. **27**, 020506 (2010).

[38] A. Yu. Cherny and J. Brand, "Polarizability and dynamic structure factor of the one-dimensional Bose gas near the Tonks-Girardeau limit at finite temperatures," Phys. Rev. A **73**, 023612 (2006).

[39] Th. Busch, B.-G. Englert, K. Rzążewski, and M. Wilkens, "Two cold atoms in a harmonic trap," Found. Phys. **28**, 549 (1998).

[40] M. D. Girardeau, E. M. Wright, and J. M. Triscari, "Ground-state properties of a one-dimensional system of hard-core bosons in a harmonic trap," Phys. Rev. A **63**, 033601 (2001).

[41] M. D. Girardeau and E. M. Wright, "Quantum mechanics of one-dimensional trapped Tonks gases," Laser Phys. **12**, 8 (2002).

[42] E. B. Kolomeisky, T. J. Newman, J. P. Straley, and X. Qi, "Low-dimensional Bose liquids: Beyond the Gross-Pitaevskii approximation," Phys. Rev. Lett. **85**, 1146 (2000).

[43] C. Menotti and S. Stringari, "Collective oscillations of a one-dimensional trapped Bose-Einstein gas," Phys. Rev. A **66**, 043610 (2002).

[44] Y. E. Kim and A. L. Zubarev, "Density-functional theory of bosons in a trap," Phys. Rev. A **67**, 015602 (2003).

[45] M. Gaudin, "Boundary energy of a bose gas in one dimension," Phys. Rev. A **4**, 386 (1971).

[46] M. Gaudin, *La fonction d'onde de Bethe* (Masson, Paris, 1983).

[47] M. T. Batchelor, X. W. Guan, N. Oelkers, and C. Lee, "The 1D interacting Bose gas in a hard wall box," J. Phys. A: Math. Gen. **38**, 7787 (2005).

[48] D. Jukić, S. Galić, R. Pezer, and H. Buljan, "Lieb-Liniger gas in a constant-force potential," Phys. Rev. A **82**, 023606 (2010).

[49] M. D. Girardeau, "Relationship between systems of impenetrable bosons and fermions in one dimension," J. Math. Phys. **1**, 516 (1960).

[50] T. Cheon and T. Shigehara, "Fermion-boson duality of one-dimensional quantum particles with generalized contact interactions," Phys. Rev. Lett. **82**, 2536 (1999).

[51] V. Yukalov and M. Girardeau, "Fermi-Bose mapping for one-dimensional Bose gases," Laser Phys. Lett. **2**, 375 (2005).

[52] D. Sen, "Perturbation theory for singular potentials in quantum mechanics," Int. J. Mod. Phys. A **14**, 1789 (1999).

[53] D. Sen, "The fermionic limit of the δ-function Bose gas: a pseudopotential approach," J .Phys. A: Math. Gen. **36**, 7517 (2003).

[54] J. C. Slater, "The theory of complex spectra," Phys. Rev. **34**, 1293 (1929).

[55] E. U. Condon, "The theory of complex spectra," Phys. Rev. **36**, 1121 (1930).

[56] M. Abramowitz and I. Stegun, *Handbook of Mathematical Functions with Formulas, Graphs, and Mathematical Tables* (Dover Publications, New York, 1972).

[57] J. Goold and T. Busch, "Ground-state properties of a Tonks-Girardeau gas in a split trap," Phys. Rev. A **77**, 063601 (2008).

[58] S. H. Patil, "Harmonic oscillator with a δ-function potential," Eur. J. Phys. **27**, 899 (2006).

[59] I. S. Gradshteyn and I. M. Ryzhik, *Table of Integrals, Series, and Products Academic* (Elsevier Academic Press, Amsterdam, 2007).

[60] Y.-Z. You, "Ground state energy of one-dimensional δ-function interacting Bose and Fermi gas," Chin. Phys. Lett. **27**, 080305 (2010).

[61] C. H. Bennett and D. P. DiVincenzo, "Quantum information and computation," Nature **404**, 247 (2000).

[62] L. Amico, R. Fazio, A. Osterloh, and V. Vedral, "Entanglement in many-body systems," Rev. Mod. Phys. **80**, 517 (2008).

[63] J. Eisert, M. Cramer, and M. B. Plenio, "Colloquium: Area laws for the entanglement entropy," Rev. Mod. Phys. **82**, 277 (2010).

[64] A. Osterloh, L. Amico, G. Falci, and R. Fazio, "Scaling of entanglement close to a quantum phase transition," Nature **416**, 608 (2002).

[65] T. J. Osborne and M. A. Nielsen, "Entanglement in a simple quantum phase transition," Phys. Rev. A **66**, 032110 (2002).

[66] G. Vidal, J. I. Latorre, E. Rico, and A. Kitaev, "Entanglement in quantum critical phenomena," Phys. Rev. Lett. **90**, 227902 (2003).

[67] F. Franchini, A. R. Its, and V. E. Korepin, "Renyi entropy of the XY spin chain," J. Phys. A: Math. Theor. **41**, 025302 (2008).

[68] F. Iglói and Y.-C. Lin, "Finite-size scaling of the entanglement entropy of the quantum Ising chain with homogeneous, periodically modulated and random couplings," J. Stat. Mech.: Theory Exp. **2008**, P06004 (2008).

[69] A. Kitaev and J. Preskill, "Topological entanglement entropy," Phys. Rev. Lett. **96**, 110404 (2006).

[70] E. Fradkin, "Scaling of entanglement entropy at 2D quantum Lifshitz fixed points and topological fluids," J. Phys. A: Math. Theor. **42**, 504011 (2009).

[71] M. Cramer, M. B. Plenio, and H. Wunderlich, "Measuring entanglement in condensed matter systems," Phys. Rev. Lett. **106**, 020401 (2011).

[72] S. Gupta, K. W. Murch, K. L. Moore, T. P. Purdy, and D. M. Stamper-Kurn, "Bose-Einstein condensation in a circular waveguide," Phys. Rev. Lett. **95**, 143201 (2005).

[73] O. Morizot, Y. Colombe, V. Lorent, H. Perrin, and B. M. Garraway, "Ring trap for ultracold atoms," Phys. Rev. A **74**, 023617 (2006).

[74] C. H. Bennett, G. Brassard, S. Popescu, B. Schumacher, J. A. Smolin, and W. K. Wootters, "Purification of noisy entanglement and faithful teleportation via noisy channels," Phys. Rev. Lett. **76**, 722 (1996).

[75] C. H. Bennett, H. J. Bernstein, S. Popescu, and B. Schumacher, "Concentrating partial entanglement by local operations," Phys. Rev. A **53**, 2046 (1996).

[76] C. H. Bennett, D. P. DiVincenzo, J. A. Smolin, and W. K. Wootters, "Mixed-state entanglement and quantum error correction," Phys. Rev. A **54**, 3824 (1996).

[77] V. Vedral, M. B. Plenio, M. A. Rippin, and P. L. Knight, "Quantifying entanglement," Phys. Rev. Lett. **78**, 2275 (1997).

[78] M. B. Plenio and S. Virmani, "An introduction to entanglement measures," Quant. Inf. Comput. **7**, 1 (2007).

[79] H. M. Wiseman and J. A. Vaccaro, "Entanglement of indistinguishable particles shared between two parties," Phys. Rev. Lett. **91**, 097902 (2003).

[80] M. R. Dowling, A. C. Doherty, and H. M. Wiseman, "Entanglement of indistinguishable particles in condensed-matter physics," Phys. Rev. A **73**, 052323 (2006).

[81] T. Sasaki, T. Ichikawa, and I. Tsutsui, "Entanglement of indistinguishable particles," Phys. Rev. A **83**, 012113 (2011).

[82] B. Sutherland, "Quantum many-body problem in one dimension: Ground state," J. Math. Phys. **12**, 246 (1971).

[83] F. Calogero, "Solution of the one-dimensional N-body problems with quadratic and/or inversely quadratic pair potentials," J. Math. Phys. **12**, 419 (1971).

[84] A. Kundu, "Exact solution of double δ function Bose gas through an interacting anyon gas," Phys. Rev. Lett. **83**, 1275 (1999).

[85] M. T. Batchelor, X.-W. Guan, and J.-S. He, "The Bethe ansatz for 1D interacting anyons," J. Stat. Mech.: Theor. Exp. **2007**, P03007 (2007).

[86] J. Schliemann, J. Ignacio Cirac, M. Kuś, M. Lewenstein, and D. Loss, "Quantum correlations in two-fermion systems," Phys. Rev. A **64**, 022303 (2001).

[87] M. Haque, O. Zozulya, and K. Schoutens, "Entanglement entropy in fermionic Laughlin states," Phys. Rev. Lett. **98**, 060401 (2007).

[88] O. S. Zozulya, M. Haque, K. Schoutens, and E. H. Rezayi, "Bipartite entanglement entropy in fractional quantum Hall states," Phys. Rev. B **76**, 125310 (2007).

[89] O. S. Zozulya, M. Haque, and K. Schoutens, "Particle partitioning entanglement in itinerant many-particle systems," Phys. Rev. A **78**, 042326 (2008).

[90] M. Haque, O. S. Zozulya, and K. Schoutens, "Entanglement between particle partitions in itinerant many-particle states," J. Phys. A: Math. Theor. **42**, 504012 (2009).

[91] F. D. M. Haldane, "'Fractional statistics' in arbitrary dimensions: A generalization of the Pauli principle," Phys. Rev. Lett. **67**, 937 (1991).

[92] H. Katsura and Y. Hatsuda, "Entanglement entropy in the Calogero-Sutherland model," J. Phys. A: Math. Theor. **40**, 13931 (2007).

[93] R. Santachiara, F. Stauffer, and D. C. Cabra, "Entanglement properties and momentum distributions of hard-core anyons on a ring," J. Stat. Mech.: Theory Exp. **2007**, L05003 (2007).

[94] H. Guo, Y. Hao, and S. Chen, "Quantum entanglement of particles on a ring with fractional statistics," Phys. Rev. A **80**, 052332 (2009).

[95] I. Klich, G. Refael, and A. Silva, "Measuring entanglement entropies in many-body systems," Phys. Rev. A **74**, 032306 (2006).

[96] I. Klich and L. Levitov, "Quantum noise as an entanglement meter," Phys. Rev. Lett. **102**, 100502 (2009).

[97] H. F. Song, S. Rachel, and K. Le Hur, "General relation between entanglement and fluctuations in one dimension," Phys. Rev. B **82**, 012405 (2010).

[98] H. F. Song, C. Flindt, S. Rachel, I. Klich, and K. Le Hur, "Entanglement entropy from charge statistics: Exact relations for noninteracting many-body systems," Phys. Rev. B **83**, 161408 (2011).

[99] M. Srednicki, "Entropy and area," Phys. Rev. Lett. **71**, 666 (1993).

[100] C. Holzhey, F. Larsen, and F. Wilczek, "Geometric and renormalized entropy in conformal field theory," Nucl. Phys. B **424**, 443 (1994).

[101] P. Calabrese, M. Mintchev, and E. Vicari, "Entanglement entropy of one-dimensional gases," Phys. Rev. Lett. **107**, 020601 (2011).

[102] P. Calabrese, M. Mintchev, and E. Vicari, "The entanglement entropy of one-dimensional systems in continuous and homogeneous space," J. Stat. Mech.: Theory Exp. **2011**, P09028 (2011).

[103] P. Calabrese, M. Mintchev, and E. Vicari, "Exact relations between particle fluctuations and entanglement in Fermi gases," Europhys. Lett. **98**, 20003 (2012).

[104] H. F. Song, N. Laflorencie, S. Rachel, and K. Le Hur, "Entanglement entropy of the two-dimensional Heisenberg antiferromagnet," Phys. Rev. B **83**, 224410 (2011).

[105] H. F. Song, S. Rachel, C. Flindt, I. Klich, N. Laflorencie, and K. Le Hur, "Bipartite fluctuations as a probe of many-body entanglement," Phys. Rev. B **85**, 035409 (2012).

[106] M. Chung and I. Peschel, "Density-matrix spectra of solvable fermionic systems," Physical Review B **64**, 64412 (2001).

[107] B.-Q. Jin and V. Korepin, "Quantum spin chain, Toeplitz determinants and the Fisher–Hartwig conjecture," J. Stat. Phys. **116**, 79 (2004).

[108] I. Peschel, "Calculation of reduced density matrices from correlation functions," J. Phys. A: Math. Gen. **36**, L205 (2003).

[109] I. Peschel, "On the reduced density matrix for a chain of free electrons," J. Stat. Mech.: Theory Exp. **2004**, P06004 (2004).

[110] I. Peschel and V. Eisler, "Reduced density matrices and entanglement entropy in free lattice models," J. Phys. A: Math. Theor. **42**, 504003 (2009).

[111] P. Calabrese, M. Campostrini, F. Essler, and B. Nienhuis, "Parity effects in the scaling of block entanglement in gapless spin chains," Phys. Rev. Lett. **104**, 095701 (2010).

[112] M. Fagotti and P. Calabrese, "Universal parity effects in the entanglement entropy of XX chains with open boundary conditions," J. Stat. Mech.: Theory Exp. **2011**, P01017 (2011).

[113] J. Molina-Vilaplana, S. Bose, and V. E. Korepin, "Pure state entanglement between separated regions using impenetrable bosons," Int. J. Quantum Inf. **6**, 739 (2008).

[114] J. Molina, H. Wichterich, V. E. Korepin, and S. Bose, "Extraction of pure entangled states from many-body systems by distant local projections," Phys. Rev. A **79**, 062310 (2009).

[115] S. D. Bartlett and H. M. Wiseman, "Entanglement constrained by superselection rules," Phys. Rev. Lett. **91**, 097903 (2003).

[116] S. D. Bartlett, T. Rudolph, and R. W. Spekkens, "Reference frames, superselection rules, and quantum information," Rev. Mod. Phys. **79**, 555 (2007).

[117] A. G. Izergin and V. E. Korepin, "Pauli principle for one-dimensional bosons and the algebraic Bethe ansatz," Lett. Math. Phys. **6**, 283 (1982).

[118] V. E. Korepin, "Calculation of norms of Bethe wave functions," Commun. Math. Phys. **86**, 391 (1982).

[119] D. N. Aristov, "Bosonization for a Wigner-Jordan-like transformation: Backscattering and umklapp processes on a fictitious lattice," Phys. Rev. B **57**, 12825 (1998).

[120] A. G. Abanov, D. A. Ivanov, and Y. Qian, "Quantum fluctuations of one-dimensional free fermions and Fisher–Hartwig formula for Toeplitz determinants," J. Phys. A: Math. Theor. **44**, 485001 (2011).

[121] A. A. Ovchinnikov, "Fisher–Hartwig conjecture and the correlators in the inpenetrable Bose gas," Phys. Lett. A **373**, 305 (2009).

[122] E. L. Basor and K. E. Morrison, "The Fisher–Hartwig conjecture and Toeplitz eigenvalues," Linear Algebra Appl. **202**, 129 (1994).

[123] P. Deift, A. Its, and I. Krasovsky, "Asymptotics of Toeplitz, Hankel, and Toeplitz+Hankel determinants with Fisher–Hartwig singularities," Ann. Math. **174**, 1243 (2011).

[124] A. Ekert and P. L. Knight, "Entangled quantum systems and the Schmidt decomposition," Am. J. Phys. **63**, 415 (1995).

[125] I. Affleck, T. Kennedy, E. H. Lieb, and H. Tasaki, "Rigorous results on valence-bond ground states in antiferromagnets," Phys. Rev. Lett. **59**, 799 (1987).

[126] I. Affleck, T. Kennedy, E. H. Lieb, and H. Tasaki, "Valence bond ground states in isotropic quantum antiferromagnets," Commun. Math. Phys. **115**, 477 (1988).

[127] F. D. M. Haldane, "Nonlinear field theory of large-spin Heisenberg antiferromagnets: Semiclassically quantized solitons of the one-dimensional easy-axis Néel state," Phys. Rev. Lett. **50**, 1153 (1983).

[128] F. D. M. Haldane, "Continuum dynamics of the 1-D Heisenberg antiferromagnet: Identification with the O(3) nonlinear sigma model," Phys. Lett. A **93**, 464 (1983).

[129] A. N. Kirillov and V. E. Korepin, "The valence bond solid in quasicrystals," Algebra i Analiz **1**, 47 (1989), English transl.: St. Petersburg Math. J. **1**, 343 (1990); arXiv:0909.2211.

[130] D. Gross and J. Eisert, "Novel schemes for measurement-based quantum computation," Phys. Rev. Lett. **98**, 220503 (2007).

[131] G. K. Brennen and A. Miyake, "Measurement-based quantum computer in the gapped ground state of a two-body Hamiltonian," Phys. Rev. Lett. **101**, 010502 (2008).

[132] T.-C. Wei, I. Affleck, and R. Raussendorf, "Affleck-Kennedy-Lieb-Tasaki state on a honeycomb lattice is a universal quantum computational resource," Phys. Rev. Lett. **106**, 070501 (2011).

[133] D. P. Arovas, A. Auerbach, and F. D. M. Haldane, "Extended Heisenberg models of antiferromagnetism: Analogies to the fractional quantum Hall effect," Phys. Rev. Lett. **60**, 531 (1988).

[134] V. E. Korepin and Y. Xu, "Entanglement in valence-bond-solid states," Int. J. Mod. Phys. B **24**, 1361 (2010).

[135] M. Fannes, B. Nachtergaele, and R. F. Werner, "Exact antiferromagnetic ground states of quantum spin chains," Europhys. Lett. **10**, 633 (1989).

[136] A. Klümper, A. Schadschneider, and J. Zittartz, "Equivalence and solution of anisotropic spin-1 models and generalized t-j fermion models in one dimension," J. Phys. A: Math. Gen **24**, L955 (1991).

[137] F. Verstraete and J. I. Cirac, "Matrix product states represent ground states faithfully," Phys. Rev. B **73**, 094423 (2006).

[138] F. Verstraete, V. Murg, and J. I. Cirac, "Matrix product states, projected entangled pair states, and variational renormalization group methods for quantum spin systems," Adv. Phys. **57**, 143 (2008).

[139] K. Totsuka and M. Suzuki, "Matrix formalism for the VBS-type models and hidden order," J. Phys. Condens. Matter **7**, 1639 (1995).

[140] Y. Xu, H. Katsura, T. Hirano, and V. E. Korepin, "Entanglement and density matrix of a block of spins in AKLT model," J. Stat. Phys. **133**, 347 (2008).

[141] Y. Xu and V. E. Korepin, "Entanglement of the valence-bond-solid state on an arbitrary graph," J. Phys. A: Math. Theor. **41**, 505302 (2008).

[142] M. M. Wolf, G. Ortiz, F. Verstraete, and J. I. Cirac, "Quantum phase transitions in matrix product systems," Phys. Rev. Lett. **97**, 110403 (2006).

[143] S. Michalakis and B. Nachtergaele, "Entanglement in finitely correlated spin states," Phys. Rev. Lett. **97**, 140601 (2006).

[144] V. G. Drinfel'd, "Hopf algebras and quantum Yang-Baxter equation," Dokl. Akad. Nauk SSSR **283**, 1060 (1985), English trans.: Sov. Math. Dokl. **32**, 254 (1985).

[145] M. Jimbo, "A q-difference analogue of U(g) and the Yang-Baxter equation," Lett. Math. Phys. **10**, 63 (1985).

[146] N. b. Reshetikhin, L. A. Takhtadzhyan, and L. D. Faddeev, "Quantization of Lie groups and Lie algebras," Algebra i Analiz **1**, 178 (1989), English transl.: St. Petersburg Math. J. **1**, 193 (1990).

[147] F. Verstraete, M. A. Martín-Delgado, and J. I. Cirac, "Diverging entanglement length in gapped quantum spin systems," Phys. Rev. Lett. **92**, 087201 (2004).

[148] B.-Q. Jin and V. E. Korepin, "Localizable entanglement in antiferromagnetic spin chains," Phys. Rev. A **69**, 062314 (2004).

[149] Y. Chen, P. Zanardi, Z. D. Wang, and F. C. Zhang, "Sublattice entanglement and quantum phase transitions in antiferromagnetic spin chains," New J. Phys. **8**, 97 (2006).

[150] M. T. Batchelor, L. Mezincescu, R. I. Nepomechie, and V. Rittenberg, "q-deformations of the O(3) symmetric spin-1 Heisenberg chain," J. Phys. A: Math. Gen. **23**, L141 (1990).

[151] A. Klümper, A. Schadschneider, and J. Zittartz, "Groundstate properties of a generalized VBS-model," Z. Phys. B **87**, 281 (1992).

[152] K. Motegi, "The matrix product representation for the q-VBS state of one-dimensional higher integer spin model," Phys. Lett. A **374**, 3112 (2010).

[153] C. Arita and K. Motegi, "Spin-spin correlation functions of the q-valence-bond-solid state of an integer spin model," J. Math. Phys. **52**, 063303 (2011).

[154] C. Arita and K. Motegi, "Entanglement properties of a higher-integer-spin AKLT model with quantum group symmetry," (2012), arXiv:1206.3653.

[155] L. Biedenharn and M. Lohe, *Quantum Group Symmetry and q-Tensor Algebras* (World Scientific, Singapore, 1995).

[156] A. N. Kirillov and N. Yu. Reshetikhin, *Infinite Dimensional Lie Algebras and Groups*, vol. 7 of *Advanced Series in Mathematical Physics* (World Scientific, Singapore, 1989).

[157] E. Ardonne and J. Slingerland, "Clebsch–gordan and $6j$-coefficients for rank 2 quantum groups," J. Phys. A: Math. Theor. **43**, 395205 (2010).

[158] H. Fan, V. Korepin, and V. Roychowdhury, "Entanglement in a valence-bond solid state," Phys. Rev. Lett. **93**, 227203 (2004).

[159] H. Katsura, T. Hirano, and Y. Hatsugai, "Exact analysis of entanglement in gapped quantum spin chains," Phys. Rev. B **76**, 012401 (2007).

[160] H. Fan, V. Korepin, V. Roychowdhury, C. Hadley, and S. Bose, "Boundary effects on entropy and two-site entanglement of the spin-1 valence-bond solid," Phys. Rev. B **76**, 014428 (2007).

[161] M. Greiter and S. Rachel, "Valence bond solids for SU(n) spin chains: Exact models, spinon confinement, and the Haldane gap," Phys. Rev. B **75**, 184441 (2007).

[162] H. Katsura, T. Hirano, and V. E. Korepin, "Entanglement in an SU(n) valence-bond-solid state," J. Phys. A: Math. Theor. **41**, 135304 (2008).

[163] S. D. Geraedts and E. S. Sørensen, "Exact results for the bipartite entanglement entropy of the AKLT spin-1 chain," J. Phys. A: Math. Theor. **43**, 185304 (2010).

[164] R. Orús and H.-H. Tu, "Entanglement and SU(n) symmetry in one-dimensional valence-bond solid states," Phys. Rev. B **83**, 201101 (2011).

[165] H. Li and F. D. M. Haldane, "Entanglement spectrum as a generalization of entanglement entropy: Identification of topological order in non-Abelian fractional quantum Hall effect states," Phys. Rev. Lett. **101**, 010504 (2008).

[166] M. B. Hastings, "An area law for one-dimensional quantum systems," J. Stat. Mech.: Theory Exp. **2007**, P08024 (2007).

[167] H. Katsura, N. Kawashima, A. N. Kirillov, V. E. Korepin, and S. Tanaka, "Entanglement in valence-bond-solid states on symmetric graphs," J. Phys. A: Math. Theor. **43**, 255303 (2010).

[168] J. Lou, S. Tanaka, H. Katsura, and N. Kawashima, "Entanglement spectra of the two-dimensional Affleck-Kennedy-Lieb-Tasaki model: Correspondence between the valence-bond-solid state and conformal field theory," Phys. Rev. B **84**, 245128 (2011).

[169] V. Karimipour and L. Memarzadeh, "Matrix product representations for all valence bond states," Phys. Rev. B **77**, 094416 (2008).

[170] A. Klümper, A. Schadschneider, and J. Zittartz, "Matrix product ground states for one-dimensional spin-1 quantum antiferromagnets," Europhys. Lett. **24**, 293 (1993).

[171] E. Bartel, A. Schadschneider, and J. Zittartz, "Excitations of anisotropic spin-1 chains with matrix product ground state," Eur. Phys. J. B **31**, 209 (2003).